

Microvascular damage, neuroinflammation and extracellular matrix remodeling in *Coll8a1* knockout mice as a model for early cerebral small vessel disease

Thesis

for the degree of

doctor rerum naturalium (Dr. rer. nat.)

approved by the Faculty of Natural Sciences of Otto von Guericke University Magdeburg

by Dr. rer. nat. Mahsima Khoshneviszadeh

born on 06.04.1988 in Shiraz

Examiner: apl. Prof. Dr. Eike Budinger
PD Dr. Dirk Montag

submitted on: 30.01.2023

defended on: 18.07.2023

Summary

The extracellular matrix (ECM), primarily composed of collagen, offers critical structural and mechanical foundations for all multicellular organisms. It plays an influential role in determining cellular activities, including cell growth, programmed cell death, morphology, movement, and differentiation. Specialized ECM structures known as basement membranes (BMs) coat most layers of epithelial and endothelial cells. Beyond their foundational and partitioning roles, BMs and their constituents participate in diverse biological signaling pathways, growth processes, and disease developments. Collagen XVIII is a well-conserved component within BMs throughout evolutionary history. This multi-domain heparan sulfate proteoglycan (HSPG) is manifested in three distinct tissue-specific forms. All three versions of collagen XVIII feature Endostatin, their C-terminal domain, known for its anti-angiogenic attributes. Earlier research on collagen IV, another primary BM element, highlighted pathological modifications in small arteries and capillaries in the absence of collagen IV in mice. These changes echo those seen in cerebral small vessel disease (CSVD), such as age-related blood-brain barrier (BBB) defects and restructuring of the vessel wall, which can lead to vessel blockages and surrounding bleeds. CSVD stands as a primary contributor to vascular cognitive issues, playing a role in numerous neurological conditions, from strokes and mild cognitive deficits to dementia.

A key objective of this thesis was to investigate if deletion of the collagen XVIII may result in development of CSVD-like pathology in terms of microvascular and neuroinflammatory alterations, and remodelling of perivascular, perineuronal and perisynaptic ECM.

Based on our observations, *Coll8a1*^{-/-} mice at 5 months of age exhibited an increased BBB permeability to mouse IgG in deep gray matter regions. There were noticeable accumulations of intravascular erythrocytes in capillaries and arterioles located in the cortex, hippocampus, and deep gray matter, though less so in white matter. As *Coll8a1*^{-/-} mice aged, BBB permeability heightened in cortical areas and the hippocampus by 12 months, yet the increase in intravascular erythrocyte accumulations seemed to plateau or even reduce in certain regions. This contrasts with the rising accumulation trend in *Coll8a*^{+/+} mice. Erythrocyte clustering seems to correspond with the noted upregulation of Vcam1, consistent with endostatin deficiency in *Coll8a1*^{-/-} mice. Subsequent qPCR analysis showcased significant alterations in the expression of BMs and components of tight

junctions. Glial cells in *Coll8a1*^{-/-} mice indicated signs of activation, including decreased branching, larger cell bodies, closer vicinity to impaired vessels, and a surge in GFAP levels within astrocytes. An in-depth look into ECM remodeling revealed that 36% of parvalbumin-expressing (PV+) interneurons in the CA1 region of *Coll8a1*^{-/-} mice were devoid of Aggrecan+ (Acan+) perineuronal nets (PNNs). Moreover, the average intensity of Acan expression dwindled in PV+ Acan+ cells. Conversely, there was a pronounced accumulation of Brevican (Bcan) in the neuropil of *Coll8a1*^{-/-} mice, especially around perisynaptic sites. This accumulation correlated with a rise in protein levels that stabilize lectican-hyaluronic acid interactions (*Hpln4*), proteins that cross-link lecticans (*Tnr*), and a decrease in presynaptic VGLUT1. Another contributing factor to the buildup of perisynaptic ECM was the increased expression of TIMP-3 in *Coll8a1*^{-/-} mice, which has been observed in the CADASIL variant of CSVD. Delving into the underlying pathways of these observations, I identified heightened signaling via the TGF- β 1/SMAD3/TIMP-3 cascade.

In essence, collagen XVIII is essential for maintaining the structural integrity of small vessels across the brain. Its absence results in small vessel impairment and pathological signs indicative of the early phases of CSVD, without evidence of hemorrhagic events or expansion of the perivascular area. This research also underscores a link between changes in perivascular ECM, extracellular proteolysis, and both perineuronal and perisynaptic ECM, suggesting these could be the foundational changes leading to synaptic and cognitive disturbances in CSVD.

Zusammenfassung

Die kollagenbasierte extrazelluläre Matrix bietet allen vielzelligen Tieren strukturelle und mechanische Unterstützung. Sie hat entscheidende Auswirkungen auf das Zellverhalten, wie Proliferation, Apoptose, Form, Migration und Differenzierung. Basalmembranen (BM) sind hochspezialisierte EZM-Strukturen, die die meisten Epithel- und Endothelzellschichten auskleiden. Neben ihren unterstützenden und trennenden Funktionen sind die BM und ihre Bestandteile an einer Vielzahl von biologischen Signalkaskaden, Entwicklungsprozessen und dem Fortschreiten von Krankheiten beteiligt. Kollagen XVIII ist einer der BM-Bestandteile, die im Laufe der Evolution stark konserviert wurden. Es handelt sich um ein Heparansulfat-Proteoglykan (HSPG) mit mehreren Domänen, das in drei gewebespezifischen Varianten exprimiert wird. Endostatin, die C-terminale (carboxyterminale) globuläre Domäne aller drei Kollagen XVIII-Varianten, hat antiangiogene Eigenschaften. Frühere Studien zu Kollagen IV, einem weiteren Hauptbestandteil der BM, zeigten pathologische Veränderungen der kleinen Arterien und Kapillaren in Mäusen mit Kollagen-IV-Mangel. Diese ähnelten den Veränderungen bei der zerebralen Erkrankung der kleinen Gefäße (*Cerebral Small Vessel Disease* CSVD), wie z. B. dem altersabhängigen Abbau der Blut-Hirn-Schranke (BHS) und dem Umbau der Gefäßwände, was sich in kleinen Gefäßverschlüssen und perivaskulären Blutungen manifestiert. CSVD ist eine der Hauptursachen für vaskuläre kognitive Beeinträchtigungen und trägt zu einem breiten Spektrum neurologischer Störungen bei, darunter Schlaganfall, leichte kognitive Beeinträchtigungen und Demenz.

Ein Hauptziel dieser Arbeit war es, zu untersuchen, ob die Entfernung von Kollagen-XVIII zur Entwicklung einer CSVD-ähnlichen Pathologie in Bezug auf mikrovaskuläre und neuroinflammatorische Veränderungen und die Umgestaltung der perivaskulären, perineuronalen und perisynaptischen EZM führen kann.

Unseren Ergebnissen zufolge wiesen 5 Monate alte *Coll18a1*-Knockout (*Coll18a1*^{-/-})-Mäuse eine erhöhte Durchlässigkeit der BHS für Maus-IgG in der tiefen grauen Substanz auf und es wurden intravaskuläre Erythrozytenansammlungen in Kapillaren und Arteriolen im Kortex, im Hippocampus und in der tiefen grauen Substanz beobachtet, wobei die Ansammlung in der weißen Substanz geringer war. Die Permeabilität der BHS nahm bei *Coll18a1*^{-/-}-Mäusen mit dem Alter zu und betraf kortikale Regionen und den Hippocampus bei 12 Monate alten Mäusen, während die

intravaskuläre Erythrozytenansammlung bei *Coll8a1*^{-/-}-Mäusen mit dem Alter nicht weiter anstieg (und in einigen Unterregionen sogar abnahm), im Gegensatz zu dem bei Wildtyp-Mäusen beobachteten Anstieg. Die Veränderungen in der Erythrozytenanhäufung scheinen die beobachtete Hochregulierung von *Vcam1* widerzuspiegeln, was mit dem Endostatinmangel bei *Coll8a1*^{-/-}-Mäusen in Einklang steht. Weitere qPCR-Analysen ergaben massive Veränderungen in der Expression von *BM* und *Tight-Junctions*-Komponenten. Die Gliazellen in *Coll8a1*^{-/-}-Mäusen zeigten Merkmale einer Aktivierung, nämlich eine geringere Verzweigung, vergrößerte Somata, eine größere Nähe zu geschädigten Gefäßen und erhöhte GFAP-Werte in Astrozyten. Bei einer detaillierten Untersuchung des EZM-Umbaus stellten wir fest, dass 36 % der Parvalbumin-exprimierenden (PV+) Interneuronen in der CA1-Region von *Coll8a1*^{-/-}-Mäusen keine Aggrecan⁺(-Acan⁺)-perineuronalen Netze (PNNs) aufweisen. Darüber hinaus war die durchschnittliche Intensität der Acan-Expression in PV⁺-Acan⁺-Zellen reduziert. Andererseits fanden wir bei *Coll8a1*^{-/-}-Mäusen eine erhöhte Akkumulation von Brevican (Bcan) im Neuropil im Allgemeinen und an perisynaptischen Stellen im Besonderen. Diese Hochregulierung war mit einer erhöhten Expression von Proteinen verbunden, die die Interaktion zwischen Lektikanen und Hyaluronsäure (*Hpln4*) stabilisieren, Lektikane vernetzen (*Tnr*) und präsynaptisches VGLUT1 herunterregulieren. Als zusätzlichen Faktor für die Anhäufung von perisynaptischer EZM fanden wir eine Hochregulierung von TIMP-3 in *Coll8a1*^{-/-}-Mäusen, die bei der zerebralen autosomal dominanten Arteriopathie mit subkortikalen Infarkten und Leukoenzephalopathie (CADASIL) gefunden wurde. Als Signalweg, der diesen Regulierungen zugrunde liegt, fand ich eine verstärkte Signalübertragung durch die TGF- β 1/SMAD3/TIMP-3-Kaskade.

Zusammenfassend lässt sich sagen, dass sich Kollagen XVIII als entscheidend für die strukturelle Integrität der kleinen Gefäße im gesamten Gehirn erwiesen hat. Sein Fehlen führt zu einer Schädigung der kleinen Gefäße und zu pathologischen Veränderungen, die typisch für frühe Stadien von CSVD sind, ohne dass es zu hämorrhagischen Veränderungen oder einer Erweiterung des perivaskulären Raums kommt. Darüber hinaus unterstreicht diese Studie einen Zusammenhang zwischen den Veränderungen der perivaskulären EZM, der extrazellulären Proteolyse und der perineuronalen/perisynaptischen EZM als möglichem Substrat für synaptische und kognitive Veränderungen bei CSVD.

Table of Contents

1	INTRODUCTION	10
1.1	CEREBRAL SMALL VESSEL DISEASE	10
1.1.1	<i>Small vessel disease: definition and classification</i>	10
1.1.2	<i>The pathogenesis of cerebral small vessel disease</i>	11
1.1.3	<i>Classification of CSVD</i>	13
1.1.4	<i>Dynamic pathological processes of CSVD</i>	16
1.1.5	<i>Experimental animal model for CSVD</i>	18
1.1.6	<i>Neurovascular unit</i>	19
1.1.7	<i>Inflammation in CSVD</i>	26
1.1.8	<i>MMP-induced disruption of the blood-brain barrier</i>	26
1.2	EXTRACELLULAR MATRIX (ECM)	27
1.2.1	<i>Perineuronal nets</i>	28
1.3	PERIVASCULAR ECM	29
1.3.1	<i>Interstitial matrix</i>	30
1.4	CEREBRAL SMALL VESSEL DISEASE AND ECM	34
1.5	BIPHASIC ECM REGULATION IN DIFFERENT CNS DISORDERS	35
1.6	ECM TURNOVER	37
1.7	TRANSLATION OF THE TWO-PHASE ECM DYSREGULATION MODEL INTO CLINICAL RESEARCH	38
1.8	COLLAGEN SUPERFAMILY	42
1.8.1	<i>Collagen XVIII</i>	42
2	AIMS AND OBJECTIVES	46
3	MATERIAL AND METHODS	47
3.1	GENE TARGETING AND GENERATION OF MUTANT MICE	47
3.2	TISSUE COLLECTION	47
3.2.1	<i>Tissue preparation for hematoxylin and eosin staining and immunohistochemistry</i>	47
3.2.2	<i>Tissue preparation for qPCR and western blot</i>	48
3.3	HISTOLOGY	48
3.4	QUANTIFICATION	49
3.5	RNA EXTRACTION, cDNA CONVERSION, AND qPCR	49
3.6	SDS-PAGE AND WESTERN BLOT ANALYSIS	52
3.7	IMMUNOHISTOCHEMISTRY	54
3.8	IMAGE ACQUISITION AND HISTOCHEMICAL MEASUREMENTS	56
3.9	DETECTION AND QUANTIFICATION OF IgG LEAKAGE AS AN INDICATOR OF BBB BREAKDOWN	56
3.10	VESSEL-ASSOCIATED MICROGLIA/PERIVASCULAR MACROPHAGES	56
3.11	MICROGLIA AND C1Q ANALYSES	57
3.12	ASTROGLIA ANALYSIS	58
3.13	NEURAL ECM ANALYSIS	58
3.14	PRESYNAPTIC AND SYNAPTIC SCAFFOLD PROTEIN ANALYSIS	59
3.15	ANALYSIS OF VGLUT1 ⁺ PUNCTA AND PERISYNAPTIC BREVICAN	60
3.16	DATA ANALYSIS AND STATISTICS	61
4	RESULT	62
4.1	ERYTHROCYTE AGGREGATIONS, MICROBLEEDS, AND PERIVASCULAR SPACE IN YOUNG AND AGED <i>COL18A1</i> ^{-/-} MICE	62
4.2	KNOCKOUT OF COL18A1 INCREASES BBB LEAKAGE IN YOUNG AND AGED MICE	65
4.3	BASMENT MEMBRANE REMODELING, ENDOTHELIAL CELLS AND PERICYTES ACTIVATION IN <i>COL18A1</i> ^{-/-} MICE	67

4.4	MICROGLIAL RECRUITMENT TO CEREBRAL SMALL BLOOD VESSELS IN <i>Col18A1</i> ^{-/-} MICE.....	68
4.5	ACTIVATION OF MICROGLIA IN <i>COL18A1</i> ^{-/-} MICE	70
4.6	ACTIVATION OF ASTROGLIA IN <i>COL18A1</i> ^{-/-} MICE	72
4.7	ACTIVATION OF PERICYTES IN <i>COL18A1</i> ^{-/-} MICE	73
4.8	REDUCED EXPRESSION OF PARVALBUMIN AND PERINEURONAL NETS IN <i>COL18A1</i> ^{-/-} MICE	74
4.9	ALTERATIONS IN GLUTAMATERGIC SYNAPSES IN <i>COL18A1</i> ^{-/-} MICE	76
4.10	UPREGULATION OF PERISYNAPTIC ECM PROTEOGLYCAN BCAN AND DOWNREGULATION OF PRESYNAPTIC VGLUT1 IN <i>COL18A1</i> ^{-/-} MICE.....	78
4.11	EVALUATION OF GENE EXPRESSION OF CSPGS, ENZYMES REGULATING THEIR PROTEOLYSIS AND TGF β 1/SMAD3/TIMP-3 SIGNALLING IN <i>COL18A1</i> ^{-/-} MICE.....	80
5	DISCUSSION	82
5.1	COLLAGEN XVIII DEFICIENCY AND MICROVASCULAR PATHOLOGY.....	84
5.2	COLLAGEN XVIII DEFICIENCY AND ACTIVATION OF GLIAL CELLS.....	85
5.3	COL18A1 KNOCKOUT AND REMODELING OF PERINEURONAL AND PERISYNAPTIC ECM.....	87
5.4	COL18A1 KNOCKOUT AND DEFECTS IN GLUTAMATERGIC SYNAPSES.....	88
5.5	TGF- β 1/SMAD3/TIMP-3 SIGNALLING PLAY A ROLE IN <i>COL18A1</i> ^{-/-} MICE ECM ALTRATIONS.....	89
6	CONCLUSIONS.....	91
7	FUTURE DIRECTIONS	92
8	REFERENCES.....	94
9	APPENDIX	113

List of abbreviations

Abbreviation	Full name
Acan, Acan	Aggrecan
AD	Alzheimer's disease
Aqp4	Aquaporin 4
BBB	Blood-brain barrier
BMs	Basement membranes
Bcan, Bcan	Brevican
BG	Basal ganglia
C1q	Complement component 1q
CADASIL	Cerebral Autosomal Dominant Arteriopathy with Subcortical Infarcts and Leukoencephalopathy
CMBs	Cerebral microbleeds
CC	Corpus callosum
Ccl2	Chemokine(C-C motif)ligand 2
CAA	Cerebral amyloid angiopathy
Cd86	Cluster of Differentiation 86
Cldn5	Claudin 5
CNS	Central nervous system
CSPG	Chondroitin sulfate proteoglycan
Cspg4	Chondroitin sulfate proteoglycan 4
CSVD	Cerebral small vessel disease
ECM	Extracellular matrix
FOV	Field of view
GfaP,GFAP	Glial Fibrillary acidic protein
GWAS	Genome-wide association studies
Homer 1	Homer protein homolog 1
Hpln1,2,3,4	Hyaluronan and proteoglycan link protein 1,2,3,4
Iba1,Iba1	Allograft inflammatory factor 1
IHC	Immunohistochemistry
Il1b	Interleukin 1 beta
Il6	Interleukin 6
ICH	intracerebral haemorrhage
IL33	Interleukin 33
Lama5	Laminin 5
Loxl2	Lysyl oxidase homolog 2
MRI	Magnetic resonance imaging
MMP	Matrix metalloproteinase
Mpo	Myeloperoxidase
Ncan	Neurocan
NVU	Neurovascular unit
Nid1	Nidogen 1
Ocln	Occludin
OPCs	Oligodendrocyte precursor cells
PBS	Phosphate-buffered saline
Pcan	Phosphacan
Pdgfrb	Platelet derived growth factor receptor, beta polypeptide
PNN	Perineuronal net
PV	Parvalbumin
PVS	Perivascular space

Plp1	Proteolipid protein 1
ROI	Region of interest
RT-qPCR	Reverse transcription-polymerase chain reaction
RSC	Retrosplenial cortex
TIMP	Tissue inhibitor of metalloproteinases
TJ	Tight junction
S100a10	S100 calcium-binding protein A10
SHRSP	Spontaneously hypertensive stroke-prone rat
Tnr	Tenascin-R
Tnfa	Tumor necrosis factor-alfa
Vcam1	Vascular cell adhesion protein 1
Vcan	Versican
VGLUT1,2	Vesicular glutamate transporter 1,2
VGAT	Vesicular GABA transporter
WFA	<i>Wisteria floribunda</i> agglutinin
WMH	White matter hyperintensities
WML	White matter lesions
Zo1	Zonula occludens-1

1 Introduction

1.1 Cerebral small vessel disease

1.1.1 Small vessel disease: definition and classification

The concept of small vessel disease (SVD) encompasses a range of medical conditions in which small blood vessels play a central role. This spectrum includes conditions such as coronary microvasculature disease (CMD), coronary artery disease (CAD), small vasculature vasculitis, and notably, cerebral small vessel disease. Much of the research centered on small vessel disease has honed in on cerebral variants, like Cerebral Autosomal Dominant Arteriopathy with Subcortical Infarcts and Leukoencephalopathy (CADASIL). Indeed, CSVD has often been associated with vascular dementia, accounting for nearly 45% of all dementia diagnoses (Inzitari, Pracucci et al. 2009).

The primary repercussions of these processes within the brain tissue are primarily lesions found in the subcortical regions. These encompass lacunar infarcts, white matter abnormalities (WML, also known as leukoaraiosis), intracerebral hemorrhages (ICHs), and cerebral microbleeds (CMBs). Given that small vessels aren't readily visible *in vivo*, these tissue abnormalities serve as indicative markers of the foundational processes, leading to the broader adoption of the term 'small vessel disease' to characterize these lesions. With the aid of neuroimaging, these abnormalities have been identified and extensively examined (Doubal, MacLulich et al. 2010, Cordonnier and van der Flier 2011). From a clinical standpoint, small vessel diseases manifest in various ways, predominantly contributing to cognitive decline and functional challenges in older individuals. They remain a significant focus for preventative and therapeutic measures and warrant attention in clinical assessments and therapeutic research.

Cerebral small vessel disease pertains to a cluster of pathological changes impacting the smaller arteries, arterioles, venules, and brain capillaries. Two primary processes are recognized: (1) age-driven and hypertension-linked arteriopathy targeting deep perforating vessels, and (2) cerebral amyloid angiopathy (CAA), which primarily affects the cortical and leptomeningeal vessels.

In terms of anatomy, cerebral arterial vessels originate from two main sources. Superficially, they branch out from the subarachnoid circulation, evolving as the end vessels from mid-sized cortical and leptomeningeal arteries, which themselves emerge from more substantial vessels. At the brain's base, these vessels spring directly from larger arteries as small arterial perforators or lenticulostriate arteries. These systems unite and traverse through cortical layers and deep grey structures, combining in the subcortical white matter's deepest regions, forming a 'borderzone' or watershed zone.

A comprehensive grasp of the underlying disease physiology is imperative for understanding its main causes, significant risk factors, and potential treatment avenues. CSVD's pathophysiology is characterized by vessel wall thickening, increased rigidity, damage, constriction of the vessel interior, diminished perfusion, and compromised vasoreactivity and self-regulation, potentially leading to vessel blockage, leakage, or rupture within the brain (Wardlaw, Smith et al. 2013). Another hallmark of CSVD is brain atrophy, which might also manifest indirectly due to vascular anomalies (Duering, Righart et al. 2012).

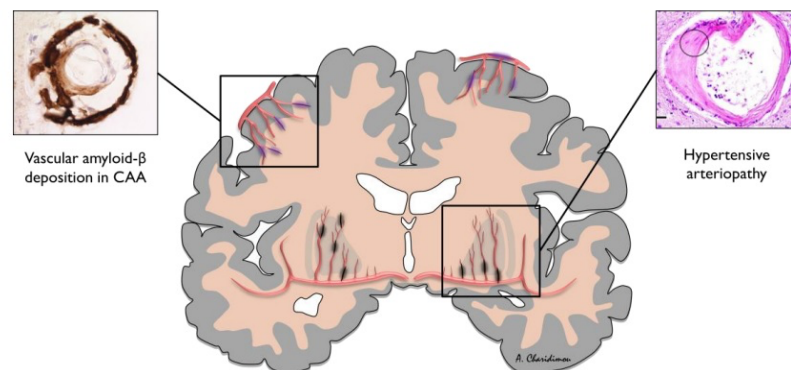


Figure 1.1 Common subtypes of small vessel disease (adapted from (Wilson, Charidimou et al. 2014)).

1.1.2 The pathogenesis of cerebral small vessel disease

Hypertension and CAA are the predominant causes of CSVD (Pantoni 2010). While hypertension results in arteriopathy mainly impacting the small end-arteries in deeper regions of the brain, CAA is distinguished by the accumulation of amyloid beta ($A\beta$) in cortical arteries (Woo, Sauerbeck et al. 2002, Vernooij, van der Lugt et al. 2008, Greenberg, Vernooij et al. 2009, Charidimou, Boulouis

et al. 2017). Corresponding to the location of these pathological occurrences, hypertensive arteriopathy frequently corresponds with microbleeds in the deeper sections of the brain, such as the basal ganglia, thalamus, and brainstem. On the other hand, CAA tends to produce (micro)bleeds with a lobar distribution. Beyond hypertension, age and vascular risk factors are other significant contributors to SVD. These vascular risk factors have been linked to cognitive deterioration and dementia (Breteler 2000, Launer 2002). Conditions and habits such as diabetes mellitus, high cholesterol levels, obesity, smoking, sedentary lifestyle, and hypertension have all been connected to an elevated likelihood of cognitive issues and dementia.

A summary of potential microcirculation pathogenesis mechanisms associated with CSVD is shown in **Table 1.1**. The analyses of molecular damage, organelle dysfunction, and cell injury in the components of the NVU and BBB, blood-cerebrospinal fluid barrier, CBF, as well as alterations in the glymphatic system have contributed significantly to the understanding of the pathophysiologic mechanism and cognitive impairment associated with CSVD. An upcoming sections will provide detailed information regarding the classification and dynamic pathological processes of CSVD, as well as the NVU components and BBB functions in the context of CSVD.

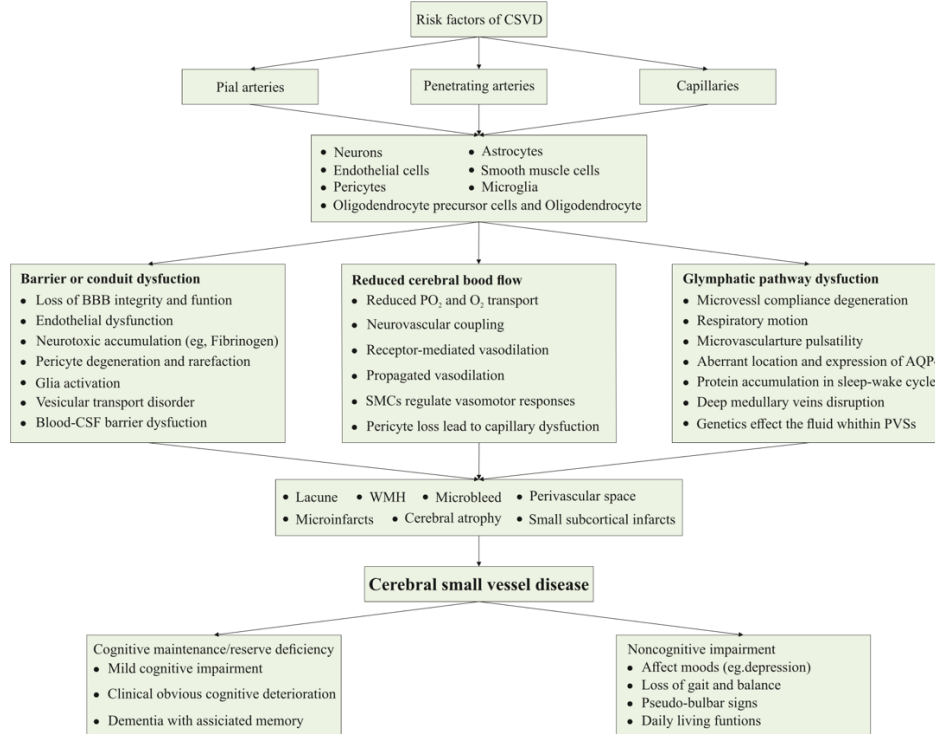


Table 1.1 Pathogenesis of cerebral small vessel disease. Schematic summarizing potential pathogenesis mechanisms of microcirculation associated with CSVD. BBB dysfunction, reductions in CBF and clearance pathway dysfunction mediated by NVU components lead to CSVD-related cognitive impairment, including the neuroimaging alternations. Adapted from (Yang, Wei et al. 2022).

1.1.3 Classification of CSVD

Several classifications exist regarding the etiopathogenesis of CSVD. The most frequently observed types include amyloidal CSVD (which can be either sporadic or hereditary, known as cerebral amyloid angiopathy [CAA]) and non-amyloidal CSVD (which arises due to age-related factors and arteriosclerosis associated with vascular risks) (Pantoni 2010). Additionally, there are rarer variants of CSVD. These encompass inherited or genetic types that are separate from CAA (like Fabry's disease and CADASIL), as well as inflammatory and immune-mediated CSVD, venous collagenosis, and other forms of CSVD (examples being non-amyloid microvessel degeneration in AD and the effects of radiation-induced angiopathy). CSVD can be divided into two main groups based on the etiology of the disease, which is described in **Table 1.2** according to its clinical and neuroimaging characteristics.

1.1.3.1 Arteriolosclerosis

Arteriolosclerosis is the most common form of CSVD, which is caused by ageing and other vascular risk factors, those being diabetes and hypertension being the most prominent. There are some pathological findings that are associated with arteriolosclerosis, including degeneration of smooth muscle cells in the tunica media, a deposition of fibrohyaline substance, and a loss of elasticity in the vessels, thickening of the vessel walls, as well as a possibility of narrowing of the vessel lumen (Pantoni 2010).

Hypertensive small vessel disease impacts various vascular structures, including arteries, arterioles, and capillaries. Two primary forms of vasculopathy arise from the vascular alterations induced by hypertension: (1) arteriosclerosis and (2) atherosclerosis. Often, these processes coexist. The first refers to a widespread stiffening of the arterial vessel wall, commonly known as fibrohyalinosis; the latter represents a subtype of arteriosclerosis where lipid deposits, or atheromas, accumulate in the endothelium. In theory, hypertension can cause the arteries' autoregulation mechanisms to falter due to the forced expansion of resistance vessels. Consequently, smaller arteries and capillaries face unchecked high blood pressure, leading to breaches in the blood-brain barrier and subsequent vasogenic edema.

1.1.3.1.1 Monogenic SVD (CADASIL)

Inherited variants of arteriolosclerosis are increasingly coming to the fore. CADASIL stands out as the predominant hereditary factor linked to strokes and cognitive decline, thereby serving as an essential model for understanding the broader and more frequent sporadic versions of CSVD (Herve and Chabriat 2010). While there exist parallels between sporadic CSVD and CADASIL, the latter manifests more acutely and at an earlier age (Charlton, Morris et al. 2006, Herve and Chabriat 2010). CADASIL is a genetic disorder transmitted in an autosomal dominant manner due to mutations in the NOTCH3 gene, which produces a transmembrane receptor protein (Joutel, Corpechot et al. 1996). This NOTCH3 gene primarily finds expression in vascular smooth muscle cells and is essential for the health and functionality of small vessels (Joutel, Corpechot et al. 1996, Joutel, Andreux et al. 2000).

Individuals diagnosed with CADASIL show evident arterial wall thickening, an accumulation of a distinct non-amyloid granular osmiophilic substance, and a degeneration of vascular smooth muscle cells, all indicative of the disease's arteriopathy (Chabriat, Joutel et al. 2009). Clinical manifestations of CADASIL include strokes and dementia, accompanied by a unique spread of white matter hyperintensities on brain scans, especially prominent in the anterior regions of the temporal lobes (O'Sullivan, Jarosz et al. 2001).

1.1.3.1.2 Cerebral amyloid angiopathy (CAA)

CAA is a prevalent age-associated small vessel condition that poses a significant risk for intracerebral haemorrhage (ICH) and cognitive decline (Viswanathan and Greenberg 2011). Essentially, CAA pertains to a spectrum of cerebral vascular disorders arising from the accumulation of amyloid fibrils within the walls of small to medium-sized cerebral vessels, as well as within the brain's leptomeninges and parenchyma (Revesz, Holton et al. 2009). Intriguingly, there's a frequent overlap between CAA and Alzheimer's disease (Kalaria and Ballard 1999). A distinguishing feature of the disease is the buildup of amyloid beta protein within the walls of leptomeningeal and cortical arteries and arterioles, making them more susceptible to fragility, breakage, and subsequent hemorrhage (Vinters 1987). CAA predominantly affects the white matter in regions like the occipital and frontal lobes. While it is distinct from systemic amyloidosis, CAA is notably prevalent among individuals in their middle age and seniors, with instances in individuals above 55 reaching between 10–40% (Banerjee, Carare et al. 2017).

Moreover, the accumulation of amyloid beta can modify the resilience of the vascular walls, leading to diminished cerebrovascular reactivity and resulting in hypoperfusion. Despite the primary research attention being on the more recurrent haemorrhagic outcomes of the condition, ischemic alterations have also been noted in CAA sufferers, and they hold clinical significance (Reijmer, Van Veluw et al. 2016).

Classification	Characteristics	Pathology	Neuroimaging features	Clinical syndromes
Form 1	<ul style="list-style-type: none"> • Non-amyloid CSVD • Arteriosclerosis (age-related and vascular risk-factor-related small vessel diseases) • Advances with age • Degenerative microangiopathy 	<ul style="list-style-type: none"> • Loss of smooth muscle cells from the tunica media (i.e., arteriosclerosis) • Deposit of fibro-hyaline material (i.e., lipohyalinosis) • Narrowing of lumen (i.e., microatheroma) • Thickening of vessel wall (i.e., microaneurysms) • Segmental arterial disorganization 	<ul style="list-style-type: none"> • Deep cerebral microbleeds • Rare cortical superficial siderosis • Basal ganglia perivascular space • Non-specific cerebral region of WMHs 	<ul style="list-style-type: none"> • Lacunar strokes • Often deep (basal ganglia, thalamus, pons, cerebellum ICH) • Cognitive impairment and dementia
Form 2	<ul style="list-style-type: none"> • Amyloid CSVD • Sporadic and hereditary CAA • Advances with age 	<ul style="list-style-type: none"> • Accumulation of amyloid-β (Aβ) in the cortical walls (type 1) and leptomeningeal small arteries, but not capillaries (type 2) due to vascular occlusion and rupture • Vasculopathy (i.e., fibrinoid necrosis, loss of smooth muscle cells, wall thickening, perivascular blood breakdown, and microaneurysm) • APOE gene polymorphism (i.e., APOE ϵ2 and APOE ϵ4 allele related to types 2 and 1, respectively) 	<ul style="list-style-type: none"> • Lobar cerebral microbleeds • Most significant feature (marker of CAA): cortical superficial siderosis • Centrum semiovale perivascular space • Posterior dominance WMHs 	<ul style="list-style-type: none"> • Lobar ICH • Non-lacunar strokes • Transient focal neurological episodes, cognitive impairment, and dementia • Hallmarks of AD

AD, Alzheimer's disease; APOE, apolipoprotein E; CAA, cerebral amyloid angiopathy; CSVD, cerebral small vessel disease; ICH, intracerebral hemorrhage; WMHs, white matter hyperintensities.

Table 1.2 Etiopathogenic classification based on clinical and neuroimaging characteristic differences in two major classes of CSVD (adapted from (Mustapha, Nassir et al. 2019)).

1.1.4 Dynamic pathological processes of CSVD

Generally speaking, the various pathological changes that resulted from CSVD not only caused damage to the cerebral parenchyma, which included axonal injury, neuronal apoptosis, demyelination, and oligodendrocytes, but also caused neurological symptoms and signs, as well as different neurological findings on neuroimaging (Li, Yang et al. 2018).

Even with the increasing volume of histopathological, epidemiological, and physiological research on CSVD, the fundamental mechanisms driving it continue to be a matter of debate. There's mounting data suggesting that factors like advanced age and chronic hypertension could weaken the capacity to self-adjust cerebral blood flow according to variations in blood pressure and arterial rigidity, leading to heightened speed and pulsatility in cerebral arterioles (Cuadrado-Godia, Dwivedi et al. 2018). Elevated shear stress brought on by these hemodynamic shifts might result in damage to the BBB's endothelial lining and changes to its permeability (Zhang, Wong et al.

2017). As such, a compromised BBB is believed to be a central characteristic of CSVD (Huisa, Caprihan et al. 2015, Wardlaw, Makin et al. 2017).

Endothelial dysfunction is also considered a pivotal contributor to the development of CSVD, as highlighted by increased biomarker levels. Beyond the endothelium, interactions between various BBB cellular components like pericytes, astrocytes, and oligodendrocyte precursor cells (OPCs) - collectively referred to as the neurovascular unit - might be implicated in microvascular harm, setting the stage for the initiation and advancement of CSVD (Ihara and Yamamoto 2016, Rajani and Williams 2017).

In connection, diminished integrity of the white matter attributed to oligodendrocyte alterations has been identified in CSVD cases. The signaling between endothelial cells (EC) and OPCs becomes disrupted, affecting the ECs' capacity to release essential factors for OPC growth and resilience, making oligodendrocytes more vulnerable (Rajashekhar, Willuweit et al. 2006). As a result, the intricate interplay among multiple BBB constituents could be pivotal for devising new preventative measures and treatments for CSVD.

1.1.4.1 Endothelial cell activation

Endothelial cells line all of the blood vessels throughout the body. There is a particular role played by endothelial cells in the brain, specifically in the BBB, in regulating the flow of cerebral blood, and in interacting with other members of the neurovascular unit. In SVD, endothelial cells are seen to survive in histological studies, even in late stages of sporadic SVD (Alistair 2002) and in CADASIL (Craggs, Hagel et al. 2013). Despite their survival, many functional studies have shown that the endothelial cells are activated, and therefore are thought to be in a state of inflammation, growth, and thrombosis as a result (Hainsworth, Oommen et al. 2015).

There is a change in the expression of surface markers on the endothelium when endothelial cells are activated. Blood biomarkers of endothelial cell activation have been widely studied in SVD and recently reviewed (Poggesi, Pasi et al. 2016). These circulating markers include, but are not limited to, intracellular adhesion molecule-1 (ICAM-1), vascular cellular adhesion molecule-1 (VCAM-1), E-selectin and P-selectin. In patients with lacunar infarcts, ICAM-1 and VCAM-1 levels are elevated compared to levels in controls (Rouhl, Damoiseaux et al. 2012). WMLs have

been associated with higher levels of ICAM-1, VCAM-1, E-selectin and P-selectin (Fassbender, Bertsch et al. 1999).

1.1.5 Experimental animal model for CSVD

It has also been noted that animal models of SVD have been used to try and uncover the pathology of SVD. There are several reasons why animal models are important for the discovery of early stage pathology in SVD, including whether endothelial cell dysfunction may be an initiating mechanism for the disease (Hainsworth and Markus 2008).

To gain deeper insights into the evolution and advancement of CSVD, researchers are turning more frequently to animal models. These models encompass rodents like rats and mice, as well as larger animals including rabbits and non-human primates. It is possible to evaluate the pathological processes of CSVD using animal models, for example, lesions in the white matter caused by ischemic white matter lesions and endothelial dysfunction caused by reduced BBB integrity. There have been several approaches and animal models identified to mimic the arterial lesion of CSVD, such as lacunar infarctions and WMHs, as well as brain injury related to CSVD.

The most common animal models used are the stroke prone spontaneously hypertensive rats (SHRSP) and the spontaneously hypertensive rats (SHR), derived from selective breeding. These rats show similar degrees of hypertension, SVD-like vessel pathology, focal infarcts, cognitive impairment and WM damage, although this varies between the models (Lin, Tomimoto et al. 2001). Since current animal models of SVD do not completely replicate the pathology seen in human SVD, results should always be interpreted with caution.

It has been shown that SHRSP and SHR rats have endothelial dysfunction, which manifests as BBB impairment histopathologically (Sadoshima and Heistad 1982, Lee, Zhai et al. 2007) and on imaging (Guerrini, Sironi et al. 2002, Sironi, Guerrini et al. 2004). Endothelial tight junction damage occurs in these rats at the earliest ages, preceding other damage (Bailey, Wardlaw et al. 2011), and treatments with endothelial cell stabilising drugs can prevent symptoms (Rajani, Quick et al. 2018); see **Table 1.3**.

Aspects of CSVD	Approaches
Hypoperfusion/ischemic injury	<ul style="list-style-type: none"> ● BCCAO and stenosis striatal ● Endothelin-1 injection ● Striatal mitotoxin 3-NPA
Hypertension-based injuries	<ul style="list-style-type: none"> ● SHRSP ● Surgical narrowing of the aorta ● Genetic mutations, usually in the renin–angiotensin system
Blood vessel damage	<ul style="list-style-type: none"> ● Injected proteases ● Endothelium targeting viral infection ● Genetic mutations affecting vessel walls

BCCAO, bilateral common carotid artery occlusion; CSVD, cerebral small vessel disease; NPA, nitropropionic acid; SHRSP, stroke-prone spontaneously hypertensive rats.

Table 1.3 Different approaches used in animal models to reflect certain aspects of CSVD (adapted from (Mustapha, Nassir et al. 2019)).

1.1.6 Neurovascular unit

The neurovascular unit (NVU) encompasses a collection of brain tissue components which include endothelial cells, pericytes, astrocytes, microglia, oligodendrocytes, neurons, and elements of the extracellular matrix forming the basement membrane (Muioio, Persson et al. 2014). At the heart of the NVU, "neurovascular coupling" describes the intricate relationship between neurons and their corresponding vascular networks, ensuring the necessary nutrient supply for optimal neuronal activities. The uninterrupted flow of blood is vital for the brain. Maintaining a robust connection between neurons and their vascular supply is essential for effectively moderating signals that dictate vascular alterations. Dysfunctions within the NVU can result in discrepancies in the metabolic needs of tissue components, a condition observed in various ailments including hypertension, Alzheimer's disease, and ischemic stroke (Girouard and Iadecola 2006).

While the blood-brain barrier (BBB) primarily acts as a protective barrier in brain capillaries, thanks to the tight junctions (TJ) amongst endothelial cells, it's imperative to recognize that surrounding cells in close proximity to these endothelial cells are instrumental in both establishing and preserving the integrity of the BBB. These include neurons, astrocytes, pericytes, basal lamina

and extracellular matrix (ECM); all collectively referred to as the “neurovascular unit” (NVU); see **Figure 1.2**.

In recent years, there has been significant progress in the understanding of the dynamic signalling that occurs between vascular endothelial cells and other cells of the NVU. Research on the BBB must take into account these interactions in order to fully comprehend BBB regulation.

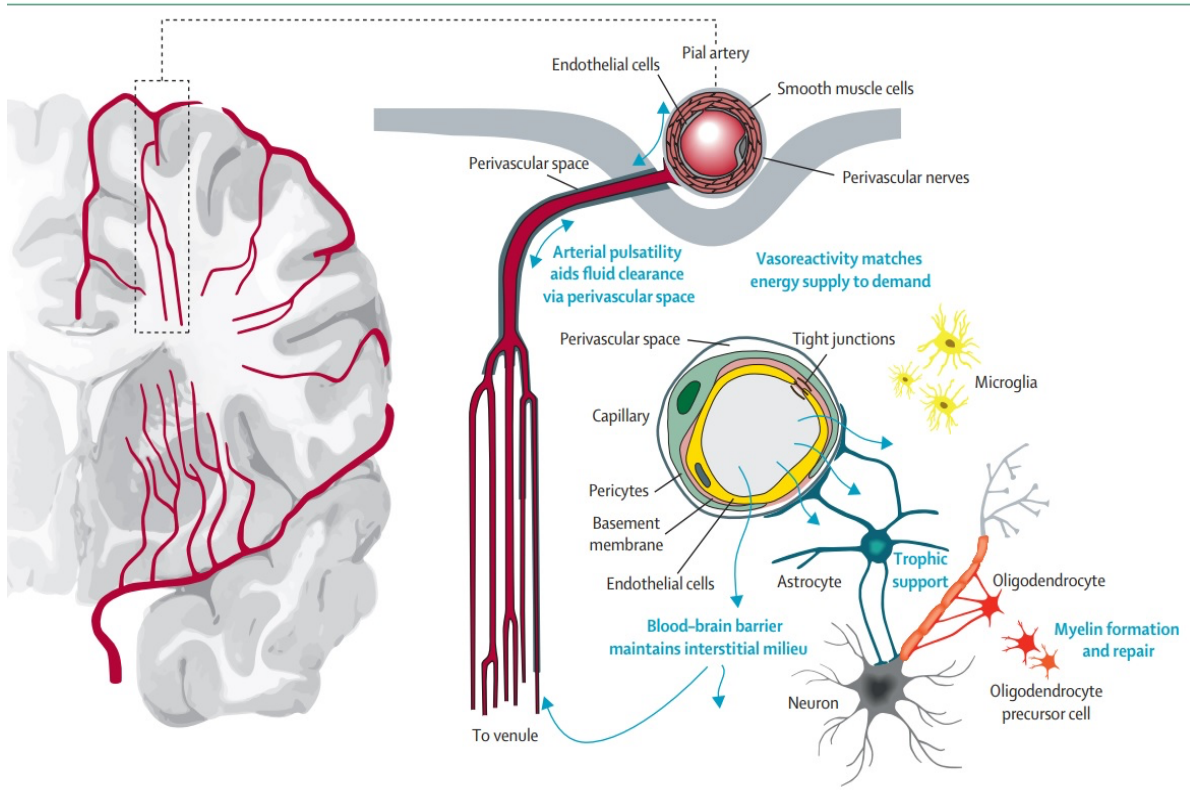


Figure 1.2 Key constituents of the vascular-glio-neuronal unit and possible entry points for disease mechanisms in cerebral small vessel disease (adapted from (Wardlaw, Smith et al. 2019)).

Brain arterioles extend and differentiate into capillaries, each encompassed by a perivascular space that links to the CSF. The combination of capillary endothelial cells, their associated tight junctions, a specialized basement membrane, pericytes, and the foot processes of astrocytes constitute the blood-brain barrier. This barrier is crucial for stabilizing the interstitial environment. Astrocytes regulate the balance of interstitial fluids, supply energy to neurons, and mediate signals between neurons and other cells, aligning blood flow with energy needs. Oligodendrocytes are

responsible for creating and mending myelin sheaths around axons and offer metabolic and trophic support.

At the cellular tier, issues with endothelial cells and blood-brain barrier functioning can escalate interstitial fluid and proteins, disrupt the connectivity of astrocyte end-feet (affecting interstitial fluid exchange), hinder the maturation of oligodendrocyte precursor cells (impacting myelination, repair, and axonal energy support), and obstruct normal astrocyte functions, thereby reducing the energy provided to neurons. The sequence in which these occurrences unfold remains under study. Multiple cellular and functional components of the vasculo-glio-neuronal unit—including endothelial cells, pericytes, astrocytes, oligodendrocytes, neurons, and the extracellular matrix—may serve as potential avenues for disease processes in the NVU associated with small vessel disease. Vascular (endothelial cells and pericytes) and brain (astrocytes, oligodendrocytes, and neurons) cells interact and function as a unit, millions of which reside in the brain (Gao, Li et al. 2022); see **Figure 1.3**.

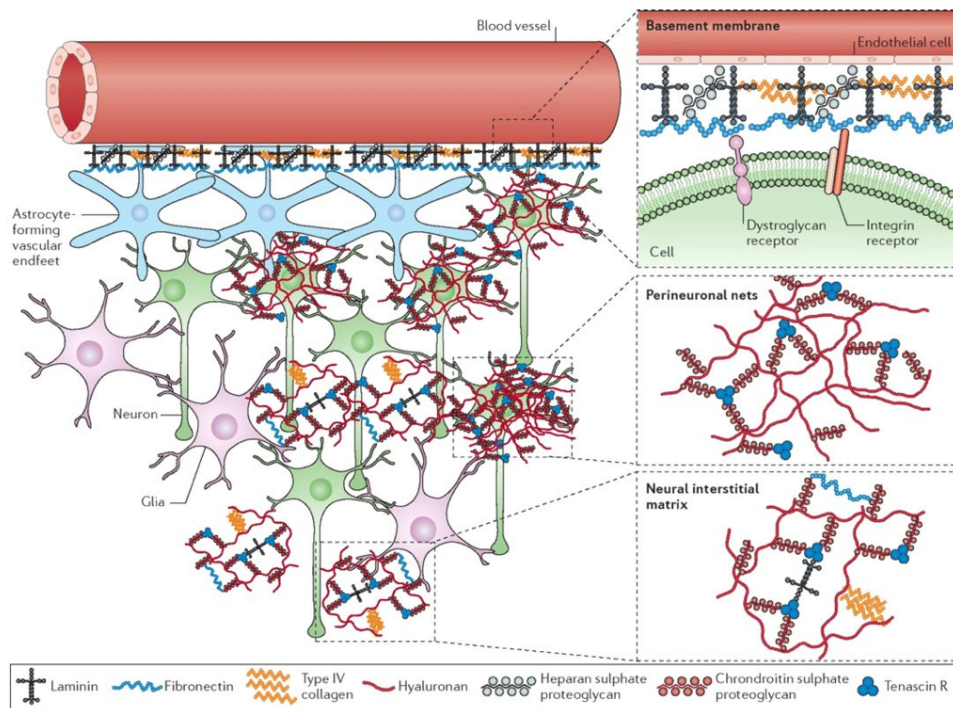


Figure 1.3 A schematic of a brain microvessel and the surrounding ECM composed by laminin, fibronectin, type IV collagen, hyaluronan, heparan sulphate proteoglycan, chondroitin sulphate proteoglycan and tenascin R, embedding astrocytes neuron and gli (left) with a close up showing a detailed view illustrating cellular attachment, perineuronal networks and the neural interstitial matrix (right) (adapted from (Lau, Cua et al. 2013)).

1.1.6.1 The blood brain barrier

A crucial component of the neurovascular unit is the blood-brain barrier (BBB). A structurally organized endothelial lining exists in the brain tissue, interacting in concert with pericytes, astrocytes, and the basement membrane in order to shield the parenchymal brain tissue from toxins and pathogens while allowing nutrients and providing the necessary chemical composition for the proper functioning of glia and neurons (Bell and Zlokovic 2009, Abbott, Patabendige et al. 2010). BBB regulates oxygen delivery and nutrient absorption, metabolic waste removal, and signaling between the endocrine glands (Cines, Pollak et al. 1998). It is widely known that the BBB properties exhibited by brain endothelial cells are predominantly controlled by tight junctions, junctional adhesion molecules that are arranged in a polarized manner between adjacent brain endothelial cells in the BBB.

1.1.6.1.1 Molecular pathways that dysregulate tight junction proteins

The tight junction proteins of the BBB are not simply static proteins; instead, they are highly dynamic structures having the ability to assemble and disassemble in response to the local microenvironment in which they are found (Deli 2009).

Claudin and occludin are the most apically located proteins on endothelial cells and the barrier function of the BBB is primarily attributed to their physical presence and correct signalling regulation (Abbott, Patabendige et al. 2010).

Claudins stand out as the primary proteins in tight junctions that signify the maturation of the BBB (Morita, Sasaki et al. 1999, Liebner, Fischmann et al. 2000). Acting as tetraspan transmembrane proteins, they play a pivotal role in establishing the BBB, ensuring the preservation of the barrier's continuity between neighboring endothelial cells (Günzel and Yu 2013). The tight junctions (claudins and occludin) are anchored to the actin cytoskeleton by Zonula occludens. In particular, Zonula occludens-1 (ZO-1) functions like a membrane-associated granulate kinase. The role of ZO-1 is critical in stabilizing tight junctions in such a way that if the gene is deleted, there will be an increase in permeability because the tight junction will be disrupted and myosin II will be redistributed among the active sites (Tornavaca, Chia et al. 2015). In general, the tight junctions at the BBB regulate the influx and efflux of biological molecules. Junctional adhesion molecules (JAM) isoforms regulate paracellular permeability at the BBB, particularly with respect to immune

cells like neurophils, monocytes/ macrophages (Sladojevic, Stamatovic et al. 2014). Loss of JAM protein expression and/or migration of JAM proteins away from the tight junction directly leads to loss of BBB properties at the microvascular endothelium (Haarmann, Deiss et al. 2010); see **Figure 1.4**.

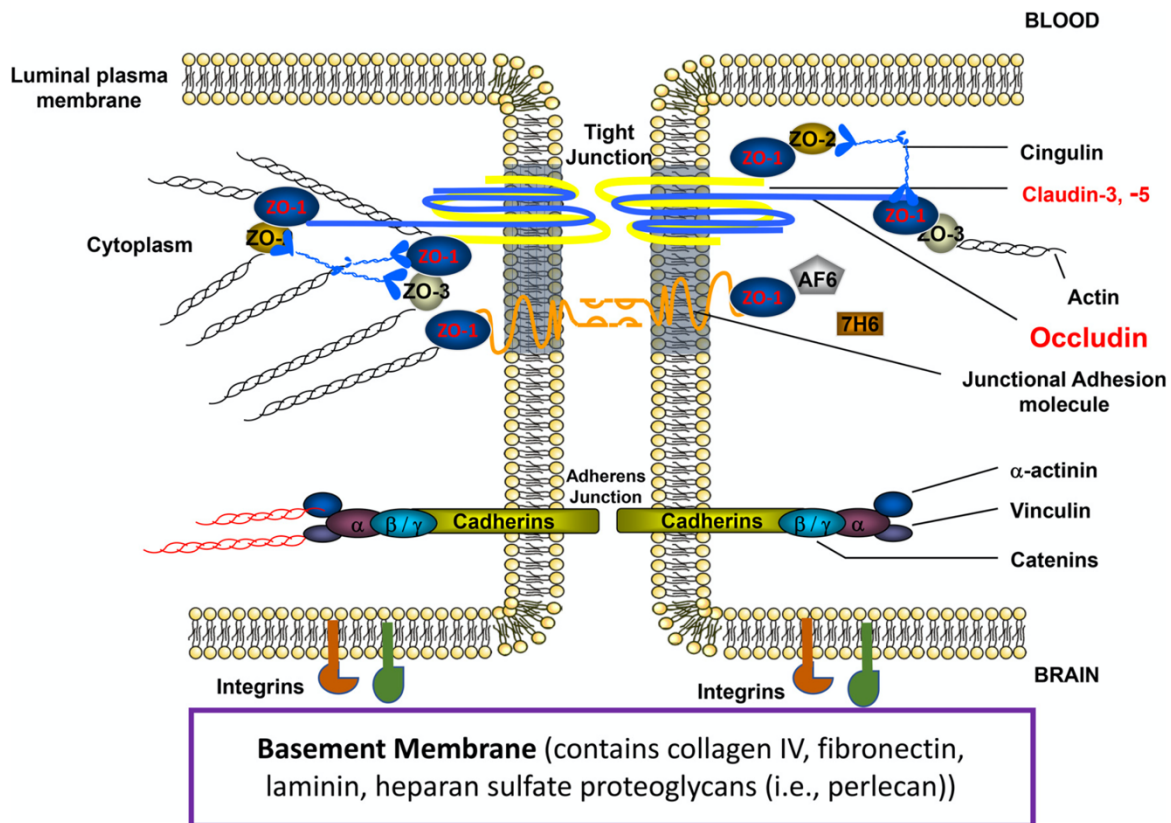


Figure 1.4 Molecular organization of tight junction protein complexes at the mammalian blood-brain barrier. Following onset of ischemic stroke, tight junction protein complexes are disrupted, which leads to breakdown of the blood-brain barrier (BBB). BBB disruption is further exacerbated by degradations of integrins, which are also expressed at the plasma membrane of brain microvascular endothelial cells. ZO-1, zonula occludens-1. Adapted from (T Ronaldson and P Davis 2012).

1.1.6.2 Pericytes

The pericytes surround the small vessels, thereby providing both structural support as well as vasodynamic support to the microvasculature. There is abundant evidence that pericytes play an essential role in cerebral autoregulation through their expression of receptors that are critical for

transmission of chemicals such as catecholamines (Elfont, Sundaresan et al. 1989), angiotensin II (Healy and Wilk 1993), vasoactive intestinal peptides (Benagiano, Virgintino et al. 1996), endothelin-1 (Dehouck, Vigne et al. 1997), and vasopressin (Van Zwieten, Ravid et al. 1988). According to studies using viable pericyte-deficient mouse mutants, a deficiency in pericytes increases the permeability of the BBB to water and to a variety of molecular weight tracers at low and high concentrations (Armulik, Genové et al. 2010). As a result of this, it can be concluded that pericyte regulation of the transcellular barrier is crucial for the normal function of the BBB (Sweeney, Ayyadurai et al. 2016). The loss of pericytic laminin also causes BBB breakdown and hydrocephalus in other conditional knockout mice models (Gautam, Zhang et al. 2016). There are numerous possible causes for this, including the degradation of the basement membrane that provides structural support for the endothelial cells, pericytes and astrocytes of the blood vessels, and also promotes the integrity of the BBB.

It has been suggested that pericyte degeneration with age may lead to BBB disruption, increased permeability of the BBB, and possibly contribute to age-associated neurodegenerative diseases like Alzheimer's disease, which are also associated with higher permeability of the BBB (Balabanov and Dore-Duffy 1998). The majority of the SVD pericyte research has been done using the CADASIL mouse model of *Notch3* mutation. The CADASIL mouse shows Notch3 aggregation in the pericytes leads to a reduction in pericyte coverage of vessels over time (Ghosh, Balbi et al. 2015).

1.1.6.3 Astrocytes

An astrocyte is one of the most abundant types of cells in the cerebral cortex of vertebrates. They have specialized endfeet covering the surface of the CNS microvessels (Liebner, Dijkhuizen et al. 2018). A significant contribution to water homeostasis in the NVU is provided by the expression of proteins such as aquaporin-4 (AQP-4) and the potassium channel Kir4 at the foot processes of the astrocytes, which are tightly associated with microvessels (Engelhardt and Liebner 2014). A growing body of evidence suggests that astrocytes can influence many aspects of the BBB, including increasing the tightness of the tight junctions, which would alter the permeability of the BBB (Abbott, Rönnbäck et al. 2006).

The interaction between endothelial cells and astrocytes is essential not just for enhancing and preserving the integrity of the BBB, but also crucial for cellular differentiation, which fosters BBB development. It is well known that astrocytes are involved in the production of lipoproteins, such as Apolipoprotein E (ApoE), which is an important component of Alzheimer's pathology and the injury to the BBB (Erdő, Denes et al. 2017).

1.1.6.4 Microglia

As a distinct class of glial cells, microglia are the primary brain immune cells that become activated and undergo morphological and functional changes following brain injuries and diseases (Nimmerjahn, Kirchhoff et al. 2005, Sá-Pereira, Brites et al. 2012). In addition to their involvement in lesions, neurodegenerative diseases, strokes, and brain tumors, they are also ontogenetically related to the mononuclear phagocyte lineage. Microglial activation increases BBB permeability by releasing pro-inflammatory mediators, including cytokines, chemokines, ROS, and interleukins (ILs). Consequently, peripheral leukocytes, including T cells and macrophages, can be infiltrated into the CNS. By increasing BBB permeability, peripheral macrophages can contribute to neuroinflammatory outcomes, causing neuronal cell death, releasing neurotoxins, and activating microglia as a negative feedback loop.

Activated microglia have been described as a double-edged sword, where they can have both toxic and beneficial roles. Research now suggests that microglia activate in a similar way to macrophages, with both an M1 and an M2 phenotype (Hu, Leak et al. 2015). The M1 phenotype represents a proinflammatory phenotype releasing inflammatory mediators such as prostaglandins, tumour necrosis factor- α (TNF- α), interleukin-6 (IL-6), interleukin-1 β (IL-1 β), ROS and glutamate. However, the M2 phenotype attempts to resolve the inflammation, with the release of anti-inflammatory mediators such as interleukin-10 (IL-10), insulin-like growth factor 1 and neurotrophic factors (Réus, Fries et al. 2015).

1.1.7 Inflammation in CSVD

Inflammation has been recognised as one of the key components of cerebrovascular and neurological diseases. Inflammatory cell infiltrations in the arteriolar wall and perivascular tissue have been noted in the elderly since 1902. Inflammation both acutely and chronically occurs in SVD. Acute inflammation occurs when lacunar infarcts are formed due to acute vessel blockage, resulting in inflammation in response to hypoxia/ischemia (Fu and Yan 2018). Hypoperfusion and BBB changes underlie chronic inflammation, and the pathophysiology is likely to be similar to chronic neurodegenerative diseases such as Alzheimer's.

Immunohistochemical techniques are useful for identifying activated microglia using specific molecular markers. Constitutive expression of ionized calcium-binding adapter molecule-1 (IBA1) is specific for microglia, irrespective of activation state. A marker of M1 microglia phenotype is CD68, while the mannose receptor CD206 can be used as a marker of M2 phenotype. Aged brains have an increase in CD68-positive microglia compared to control brains, according to postmortem studies (Simpson, Ince et al. 2007). Studies into Alzheimer's disease patients showed a similar pattern of increased CD68 expression in activated microglia in the patient brain compared to control (Hopperton, Mohammad et al. 2018).

Matrix metalloproteinase-2 (MMP2), matrix metalloproteinase-3 (MMP3) and matrix metalloproteinase-9 (MMP9) are produced by microglia, astrocytes and endothelial cells as part of the inflammatory response (Asahi, Wang et al. 2001, Rosenberg, Cunningham et al. 2001). A reversible disruption of basal lamina proteins and opening of tight junction proteins occurs early in hypoxia, as a result of the activation of MMP-2 (Yang, Estrada et al. 2007); this is thought to be short lived. Increasing hypoxia level, however, activates inducible MMP-3 and MMP-9, which irreversibly degrade the basal lamina and tight junction proteins (Rosenberg 2016).

1.1.8 MMP-induced disruption of the blood-brain barrier

There is a well-established link between MMP activity and neuroinflammation (Yong, Power et al. 2001), (McColl, Rothwell et al. 2008), particularly after infection (Gurney, Estrada et al. 2006) and ischemia (Yang, Estrada et al. 2007), leading to BBB disruption. MMPs are secreted by

endothelial cells, microglia, astrocytes, and neutrophils (Rosenberg 2002). MMPs have been shown to disrupt TJ directly *in vivo* as well; decreased claudin-5 and occludin expression was attributed to increased MMP activity in mice injected with LPS, a result that was not observed in MMP-3 knockout mice (Gurney, Estrada et al. 2006), indicating that MMPs may be damaging the substrate for which endothelial cells are anchored, which could in turn, lead to disrupted TJ. A study by Yang et al. in 2007 found that MMP-2 and -9 in particular, directly led to a decrease in claudin-5 and occludin levels following middle cerebral artery occlusion in rats (Yang, Estrada et al. 2007). This in turn resulted in an increase in BBB permeability. In addition, there have been numerous *in vitro* studies that support the *in vivo* observations above, which have implicated MMPs in signaling events that involve the degradation of TJ protein (Reijerkerk, Kooij et al. 2006), (Lischper, Beuck et al. 2010).

The balance between MMPs and tissue inhibitors of metalloproteinases (TIMPs) is responsible for maintaining basal lamina stability (Yang, Estrada et al. 2007). It is also known that MMP-2 and -9 play a role in modulating the NVU. Furthermore, MMP-9 may contribute to laminin disruption following focal ischemia in mice (Gu, Cui et al. 2005).

A number of studies suggest that (i) MMP-mediated proteolysis of the basal lamina loosens the base upon which the TJ proteins are anchored, and/or (ii) MMP-mediated proteolysis of the extracellular matrix exposes the endothelial TJ proteins to damage, making them more susceptible to damage in the future (Gurney, Estrada et al. 2006). An MMP-9 inhibitor was found to be effective in preventing laminin proteolysis in the brain following cerebral ischemia in mice (Gu, Cui et al. 2005) and additionally in cultured human brain endothelial cells (Haorah, Ramirez et al. 2007).

1.2 Extracellular matrix (ECM)

The emergence of multicellular organisms necessitated the creation of methods for intercellular communication and bonding. This challenge was addressed by the development of ECMs based on collagen, a feature found in all multicellular species.

There is a complex network of macromolecules called the ECM that is present within tissues and organs, which contains collagen, fibronectin, laminin, fibrillin, proteoglycans, and several other glycoproteins [83, 148]. There has been a tendency in the past to view ECMs solely as structures

providing structural support to cells and tissues within their microenvironment, such as providing strength and elasticity [38]. Now the functional role of ECM is recognized in modulation of cell to cell signaling, volume transmission, cell proliferation and differentiation [83, 144].

Generally, the ECM occupies the space outside cells, but its makeup varies. Three primary forms of ECM can be identified: (1) perineuronal nets (PNNs) rooted in hyaluronic acid and lecticans, (2) the perivascular ECM, which is based on collagen and laminin, and (3) a mixed interstitial matrix that combines lecticans, collagens, and laminins in varying ratios. **Table 1.4** displays the expression trends of both perineuronal and perivascular ECM components. Meanwhile, **Figure 1.5** showcases their interplay to form diverse ECM structures within the CNS.

1.2.1 Perineuronal nets

PNNs consist of a densely packed version of ECM. They are primarily linked with parvalbumin (PV)-expressing, gamma-aminobutyric acid (GABA)-ergic interneurons but are also observed around excitatory pyramidal cells and motoneurons. The intricate structure of PNNs surrounds the neuronal cell bodies, early dendrites, and the initial segment of axons. They are evident in various brain areas such as the cerebral cortex, hippocampus, cerebellum, and basal ganglia (Brauer, Ha et al. 1993, Song and Dityatev 2018). These structures predominantly consist of chondroitin sulfate proteoglycans (CSPGs) from the lectican family, which connect to tenascin-R (Tn-R) at their C-terminus and to the hyaluronan (HA) backbone through hyaluronan and proteoglycan link proteins (Hapln1-4). The HA framework is crafted by transmembrane hyaluronan synthases (HAS1-4), essential for binding the ECM to the neuron surface (Rooney and Kumar 1993, Djerbal, Lortat-Jacob et al. 2017). **Figure 1.5.a** shows how these molecules interact and affix to the neuronal surface. The lectican group encompasses aggrecan, brevican, neurocan, and versican. These elements and the CSPG phosphacan connect with membrane receptors like the neuronal cell adhesion molecule (NCAM) and receptor protein tyrosine phosphatases (RPTP δ or RPTP σ) (Djerbal, Lortat-Jacob et al. 2017). These receptors bind to CSPGs with a high affinity, leading to the dephosphorylation of protein tyrosine residues. This cellular signaling pathway results in neurite outgrowth inhibition and plays a role in managing axonal development, direction, synaptic adaptability, and post-injury regeneration. Mature PNNs can limit synaptic adaptability and are linked with the ending of crucial phases during which experience-driven adaptability solidifies

(Shen, Tenney et al. 2009, Djerbal, Lortat-Jacob et al. 2017). Additionally, PNNs regulate the excitability of PV⁺ interneurons and the excitatory inputs they receive (Dityatev, Brückner et al. 2007, Hayani, Song et al. 2018).

1.3 Perivascular ECM

Brain blood vessels comprise a luminal layer of endothelial cells bound tightly through TJs, encased by pericytes and vascular smooth muscle cells (vSMCs) (Armulik, Abramsson et al. 2005). Astrocytic endfeet embed the vessel wall's outermost section. In this context, the perivascular ECM serves a pivotal role in preserving and bolstering the BBB's mechanical and chemical defenses. The perivascular ECM layers, moving from luminal to outer regions, include (i) the endothelial basement membrane (BM), also encompassing pericytes; (ii) the distinct BM surrounding vSMCs; (iii) the astroglial and pial BM; and (iv) the fibrous interstitial matrix linking these layers. The parenchymal BM, which includes astroglial and pial layers, represents the external part of the brain tissue and encloses arterioles entering the brain. A layer made up of flat pial cells, astrocytic processes, and the ECM they generate is isolated from the rest of the vessel by a fluid-filled perivascular gap. This gap vanishes as the parenchymal arteriole divides into the microvascular capillary system (Wardlaw, Benveniste et al. 2020). **Figure 1.5.b** visualizes a CNS capillary's ECM architecture. The capillary BM, varying in thickness from 20-200 nm, is a conjoined remnant of the endothelial and parenchymal BMs. The ECM components are produced by all neighboring cells, such as pericytes, endothelial cells, and astroglial cells, but not by pial cells anymore (Yousif, Di Russo et al. 2013, Thomsen, Routhe et al. 2017). Two primary components of vascular BMs, laminins and collagen IV, create interconnected three-dimensional structures, linked non-covalently through perlecan and agrin (two heparan sulfate proteoglycans, HSPGs) and nidogen. Notably, perlecan plays a part in binding various growth factors, and the amount produced and its cleavage determines the influence of these growth factors on ECM formation or angiogenesis (Göhring, Sasaki et al. 1998, Whitelock, Melrose et al. 2008, Thomsen, Routhe et al. 2017). Several other structural proteins like fibronectin, fibulin 1 and 2, and SPARC are also part of the vascular BM (McKee, Harrison et al. 2007, Yurchenco 2015, Thomsen, Routhe et al. 2017). Different compositions of ECM molecules are observed between capillaries and pial

arterioles. For example, laminin $\alpha 1$ chains or a specific form of type IV collagen were found more associated with pial cells than capillaries (Joutel, Haddad et al. 2016).

The perivascular ECM differs in structures like the circumventricular organs and the choroid plexus, areas requiring permeable capillaries for sensory or secretory functions. In these regions, the BBB doesn't exist at the capillary level, and TJs shift from endothelial to ependymal cells lining the brain's ventricles. An additional ependymal BM is distanced from the capillary BM by a perivascular area. This BM resembles the renal glomerular BM and might perform size-selective filtration (Urabe, Naito et al. 2002, Jiménez, Domínguez-Pinos et al. 2014). In the subventricular zone of the lateral ventricle, a neurogenically active area, unique ECM structures called fractones exist (Sato, Kiyozumi et al. 2019). Fractones are discrete from vascular BMs in structure and composition and interact with neural stem cells.

The integrity of the ECM and the structure of blood vessels are deeply interconnected, with cellular surface receptors, mainly from the integrin and dystroglycan families, playing a crucial role. Studies have drawn links between collagen IV's connection to endothelial $\beta 1$ -integrin and the appearance of the TJ protein claudin-5, with significant implications for BBB stability (Osada, Gu et al. 2011). In mice, the absence or mutations in laminin or collagen IV genes might lead to brain bleeding due to a compromised BBB (Gautam, Zhang et al. 2016, Joutel, Haddad et al. 2016). Therefore, the precise composition of the ECM and the concentration of specific molecules greatly influence BBB formation. Persistent alterations in these molecules, resulting from increased synthesis or degradation, might destabilize the BBB and pose potential threats to surrounding CNS tissue.

1.3.1 Interstitial matrix

The interstitial matrix pervades the remaining extracellular space within the CNS tissue. This matrix is characterized as a "composite" ECM encompassing components of the PNN, including an HA backbone fused with CSPGs, Tn-R, and link proteins. Additionally, it consists of adhesive ECM glycoproteins like laminins, fibronectin, and fibrillary proteins such as collagens, which are primarily expressed perivascularly (Lau, Cua et al. 2013). Molecules that exhibit a strong affinity to HA, including CSPGs and HSPGs, have also been demonstrated to bind to collagen, laminin,

and fibronectin, albeit with diminished affinity (Rooney and Kumar 1993, Lasek 2016). **Figure 1.5.c** depicts some of these molecular associations. The "composite" aspect of the ECM is intriguing as its make-up mirrors the activity of neuronal, glial, immune, and vascular cells. All these cells play a role in either producing or breaking down ECM molecules (**Table 1.4**). It is conceivable that ECM molecules concentrated in perineuronal and perivascular regions might spread and alter the composite ECM's composition associated with adjacent synapses, neurons, and glial cells. The assimilation of perivascular ECM molecules into the composite ECM might have significant functional relevance due to their ability to bind and signal via integrins. For example, laminin $\alpha 5$ functions through an integrin $\alpha 3\beta 1$ -Abl2 kinase-p190RhoGAP signaling pathway and collaborates with laminin $\beta 2$ to modulate dendritic spine density and behavior (Omar, Campbell et al. 2017). Furthermore, studies have shown that synaptic plasticity regulation was disrupted in mice deficient in integrin-binding fibronectin, laminins, and tenascins (Dityatev and Schachner 2003, Dityatev 2010, Senkov, Andjus et al. 2014, Lasek 2016).

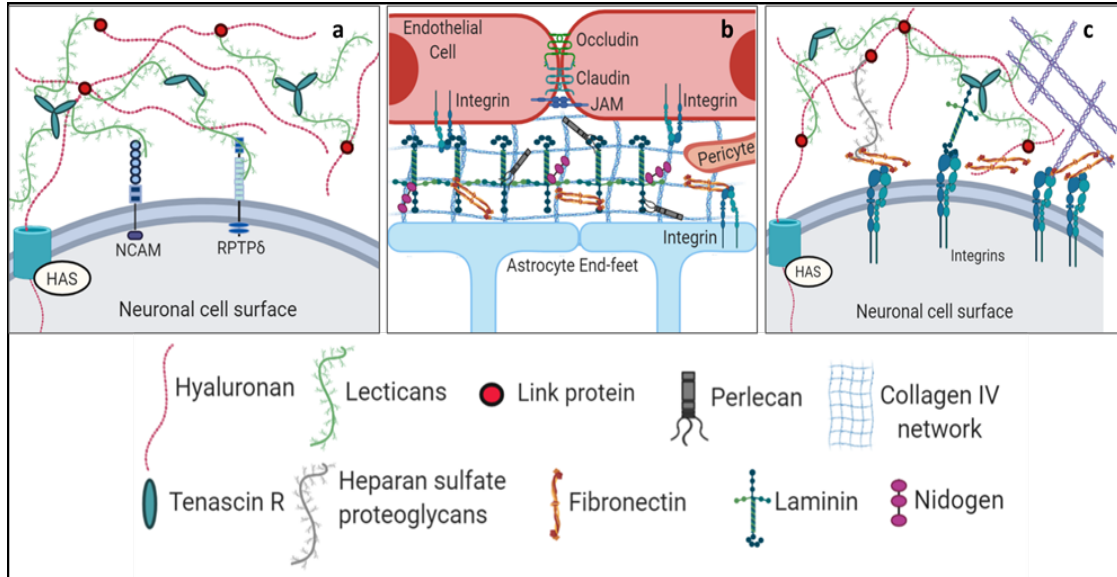


Figure 1.5 Three forms of ECM in the CNS. (a) The structure of a PNN: this dense mesh-like ECM is composed of an HA backbone connected to lecticans and stabilized by tenascins. Lecticans signal through NCAM and RPTP δ and other receptors. (b) The structure structure of the perivascular ECM in a CNS capillary: laminin and collagen IV form molecular networks that are connected to each other through nidogen, perlecan and fibronectin. The ECM is connected to the surfaces of perivascular cells through integrins. Closely apposed TJ proteins (occludins, claudins or JAM) enable BBB integrity. (c) The interstitial “hybrid” matrix: next to HA, PGs and tenascins, smaller amounts of adhesive glycoproteins (e.g., fibronectin, laminin) and collagens enable signal transduction to intracellular cascades by binding integrins. Abbreviations: HA, hyaluronan; BBB, blood-brain barrier; ECM, extracellular matrix; HAS, hyaluronan synthase; JAM, junctional adhesion molecule; NCAM, neuronal cell adhesion molecule; PG, proteoglycan; PNN, perineuronal net; RPTP δ , receptor protein tyrosine phosphatase δ ; TJ, tight junction. The image was created using Biorender graphic software. Adapted from (Ulbrich, Khoshneviszadeh et al. 2021).

Colour scale for each gene and each species		100%	80%	50%	25%	10%	5%	1%	0%											
Molecule	Gene	Human						Mouse												
		Foetal astrocyte	Mature astrocyte	Neuron	Oligodendrocyte	Microglia	Endothelial cell	Astrocyte	Neuron	OPC	Oligodendrocyte	Microglia	Endothelial cell							
Perineuronal ECM																				
Hyaluronan synthase	HAS1	0.1	0.1	0.1	0.1	0.1	0.1	0.1	0.1	0.1	0.1	0.1	0.1	0.1	0.1	0.1	0.1	0.1	0.1	0.1
	HAS2	2.5	0.1	0.2	1.6	0.1	0.1	0.1	0.1	0.1	0.1	0.1	0.1	0.1	0.1	0.1	0.1	0.1	0.1	0.1
	HAS3	2.5	0.2	0.2	0.7	0.1	0.1	0.1	0.1	0.1	0.1	0.1	0.1	0.1	0.1	0.1	0.1	0.1	0.1	0.1
Lecticans	ACAN	0.1	0.1	0.1	0.1	0.1	0.1	0.1	0.1	0.1	0.1	0.1	0.1	0.1	0.1	0.1	0.1	0.1	0.1	0.1
	BCAN	8.5	14.9	0.9	4.6	0.1	0.4	0.1	0.4	817.8	47.3	556.0	75.5	12	1.7	0.1	0.1	0.1	0.1	
	VCAN	55.9	4.9	3.2	28.9	1.4	1.4	0.1	0.1	30.7	10.1	161.0	1.8	0.2	0.2	0.1	0.1	0.1	0.1	0.1
	NCAN	45.4	80.7	6.6	3.1	0.2	2.1	0.1	0.1	280.1	33.3	46.8	2.9	1.5	0.8	0.1	0.1	0.1	0.1	0.1
	PTPRZ1	259.8	140.5	20.5	131.7	2.0	4.2	0.1	0.1	1021.1	45.5	416.6	2.7	1.7	0.8	0.1	0.1	0.1	0.1	0.1
Tenascin-R	TNR	1.0	2.4	1.4	16.4	0.3	1.0	0.1	0.1	0.7	3.3	111.4	5.0	0.1	0.1	0.1	0.1	0.1	0.1	0.1
Tenascin-C	TNC	26.6	0.6	0.1	0.2	0.1	0.1	0.1	0.1	118.2	10.4	0.3	0.1	0.2	0.7	0.1	0.1	0.1	0.1	0.1
Link proteins	HAPLN1	1.2	0.4	7.6	0.8	0.1	0.1	0.1	0.1	63.3	11.8	13.3	0.5	0.3	0.5	0.1	0.1	0.1	0.1	0.1
	HAPLN4	0.7	0.1	0.8	0.1	0.1	0.1	0.1	0.1	1.4	0.4	1.1	0.5	0.3	0.1	0.1	0.1	0.1	0.1	0.1
Collagens	COL1A1	0.1	0.1	0.1	0.1	0.1	0.1	0.1	0.1	0.8	3.1	19.5	0.4	0.4	0.4	0.1	0.1	0.1	0.1	0.1
	COL1A2	1.5	0.1	0.4	0.1	0.1	2.4	0.1	0.1	6.4	1.6	34.5	0.5	0.7	2.9	0.1	0.1	0.1	0.1	0.1
	COL3A1	0.4	0.1	0.2	0.1	0.1	0.4	0.1	0.1	0.2	0.8	23.4	0.1	0.3	2.4	0.1	0.1	0.1	0.1	0.1
	COL5A2	0.9	0.3	0.8	0.1	0.1	0.2	0.1	0.1	2.6	2.1	2.3	0.1	0.1	2.9	0.1	0.1	0.1	0.1	0.1
	COL5A3	2.7	0.1	0.1	0.1	0.1	0.2	0.1	0.1	2.4	0.2	2.9	0.1	0.1	1.0	0.1	0.1	0.1	0.1	0.1
	COL6A1	5.9	1.1	0.3	0.3	0.1	0.5	0.1	0.1	0.3	6.4	6.1	0.2	0.3	0.2	0.1	0.1	0.1	0.1	0.1
	COL6A2	1.2	0.1	0.1	0.1	0.1	0.4	0.1	0.1	0.4	43.4	4.6	5.7	0.1	0.3	0.1	0.1	0.1	0.1	0.1
	COL19A1	0.1	0.1	0.6	0.2	0.1	0.1	0.1	0.1	0.1	0.1	2.8	1.1	0.1	0.1	0.1	0.1	0.1	0.1	0.1
Extracellular proteolytic pathway																				
Matrix metalloproteinases	MMP2	1.0	0.3	0.3	1.8	3.3	0.9	0.1	0.1	0.1	8.0	19.8	3.0	23.7	1.1	0.1	0.1	0.1	0.1	0.1
	MMP3	0.1	0.1	0.1	0.1	0.1	0.1	0.1	0.1	0.1	0.1	0.1	0.1	0.1	0.1	0.1	0.1	0.1	0.1	0.1
	MMP9	0.1	0.1	0.1	0.1	0.1	0.1	0.1	0.1	0.1	0.3	0.4	0.1	7.8	0.7	0.1	0.1	0.1	0.1	0.1
ADAMs	ADAM10	6.8	7.4	9.1	15.6	22.6	6.3	0.1	0.1	24.9	12.7	31.4	6.5	17.6	104.7	0.1	0.1	0.1	0.1	0.1
	ADAM17	7.0	4.6	4.4	4.4	20.4	3.0	0.1	0.1	18.9	2.9	17.5	8.0	18.6	19.4	0.1	0.1	0.1	0.1	0.1
ADAMTSs	ADAMTS4	0.1	0.1	0.2	3.0	3.8	0.5	0.1	0.1	0.5	1.1	1.5	61.4	0.4	3.9	0.1	0.1	0.1	0.1	0.1
	ADAMTS5	0.2	0.1	0.3	0.2	0.1	0.1	0.1	0.1	2.8	0.5	1.4	0.1	0.1	0.2	0.1	0.1	0.1	0.1	0.1
Plasminogen activators	PLAT	3.2	0.2	1.0	2.0	0.2	7.0	0.1	0.1	120.3	13.5	29.5	78.8	0.8	160.9	0.1	0.1	0.1	0.1	0.1
	PLAU	0.2	0.4	0.1	1.5	28.6	0.5	0.1	0.1	0.8	0.4	4.8	2.9	213.0	0.8	0.1	0.1	0.1	0.1	0.1
Tissue inhibitors of metalloproteinases	TIMP1	7.8	4.2	1.3	1.1	3.3	3.7	0.1	0.1	0.6	0.6	0.3	0.2	0.2	11.4	0.1	0.1	0.1	0.1	0.1
	TIMP2	17.3	15.6	61.6	27.9	23.6	10.3	0.1	0.1	21.2	142.2	51	31.9	106.5	2.5	0.1	0.1	0.1	0.1	0.1
	TIMP3	10.2	54.3	6.9	4.2	0.3	56.9	0.1	0.1	144.7	7.8	34.6	1.7	0.9	46.4	0.1	0.1	0.1	0.1	0.1
	TIMP4	0.9	1.1	0.6	0.1	3.5	0.1	0.1	0.1	48.7	5.2	73.4	7.6	1.8	0.3	0.1	0.1	0.1	0.1	0.1
Perivascular ECM																				
Laminins	LAMA1	5.0	2.4	0.1	0.1	0.1	0.1	0.1	0.1	0.3	0.4	3.3	0.1	0.1	6.7	0.1	0.1	0.1	0.1	0.1
	LAMA2	0.3	0.1	0.7	1.3	0.1	4.3	0.1	0.1	6.9	0.3	1.7	2.5	0.1	1.8	0.1	0.1	0.1	0.1	0.1
	LAMA4	2.3	2.1	0.5	1.2	0.1	4.3	0.1	0.1	6.6	0.7	3.7	0.2	0.2	112.4	0.1	0.1	0.1	0.1	0.1
	LAMA5	0.4	0.1	0.1	0.1	0.1	0.1	0.1	0.1	7.1	1.2	0.2	0.1	0.2	15.5	0.1	0.1	0.1	0.1	0.1
	LAMB2	1.25	2.0	0.1	0.1	0.1	2.7	0.1	0.1	30.1	1.4	2.4	0.5	13.5	54.1	0.1	0.1	0.1	0.1	0.1
Collagens	LAMC1	5.9	4.0	1.6	0.7	0.1	3.0	0.1	0.1	16.0	2.7	22.2	9.7	2.1	95.2	0.1	0.1	0.1	0.1	0.1
	COL4A1	1.3	0.2	0.5	0.1	0.1	1.2	0.1	0.1	13.3	6.1	30.5	1.6	2.4	413.7	0.1	0.1	0.1	0.1	0.1
	COL4A2	0.4	0.2	0.1	0.1	0.1	0.5	0.1	0.1	6.9	5.2	16.4	0.7	2.1	312.6	0.1	0.1	0.1	0.1	0.1
	COL18A1	0.2	0.1	0.1	0.1	0.1	0.6	0.1	0.1	0.6	1.0	12.8	0.1	0.2	24.9	0.1	0.1	0.1	0.1	0.1
Fibronectin	FN1	7.8	2.6	3.2	0.1	1.0	65.2	0.1	0.1	3.7	1.1	4.4	0.3	1.1	292.6	0.1	0.1	0.1	0.1	0.1
Perlecan	HSPG2	0.2	0.1	0.1	0.1	0.1	0.1	0.1	0.1	2.5	1.2	3.1	5.6	0.3	42.9	0.1	0.1	0.1	0.1	0.1
Agrin	AGRN	0.8	0.2	0.1	0.1	0.1	1.0	0.1	0.1	115.8	61.5	52.8	8.7	6.8	186.5	0.1	0.1	0.1	0.1	0.1
	NID1	3.4	3.6	0.5	0.2	0.2	4.2	0.1	0.1	3.9	1.7	7.5	1.2	0.3	116.9	0.1	0.1	0.1	0.1	0.1
Nidogens	NID2	0.4	0.1	0.4	0.5	0.1	2.1	0.1	0.1	7.9	0.9	4.0	0.3	8.3	70.7	0.1	0.1	0.1	0.1	0.1

Table 1.4 Expression pattern of diverse ECM molecules in the human and mouse brains. The table is divided into perineuronal and perivascular components and molecules involved in the extracellular proteolytic pathway. The presented data were collected using an online mRNA databank (available at <http://www.brainrnaseq.org>). Numbers represent FPKM (fragments per kilobase of exon model per million reads mapped) values of mRNA. A colour scale for each gene in each species depicts the highest mRNA expression level among all considered cell types in red and the lowest in green. Yellow and orange colour coding represents intermediate expression levels. Abbreviations: ADAM, a disintegrin and metalloproteinase; ADAMTS, ADAM with thrombospondin motifs; ECM, extracellular matrix; OPC, oligodendrocyte precursor cell. Adapted from (Ulbrich, Khoshneviszadeh et al. 2021).

1.4 Cerebral small vessel disease and ECM

Age and hypertension have been highlighted as primary risk factors for CSVD (Santisteban and Iadecola 2018). Additionally, findings from genetic animal models with mutations in genes related to perivascular ECM molecules indicate that changes in the brain ECM could also be a significant risk factor. With aging, cerebral arterioles undergo stiffening and fibrosis due to vascular smooth muscle cell reduction, diminished elastin production, and increased elastin breakdown and collagen formation. Such changes in perivascular ECM are believed to be connected to elevated TGF- β secretion (Hajdu, Heistad et al. 1990, Morgan, Ives et al. 2014, Joutel, Haddad et al. 2016). During healthy aging, perineuronal ECM undergoes alterations, including increased lectican and HA accumulation, resulting in more pronounced and numerous PNNs. This boost in HA synthesis correlates with HAS1's heightened activity in reactive astrocytes in an aging brain (Cargill, Kohama et al. 2012, Song and Dityatev 2018).

Typically, hypertension is linked with cellular and ECM transformations of the vessel wall, culminating in constricted, fibrotic cerebral vessels and endothelial malfunction. Consequently, during heightened metabolic demands, these vessels can't expand sufficiently. This leads to a series of hypoxic injuries triggering an inflammatory reaction and the secretion of MMPs, notably MMP-3 and MMP-9, by activated microglial cells (Rosenberg 2017). Yet, this protease release aimed at reshaping the blood vessel wall inadvertently compromises the BBB and injures myelin fibers. Supporting this perspective, treating SHRSP, an animal model emulating sporadic CSVD, with minocycline, an anti-inflammatory MMP suppressor, led to diminished white matter damage, better learning outcomes in water-maze evaluations, and prolonged lifespan (Jalal, Yang et al. 2015). CADASIL is a hereditary version of CSVD showing similar complications as sporadic CSVD, like microbleeds and minuscule infarcts. In a genetic mouse CADASIL model, changes like reduced laminin, increased fibronectin, collagen IV, MMP-2, and MMP-9 were noted in cerebral arteries, mirroring findings in SHRSP (Dziewulska, Nycz et al. 2017, Held, Morris et al. 2017). Additionally, a spike in perivascular TIMP-3 was detected in the ECM, causing the metalloproteases ADAM17 and HB-EGF's inability to control cerebral arterial dynamics and blood flow reactions. Typically, the ADAM17/HB-EGF/(ErbB1/ErbB4) pathway's ongoing activity deters excessive Kv channel build-up on vSMCs' plasma membrane, preserving myogenic tone. Thus, a surge in TIMP-3 might modify vSMC contractility, obstructing vasodilation and standard cerebral blood flow (Capone, Dabertrand et al. 2016).

In summation, in sporadic CSVD, persistent vascular changes cause numerous, asynchronous cellular responses in the impacted vicinity. In both human and animal brains examined postmortem, one can detect simultaneous acute and chronic tissue changes, complicating distinguishing between them. This blurring of acute and chronic reactions may be why clear CSVD markers are missing in serum or CSF. Another critical point is the excessive TIMP-3 production in perivascular zones possibly creating a diffusion gradient of TIMP-3, influencing the neighboring neuropil. A logical inference would be that the consequent build-up of perisynaptic ECM molecules in CSVD, which might be a factor in cognitive deterioration.

1.5 Biphasic ECM regulation in different CNS disorders

In our recent studies on CSVD, we were led to delve into the mechanisms that oversee ECM management in such long-standing conditions. When we drew parallels between the time-sensitive regulation of ECM in other CNS ailments, a pattern emerged. Following vascular injuries, oxygen deprivation, CNS trauma, seizures, or mental stress, an immediate inflammatory reaction is triggered, marked by a surge in the expression and activity of external proteases like MMPs, ADAMTSSs, and tPA, leading to ECM breakdown. Conversely, during the recuperative or prolonged phase, there's an upswing in ECM production, usually tied to an increased expression of TIMPs. **Figure 1.6** provides a graphic representation of the progression of these events..

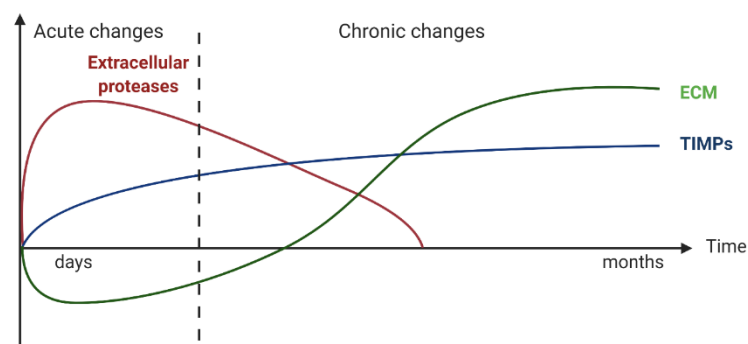


Figure 1.6 Schematic timeline of ECM regulation in different neurological and psychiatric disorders. Acute elevation of extracellular proteases leads to net ECM degradation, whereas a long-term increase in TIMP and ECM expression causes chronic ECM accumulation. ECM, extracellular matrix; TIMP, tissue inhibitor of metalloproteinases. The graphic was made using Biorender graphic software (<https://biorender.com>). Adapted from (Ulbrich, Khoshneviszadeh et al. 2021).

In this discussion, we begin by analyzing the mechanisms activated by vascular injuries, notably the breakdown of the BBB or microbleeds in capillaries. In the initial 24 hours post-injury, microglial cells, the resident immune cells of the CNS tissue, spring into action, discharging cytokines and a substantial amount of proteases, particularly MMPs, in a broad manner. This surge in proteolytic activity, meant to clear the injury site by engulfing cell remnants and reconfiguring the ECM, unfortunately also targets and splits TJ proteins, BM proteins, and myelin in the nearby intact tissue. As a result, the efficacy of axonal signal transmission diminishes, the vascular wall becomes thinner, and the BBB's structural integrity is compromised. This degradation allows plasma proteins and immune cells to infiltrate the CNS tissue, intensifying the inflammatory reaction. Triggered by cytokine release, for instance from microglial cells, astrocytes become active. Within days of tissue trauma or oxygen deprivation, they initiate scar formation to enclose the affected tissue, as depicted in **Figure 1.7**.

In the subsequent 2-3 weeks, though proteases remain elevated, their role is more limited, aiding beneficially in angiogenesis, axonal growth, and PNN disintegration. This localized degradation of ECM is pivotal for cellular differentiation and movement to develop new blood vessels or axonal extensions. The formation of new blood vessels and the restructuring of neuronal circuits provide some degree of compensation for neuronal injury or loss. Concurrently, there's a rise in the expression of ECM components, yet the primary process is still ECM proteolysis. It's only when the balance of extracellular proteases to TIMP swings back to its base levels that there's a net increase in ECM. As a result, the tissue regains its structural stability, and alterations in cellular adhesion and neuronal connectivity become more permanent.

Long-term changes spanning several months are largely tied to reactive astrogliosis. During this phase, there's a rise in the levels of TIMPs, CSPGs, and HA in the scar and neighboring areas. Notably, there's a surge in the number of PNNs and their component expression, potentially altering cellular reactivity and the principles governing precision and updating of memories. CSPGs and HA may hinder the differentiation and movement of OPCs and disrupt axonal remyelination. Additionally, significant quantities of ECM components associated with perivascular ECM, like fibronectin, laminins, and collagens, appear within and around the scar. These molecules also play a role in guiding tissue regeneration by amplifying integrin receptor engagement and signaling.

In various CNS conditions, there's an imbalance in the long-term equilibrium between ECM breakdown and formation. Any shift in this balance can have both positive and negative impacts on synaptic plasticity and tissue repair, contingent on the specific molecules at play. In the subsequent sections, we'll delve into a range of diseases, emphasizing parallels in their ECM dynamics and examining specific signaling pathways and their influence on regeneration.

1.6 ECM turnover

The CNS's ECM undergoes constant dynamic changes, maintained by a finely-tuned coordination of proteases and their corresponding inhibitors. The CNS hosts extracellular proteases such as the plasmin system, which is activated by tissue-type (tPA) and urokinase-type plasminogen activators (uPA) (Stevenson 2018). Furthermore, the system includes over 20 matrix metalloproteinases (MMPs), the ADAM protein group, ADAMTS proteins with thrombospondin motifs, and the cathepsins family which primarily targets intracellular protein breakdown (Wilkinson, Williams et al. 2015; Bonnans, Chou et al. 2014; Lasek 2016). Since ECM molecules play a pivotal role in synaptic adaptability and learning, a perpetual modification of the ECM structure, driven by neuronal activity or experiences, becomes essential. Notably, MMP-9's involvement in learning and memory processes has garnered significant attention (Dzwonek, Rylski et al. 2004; Lasek 2016; Rosenberg 2017). Also, ADAMTS-4 and ADAMTS-5 stand out due to their ability to break down proteoglycans like aggrecan, brevican, neurocan, and versican, all crucial constituents of PNNs (Gottschall and Howell 2015). Additionally, certain proteases cleave cell surface receptor extracellular parts such as β -dystroglycan (by MMP-9), while others target membrane receptor substrates like HB-EGF (cleaved by ADAM17) or initiate growth factors like the brain-derived growth factor (BDNF) (activated by MMP-3, 7, and 9). Consequently, they can influence intracellular signaling pathways (Dzwonek, Rylski et al. 2004; Mizoguchi and Yamada 2013; Capone, Dabertrand et al. 2016).

This exterior proteolytic system is controlled both at the biosynthesis phase and via TIMP proteins. The TIMP family consists of four analogous members that, in general, can suppress all identified MMPs, though their efficacy may differ. Notably, TIMPs also counteract ADAMs and ADAMTSs, with TIMP-3 being particularly effective in this inhibition (Arpino, Brock et al. 2015). The localized expression and activity modifications of extracellular proteases, based on activity,

are pivotal for managing physiological processes. Maintaining a long-term equilibrium between proteases and their inhibitors is crucial for the stability of the CNS. Subsequent discussions will illuminate how disturbances in this equilibrium can influence the evolution of various CNS diseases, either boosting or thwarting regeneration and recuperation.

1.7 Translation of the two-phase ECM dysregulation model into clinical research

Various CNS disorders, when studied in animal models and human post-mortem samples, display comparable patterns of time-related pathophysiological ECM regulation. Applying this understanding to translational research necessitates the creation of biomarkers to oversee ECM alterations in a clinical environment. Both CSF and blood serum serve as *in vivo* biomarkers and could be vital in denoting the presumed temporal regulation of specific ECM molecules within the human CNS. Under normal circumstances, the CSF plays a role in the clearance of CNS waste and has a connection with the interstitial fluid found in the extracellular space. This connectivity allows CNS ECM molecules to permeate into the CSF, suggesting that CSF may reflect increases or decreases of certain ECM molecules in the CNS. Since CSF is drained into the venous blood system, any modifications might also manifest in blood serum samples. Some research has probed into the presence of ECM molecules in CSF and blood serum in relation to neurological disorders such as brain cancers, traumatic brain injuries, and strokes (Al'Qteishat, Gaffney et al. 2006).

The detection of perineuronal ECM components like brevican and neurocan in the serum and CSF of humans has recently provided an opportunity to investigate their concentration *in vivo* and identify novel biomarkers for neural reorganization of ECM. There have been several studies that have examined serum and CSF biomarkers of traumatic brain injury (TBI), vascular and neurodegenerative dementia. The results of these studies have shown that CSF brevican, consisting of its N-terminal peptides, and neurocan levels in the patients have been decreased, while total brevican levels have decreased, but the C-terminal fragments have increased in serum levels (Minta, Cullen et al. 2019, Jonesco, Karsdal et al. 2020). Hessler and colleagues concluded in their recent work that proteolytic cleavage products of brain-derived perineuronal ECM molecules, such as neurocan fragments, might provide insight into the integrity of the brain's extracellular environment. Especially when normalized to the total proteoglycan concentration, CSF is a potent

indicator of proteolytic ECM fragmentation in the CNS tissue. In the clinic, the correlation with established markers for neurodegeneration and BBB leakage may pave the way to a more differentiated diagnosis of neurological disorders, based on body fluids. To improve the accuracy of detecting disorders, their study suggests incorporating the ratio of cleaved vs total neurocan into informative biomarker panels (Hubler, Höhn et al. 2022).

In various CNS disorders, there is a notable gap in extensive correlation studies involving blood and CSF samples, as well as in understanding the fluctuations of several molecules in body fluids in relation to CNS and ECM changes. The depth of knowledge about how, and to what extent, ECM molecules permeate into the CSF under different health conditions is limited.

When there's a breakdown in the BBB, the passage of extracellular neural ECM molecules and extracellular proteases into the vascular system increases. Hence, the analysis of ECM molecules in the blood could be particularly valuable in illnesses where BBB breakdown is evident.

For instance, those with epilepsy or traumatic brain injuries display a swift rise in CSF MMP-9 concentrations. Stroke victims also experience elevated MMP-9 concentrations in their serum shortly after the event (Grossetete, Phelps et al. 2009, Worthmann, Tryc et al. 2010, Li, Wang et al. 2013). In cases of ischemic stroke, elevated serum MMP-9 levels align with a heightened risk of hemorrhagic transformation, significant walking disability, and increased mortality, positioning blood MMP-9 as a potential predictive biomarker (Montaner, Alvarez-Sabin et al. 2001, Iemolo, Sanzaro et al. 2016, Zhong, Yang et al. 2017). This underlines the notion of a rapid surge in proteases in the CNS after damage in various neurological conditions. Additionally, a week post-stroke, there's a correlation between heightened serum TIMP-1 levels and clinical severity of the stroke (Worthmann, Tryc et al. 2010). Elevated TIMP-1 levels are believed to reflect the degree of astrocyte activation, which is in proportion to the extent of stroke-induced brain damage. An ongoing prospective clinical study is examining the aftereffects of ischemic stroke by linking a comprehensive analysis of blood biomarkers to brain imaging and clinical outcomes at multiple intervals (Piccardi, Arba et al. 2018). Another noteworthy finding is the correlation between HA levels in post-stroke human brains and serum HA levels, which seem to rise for up to two weeks following a stroke. This increase may indicate a longer-term upregulation of brain ECM.

In patients with recurring depression, long-term studies show a decrease in serum MMP-2 and MMP-9 activity, which aligns with cognitive decline (Bobińska, Szemraj et al. 2016). Although this doesn't solidify the chronic upsurge of ECM molecules, it draws a link between diminished proteolytic activity and cognitive deficits. Animal studies, particularly the SDPS rat model, offer more direct evidence, underscoring the ECM's long-term impact on memory (Riga, Kramvis et al. 2017, Koskinen, van Mourik et al. 2020).

Regarding the evaluation of extracellular proteases in CSF and blood, there is a correlation between the concentration of latent proteases, like MMP-9, and respective clinical results. Still, the mere presence of proteolytic enzymes doesn't necessarily reflect their true activity in the CNS ECM. Hence, combining expression and activity assessments would be ideal. A significant challenge in data interpretation stems from the fact that MMPs, TIMPs, and many ECM molecules are expressed beyond the CNS, making it hard to tie measurements exclusively to brain processes. Consequently, a promising direction might be examining ECM molecules unique to the CNS, like neurocan or brevican. For acute phases, the degradation products of these molecules might offer insights into actual degradation activity in CNS tissue. Therefore, future work should prioritize comprehensive studies, considering both the acute and chronic disease phases and analyzing various CNS ECM molecules and proteases in both serum and CSF.

In addition to serum and CSF indicators, molecular imaging techniques, like PET, may help in the early detection of CNS ECM remodeling. A few MMP inhibitors have been crafted as imaging agents for various conditions. Notably, pilot clinical studies involving [18F]15 in MS patients, as detailed by Wagner and associates, provide a solid foundation for the potential of MMP inhibitor probes in clinical trials (Wagner, Faust et al. 2011).

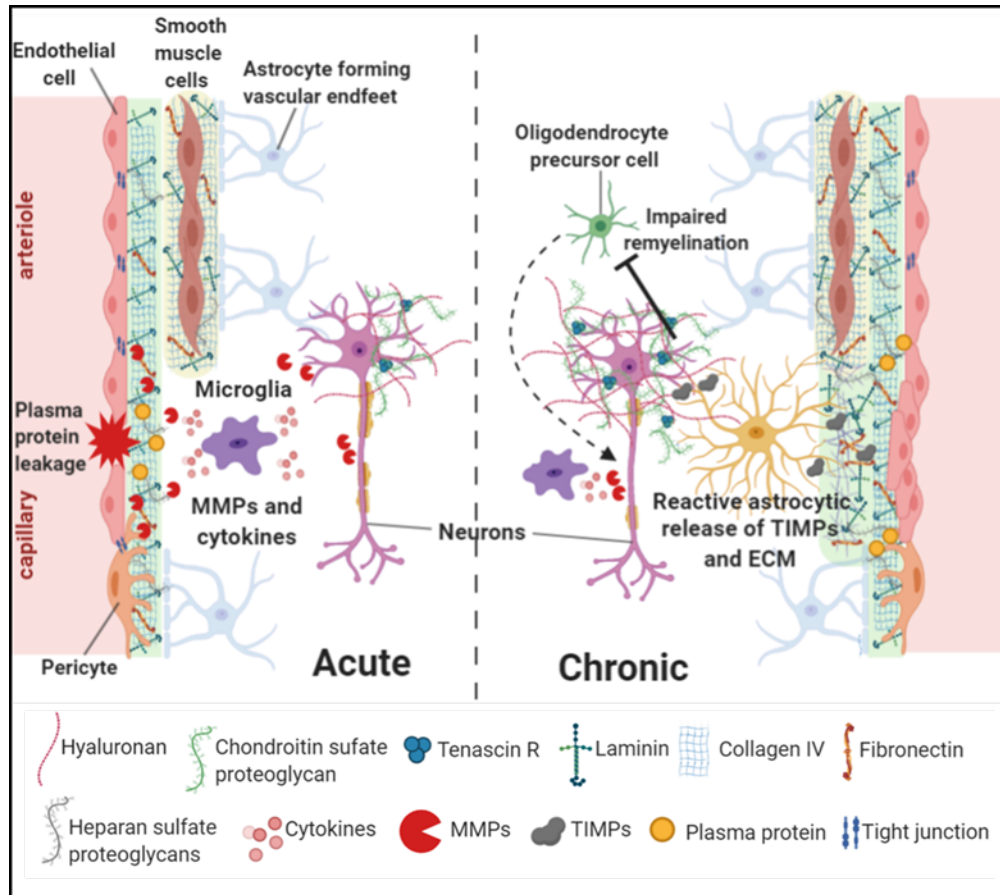


Figure 1.7 Schematic presentation of biphasic ECM regulation following vascular damage. After a vascular damage event, plasma proteins such as fibrinogen, and circulating immune cells (not shown here), leak into the CNS parenchyma and activate an initial inflammatory response. Amoeboid microglial cells phagocytize cell debris and release cytokines and extracellular proteases, which degrade perivascular ECM (BM) and TJ, perineuronal ECM (PNNs) and myelin. BBB opening and myelin degradation further restrict tissue repair, whereas PNN degradation can enable developmental forms of structural plasticity to compensate for partial neuronal death and loss of neuronal connections. In the chronic period, reactive astrocytes synthesize high amounts of ECM molecules and upregulate TIMP expression, leading to net perivascular and perineuronal ECM accumulations and to the appearance of more frequent and prominent PNNs. Microglial cells are still active and degrade myelin. Inhibition of OPC differentiation and migration by ECM overproduction leads to long-lasting demyelination and impairs functional recovery. Abbreviations: CNS, central nervous system; BBB, blood-brain barrier; BM, basement membrane; ECM, extracellular matrix; MMP, matrix metalloproteinase; OPC, oligodendrocyte precursor cell; PNN, perineuronal net; TIMP, tissue inhibitor of metalloproteinases; TJ, tight junction. The graphic was made using Biorender graphic software (<https://biorender.com>) (Adopted from (Ulbrich, Khoshneviszadeh et al. 2021)).

1.8 Collagen superfamily

Collagen is one of the most abundant proteins in the body and is the major macromolecule of most connective tissues. In particular, collagen is found in bones, skin, tendons, cartilage, ligaments, and vascular walls. Collagens are responsible for maintaining the structure and strength of tissues and organs. Additionally, collagens are crucial for early organogenesis and development, cell attachment, chemotaxis, and filtration via basement membranes. Collagens are recognized as fundamental proteins of the extracellular matrix, characterized by one or more unique triple-helical domains made up of three polypeptides that follow the Gly-X-Y amino acid pattern. This unique triple-helical structure is attributed to the presence of glycine at every third amino acid position. Each of these triple-helical sections showcases a rich proline content in the X position and hydroxyproline in the Y position of the recurring Gly-X-Y sequence. Collagen molecules are comprised of three α -chain polypeptides that intertwine in a right-handed helical formation, crafting the distinctive collagen triple-helix. While some collagens possess three identical α chains, others may have two or even three distinct α chains. Collagen molecules also feature non-collagenous sequences at their endpoints. Additionally, certain collagens display these sequences within their collagenous areas, disrupting the Gly-X-Y sequence. The significance of collagens is further underscored by a range of diseases arising from mutations in the collagen genes (Brodsky and Shah 1995, Ricard-Blum 2011).

1.8.1 Collagen XVIII

BMs, or basement membranes, are intricate molecular frameworks. They function as anchoring platforms for cells, influencing a range of cellular activities and facilitating the transport of nutrients. Constituents of their structure encompass laminin and collagen IV polymers, intertwined with other elements such as nidogen and perlecan. BMs are pivotal for structuring developing tissues and sustaining the functions of mature tissues. Consequently, mutations in various BM components can manifest in developmental anomalies or irregularities in mature tissues (Yurchenco, Amenta et al. 2004).

A recently discerned element of the majority of epithelial and endothelial BMs is collagen XVIII/endostatin (Rehn, Hintikka et al. 1994, Rehn and Pihlajaniemi 1994, Muragaki, Timmons

et al. 1995, Rehn and Pihlajaniemi 1995, Fukai, Eklund et al. 2002). Characterized as a heparan sulfate proteoglycan (Dong, Cole et al. 2003), this collagen boasts 10 collagenous (COL) domains which are interspersed and bordered by noncollagenous domains (NC)(Oh, Warman et al. 1994, Dong, Cole et al. 2003). A segment derived from the C-terminal noncollagenous domain (NC1), named endostatin, exhibits anti-angiogenic properties both in a lab setting and within living organisms (O'Reilly, Boehm et al. 1997, Marneros and Olsen 2001); see **Figure 1.8**. Nevertheless, the absence of collagen XVIII and endostatin in both mice and humans doesn't spur angiogenesis in primary organs. This implies that neither this specific collagen nor its byproduct, endostatin, stands as the sole pivotal inhibitor of angiogenesis throughout development and subsequent growth (Sertié, Sossi et al. 2000, Fukai, Eklund et al. 2002).

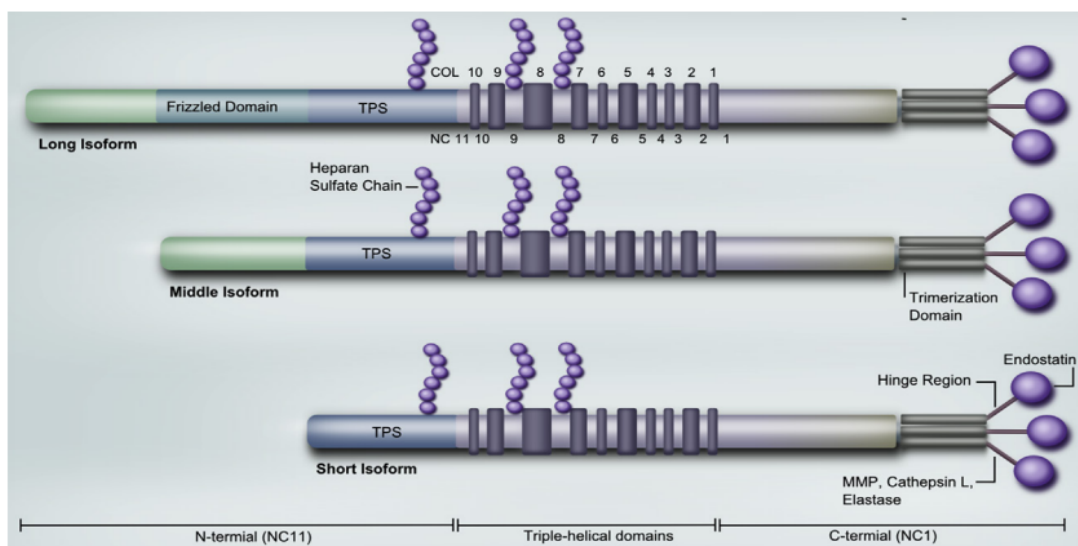


Figure 1.8 Schematic illustration of type XVIII collagen. The COL18A1 gene encodes three distinct isoforms: short, middle, and long. All three isoforms contain a thrombospondin (TSP) 1-like domain and 10 triple helical collagenous domains (Col1–10) flanked by 11 noncollagenous regions (NC1–11). The NC1 domain contains three functionally distinct subdomains: a trimerization domain, a protease sensitive hinge region, and a C-terminal endostatin domain. The long isoform contains an additional cysteine-rich Frizzled domain. Adapted from (Bager and Karsdal 2016).

1.8.1.1 Collagen XVIII/endostatin gene mutations in Knobloch syndrome

Collagen XVIII deficiency is associated with several developmental and age-related irregularities, prominently manifesting as deteriorating visual abilities and an increased risk of hydrocephalus. Studies on patients with Knobloch syndrome and corresponding mouse models carrying nonfunctional mutations in collagen XVIII/endostatin underscore the significance of this collagen in upholding epithelial operations in particular tissues.

Knobloch syndrome manifests as an autosomal recessive condition, hallmarked by vitreoretinal degeneration leading to retinal detachment, significant myopia, macular degeneration, and an occipital encephalocele (Knobloch and Layer 1972). Variability is noted in ocular anomalies, which might also encompass congenital cataracts, abnormalities of the iris, or lens dislocation in certain patients. Apart from the signature occipital encephalocele, additional abnormalities outside the eye are uncommon and not characteristic of the syndrome. However, ocular complications are severe, often culminating in blindness early in life (Sertié, Sossi et al. 2000).

Different isoforms of collagen XVIII are identifiable across a broad spectrum of tissues. The shorter version appears predominantly in vascular and epithelial BMs, while the lengthier ones find expression chiefly in the liver. The endostatin domain potentially orchestrates its biological impacts by interacting with BM heparan sulfate proteoglycans like perlecan or cell-surface variants like glypicans. Empirical binding assays have confirmed endostatin's direct bond with perlecan (Sasaki, Fukai et al. 1998), and significant colocalization of endostatin with perlecan in BMs is documented (Miosge, Simniok et al. 2003, Marneros, Keene et al. 2004).

It's plausible that diverse pathological mechanisms are responsible for the variances observed in *Coll8a1* null mice and Knobloch syndrome patients. Potential consequences of this deficiency, such as impaired neuronal cell migration, disruptions in the retinal vascular pattern, iris malformations, predisposition to hydrocephalus, delayed dissolution of hyaloid vessels, or enhanced vascular leakiness, might stem from the missing functionalities linked to the endostatin domain. Su et al. discovered that collagen XVIII and its derivative endostatin are produced by cerebellar Purkinje cells, crucial for organizing climbing fiber endpoints. Moreover, endostatin alone can trigger climbing fiber terminal formations via $\alpha 3\beta 1$ integrin pathways, offering insights

into how a lack of collagen XVIII in Knobloch syndrome might predispose individuals to neurological shortcomings (**Table 1.5**) (Su, Stenbjorn et al. 2012).

The missing promigratory traits of endostatin-oligomers could modify the astrocytic blueprint that ordinarily precedes the spread of retinal vasculature. This alteration could contribute to the unusual retinal vascular layout seen in *Coll8a1*^{-/-} mice. It's plausible that an absence of collagen XVIII disrupts vascular BM and endothelial cell interactions, as there is noted elevated vascular permeability in *Coll8a1* mutant mice and increased angiogenic growth in controlled experiments using these mice's aortas (Moulton, Olsen et al. 2004).

Subsequent research comparing the phenotypes of mutant mice carrying specific domain mutations in collagen XVIII with the abnormalities seen in *Coll8a1* null mice might elucidate the relationship between particular domains of collagen XVIII and their associated pathological processes. Additionally, by examining mutant mice devoid of collagen XVIII/endostatin and other angiogenesis-regulating elements, it might be possible to identify variances in angiogenic reactions in tissues that remain unaffected in *Coll8a1* null mice. These investigations could further clarify the significance of collagen XVIII/endostatin in physiologically modulating angiogenesis.

	Knobloch syndrome patients	<i>Coll8a1</i> ^{-/-} mice
Ocular system		
Progressive loss of vision	+++	++
Vitreoretinal degeneration	+++	++
Iris abnormalities	+	+++
Cataract	++	+?
Lens subluxation	+	?
Extraocular systems		
Occipital encephalocele	+++	-
Hydrocephalus predisposition	(+)	++
Renal abnormalities	(+)	?

Table 1.4 Comparison between major findings in Knobloch syndrome patients (COL18A1 mutations) and mutant mice in (*Coll8a1*^{-/-} mice) (adapted from (Marneros and Olsen 2005)).

2 AIMS AND OBJECTIVES

In this study, the main objective was to investigate the role of collagen XVIII in the integrity of the vascular system as well as the maintenance of the neurovascular unit in the context of CSVD. Also, I aimed to investigate if vascular changes are associated with alterations in synapses and perisynaptic ECM.

This thesis work includes the following objectives:

1. To investigate the validity of *Coll8a1*^{-/-} mice as a novel animal model to study early stages of CSVD.
2. To assess erythrocytes thrombi and BBB breakdown in young and aged *Coll8a1*^{-/-} mice.
3. To investigate the hallmarks of CSVD in this mouse model.
4. To investigate the expression of neural ECM molecules and related genes including the sulfotransferases and proteases using q-PCR and Western blot.
5. To investigate mRNA and protein expression levels of TJ proteins (occludin) and pericytes in *Coll8a1*^{-/-} mice.
6. To unravel the possible cellular and molecular mechanism(s) behind ECM alterations.

3 Material and Methods

In this thesis, the chemicals used for all experiments were from the following manufacturers: Invitrogen, Sigma-Aldrich, ThermoScientific, Abcam, Roche, Merck, and Gibco. In addition, buffers for RT-qPCR were prepared with deionized-double distilled water whereas, for immunohistochemistry and western blot, I used ultra-pure water. Details and composition of buffers are described below.

3.1 Gene targeting and generation of mutant mice

The generation of *Coll8a1*^{-/-} mice (B6.129S4-Coll8a1^{tm1Hms}; <http://www.informatics.jax.org/allele/MGI:2179134>) has been described (Seppinen and Pihlajaniemi 2011). Heterozygous *Coll8a1*^{+/-} mice underwent backcrossing with the C57BL/6J mouse strain (Jackson Laboratory) for over 15 generations. They were also crossbred with the C57BL/6JOlaHsd strain (Harlan) for over 10 generations and additionally with the C57BL/6NCrl strain (Charles River) on four occasions to develop a purebred C57BL/6 *Coll8a1*^{-/-} mouse lineage. This strain was sustained via backcrossing methods and breeding between heterozygous *Coll8a1*^{+/-} pairs. For all experimental evaluations, wild-type siblings (*Coll8a1*^{+/+}) served as the reference points. The genetic makeup of the mice was authenticated using polymerase chain reaction (PCR), following methods previously outlined (Ylikärppä, Eklund et al. 2003). The study made use of two groups: one set was fixated for histological inspection, while the other was utilized for both histological observations and q-PCR assessments as elaborated subsequently.

3.2 Tissue collection

3.2.1 Tissue preparation for hematoxylin and eosin staining and immunohistochemistry

For tissue preparation, animals were injected s.c. with ketamine (90 mg/kg body weight) and xylazine (18 mg/kg body weight), fentanyl (0,6 mg/kg body weight), midazolam (15 mg/kg body weight) and medetomidin (2,25 mg/kg body weight) in 0.9% NaCl solution and then transcardially perfused with phosphate buffered saline (PBS), followed by 4% paraformaldehyde containing PBS

(pump speed of 15 ml/min, duration 240 s each). The following day, the tissue was transferred through PBS washes from PFA to 30% sucrose in PBS for overnight cryoprotection, frozen in methylbutane (Carl Roth GmbH + Co. KG, Karlsruhe, GER) and stored at -80°C until sectioning. Coronal slices (thickness 30 μm) of the whole brain were prepared using a cryostat and stored in cryo-protection solution (25% ethylene glycol, 25% glycerin, 50% 0.1 M PBS pH 7.4) at 4°C . From the frontal to the occipital pole, 3 brain slices were taken from each of the 6 sectional planes with a distance of 750 μm between each sectional plane (18 brain slices per animal in total) for hematoxylin and eosin (HE) staining and immunohistochemistry (IHC) analysis. In this study, HE analysis was performed on sections from 7 wild-type (*Coll8a1*^{+/+}) and 5 *Coll8a1*^{-/-} 5-month-old mice as well as from 5 *Coll8a1*^{+/+} and 6 *Coll8a1*^{-/-} 12-month-old mice. Furthermore, IHC analysis was performed on sections from 6 *Coll8a1*^{+/+} and 5 *Coll8a1*^{-/-} 5-month-old mice and 5 *Coll8a1*^{+/+} and 5 *Coll8a1*^{-/-} 12-month-old mice.

3.2.2 Tissue preparation for qPCR and western blot

After an overdose with i.p. injection of ketamine (75 mg/kg body weight), xylazine (10 mg/kg body weight) and acepromazine (3 mg/kg body weight), tissue isolation for quantitative PCR (qPCR) and western blot was performed by intracardial perfusion with ice-cold PBS (pump speed of 15 ml/min, duration 70 s), quick decapitation, and dissection of the brain into ice-cold PBS. Left hippocampi and right cortex from the second batch of animals were stored for RNA extraction and western blot, respectively. Six *Coll8a1*^{+/+} and 11 *Coll8a1*^{-/-} 12-month-old mice were used for qPCR and western blot analysis.

3.3 Histology

For HE staining, brain slices were washed with distilled water twice, incubated with hematoxylin (Carl Roth GmbH + Co. KG, Karlsruhe, GER) for 5 min and washed again, followed by bluing under running tap water for 10 min and another rinse with distilled water. Afterwards, staining was performed with 1% eosin solution (Carl Roth GmbH + Co. KG, Karlsruhe, GER) for 40 s. After dehydration with increasing concentrations of alcohol (Rotisol, Carl Roth GmbH + Co. KG,

Karlsruhe, GER), slices were finally placed in Xylene (Carl Roth GmbH + Co. KG, Karlsruhe, GER) and mounted with coverslips using Histomount (Fisher Scientific GmbH, Schwerte, GER).

3.4 Quantification

The following CSVD hallmarks were quantified in the HE-stained brain slices: (i) nonocclusive erythrocyte thrombi defined as the accumulation of erythrocytes in the lumen of the vessels (subsequently referred to as erythrocyte thrombi)(Jandke, Garz et al. 2018), (ii) small perivascular bleeds/microbleeds defined as leakage of erythrocytes out of the vessel, and (iii) enlarged PVS defined as distended, white, nonstained perivascular areas.

Erythrocyte thrombi and small perivascular bleeds were counted in 25 randomly chosen fields of view (FOVs) in different brain regions (retrosplenial cortex (RSC), basal ganglia (BG), hippocampal CA1 region, corpus callosum (CC) and thalamus) in both hemispheres. When quantifying, we additionally differentiated between two different types of vessels: (i) capillaries with a luminal diameter $< 10 \mu\text{m}$ and (ii) small vessels defined through a luminal diameter $> 10 \mu\text{m}$ (Carare, Bernardes-Silva et al. 2008). For statistical analysis, the mean of all FOVs per brain region was calculated.

For PVS measurements, 18 FOVs per brain region (see above) were quantified in each animal. In each FOV, all arterioles and the number of arterioles with PVS in the same FOV were counted. Percentages of arterioles with PVSs per FOV were then calculated, and mean values per animal were used for statistical analysis.

3.5 RNA extraction, cDNA conversion, and qPCR

A total RNA extract was prepared from the frozen hippocampal region using the EURx GeneMatrix DNA/RNA Extracol kit (Roboklon Cat. No. E3750), following the manufacturer's recommendations (Ventura Ferreira, Bienert et al. 2018). Nano-drops were used to measure the yield, purity, and integrity of RNA. Furthermore, the High-Capacity cDNA Reverse Transcription Kit (Cat. 4368814) was used for the conversion of $1.5 \mu\text{g}$ of RNA to cDNA, and then real-time (RT)-qPCR was performed using a TaqMan gene expression array (Cat. 4331182) from ThermoFisher Scientific using Quant-Studio-5 from Applied Biosystems (**Table 3.1**). Overall, 50 genes

were analyzed, comprising five chondroitin sulfate proteoglycan (CSPG) genes, namely, aggrecan (*Acan*), versican (*Vcan*), neurocan (*Ncan*), phosphacan (*Pcan*) and brevican (*Bcan*), four genes coding for link proteins, hyaluronan and proteoglycan link protein (*Hpln2*, *Hpln3*, *Hpln4*) and tenascin-R (*Tnr*), five genes for major metalloproteinases degrading neural ECM proteins, namely, matrix metalloproteinase 2 (*Mmp2*), matrix metalloproteinase 9 (*Mmp9*), cathepsin S (*Ctss*), a disintegrin-like and metalloproteinase with thrombospondin type 1 motif, 4 (*Adamts4*), a disintegrin-like and metalloproteinase with thrombospondin type 1 motif, 5 (*Adamts5*) and four genes coding for tissue metalloproteinases inhibitors (*Timp1*, *Timp2*, *Timp3*, *Timp4*). In addition, three genes coding for tight junction proteins - occludin (*Ocln*), claudin-5 (*Cldn5*) and zonula occludens-1 (*Zo1*) - and six genes coding for basement membrane proteins laminin alpha5 (*Lama5*), nidogen1 (*Nid1*), collagen III alpha 1 (*Col3a1*), collagen IV alpha 1 (*Col4a1*), collagen VIII alpha 1 (*Col8a1*), vascular cell adhesion molecule 1 (*Vcam1*) and lysyl oxidase-like 2 (*Loxl2*) were also analyzed. Additionally, the expression of three astrocyte markers, glial fibrillary acidic protein (*Gfap*), aquaporin 4 (*Aqp4*), and S100 calcium-binding protein A10 (*S100a10*); microglial genes, allograft inflammatory factor 1 (*Iba1*), targeting receptor expressed on myeloid cell 2 (*Trem2*), complement component 1 (*C1q*), complement component 3 (*C3*), myeloperoxidase (*Mpo*), *Cd68*, *Cd86*, *Cd13*, *Cd47*, chemokine (C-C motif) ligand 2 (*Ccl2*); transforming growth factor beta 1 (*Tgfb1*); two oligodendrocyte/oligodendrocyte progenitor cell (OPC) markers, proteolipid protein (myelin) 1 (*Plp1*) and chondroitin sulfate proteoglycan 4 (*Cspg4*); pericyte marker (*Pdgfrb*), alpha smooth muscle (*Asma*); and three interleukins (*Il1b*, *Il6*, and *Il33*) and Tumor necrosis factor (*Tnfa*) were also quantified and analyzed relative to the expression of glyceraldehyde 3-phosphate dehydrogenase (*Gapdh*). The *Gapdh* gene was used to normalize the expression levels of these genes as a housekeeping gene whose expression was not altered in the compared conditions (Meldgaard, Fenger et al. 2006).

Gene	Full description	Reference Sequence	Sequence (5' to 3')
<i>Acan</i>	Mouse_Aggrecan_Mm00545794_m1	NM_007424.2	Fw CCCCCCGCGCAGAGCATCCC
			Rv AAGACATTGGAAGAGATCTA
<i>Vcan</i>	Mouse_Versican_Mm01283063_m1	NM_001081249.1	Fw GCCTGTTTCCAAGCTGGGGC
			Rv AAAATTCCTCTTTTACTACA
<i>Ncan</i>	Mouse_Neurocan_Mm00484007_m1	NM_007789.3	Fw GGAGGCTGCGCCTGGCGTGC
			Rv TTAATAAAAAAAAAAAAAAAAAA
<i>Pcan</i>	Mouse_PTPRZ1_Phosphocan_Mm00478484_m1	NM_001081306.1	Fw AATTCCGCGCCGCTGCGCTG
			Rv AATATAAATATTGCTATTAA

<i>Bcan</i>	Mouse_Brevican_Mm00476090_m1	NM_001109758.1	Fw CGCTGTCGCCCCGGAACCCGC Rv ATTAAACTGCTTTGTACCCA
<i>Hpln2</i>	Mouse_Hpln2_Mm00480745_m1	NM_022031.2	Fw AGAAAAGAAAAGGACAGACA Rv TACTATAATAAATCCACTTG
<i>Hpln3</i>	Mouse_Hpln3_Mm00724203_m1	NM_178255.3	Fw AGGCCATTCAAGATCCCAAA Rv TTATTATTATTTTATTTTAC
<i>Hpln4</i>	Mouse_Hpln4_Mm00625974_m1	NM_177900.4	Fw GCACTGGCCGCTCAGCAAGG Rv ATTAAAGGTGTAAGCCACCA
<i>Tnr</i>	Mouse_TenascinR_Mm00659075_m1	NM_022312.3	Fw AGTAAGAGGGGAAAAGAGAG Rv AATCATTGTCGTGTAATAAC
<i>Ocln</i>	Mouse_Occludin_Mm00500912_m1	NM_008756.2	Fw GGGTGGGGGAAGCGGAGGAC Rv AATTTAAATAATGTTTTTGT
<i>Cldn5</i>	Mouse_Claudin5_Mm00727012_s1	NM_013805.4	Fw AGTTGGTGTAGTTAAAACCT Rv GTTTGAACACTTTCAAAAAA
<i>Zol1</i>	Mouse_Tjp1_Mm01320638_m1	NM_001163574.1	Fw GTGGCCGCCTGAGTTGCCCG Rv AAAAAAAAAAAAAAAAAAAAAA
<i>Lama5</i>	Mouse_Laminin, alpha5_Mm01222029_m1	NM_001081171.2	Fw ACTTGCCGGCTCCTGCGGT Rv TTGAAAAAAAAAAAAAAAAAAAAA
<i>Nid1</i>	Mouse_Nidogen1_Mm00477827_m1	NM_010917.2	Fw GGGAGGTGAGGAGGACTGC Rv AAAATAAAATCTTATTTTGA
<i>Col3a1</i>	Mouse_Collagen, typeIII, alpha 1_Mm00802300_m1	NM_009930.2	Fw GGATGGGTTCTGCTCTCATA Rv TAAAATATCATAATGAAACA
<i>Col4a1</i>	Mouse_Collagen, type IV, alpha 1_Mm01210125_m1	NM_009931.2	Fw TTGAGACGCCGCCCGCGCA Rv AAAAAAAAAAAAAAAAAAAAAA
<i>Col8a1</i>	Mouse_Collagen, type VIII, alpha 1_Mm01344184_m1	NM_007739.2	Fw AAGTGCAAGTTACCCGCAGA Rv TAAATATCTCTAAAAATATG
<i>Vcam1</i>	Mouse_Vascular cell adhesion molecule 1_Mm01320970_m1	NM_011693.3	Fw GCCCTTCGAGCTGAAGGT Rv AATACAGATACTCGAAACAT
<i>Loxl2</i>	mOUSE_Lysyl oxidase-like 2_Mm00804740_m1	NM_033325.2	Fw GTCTCACTTTGCCCGGTCC Rv AACTCTCTGCTTTAAAAAAA
<i>Mmp2</i>	Mouse_Matrix metallopeptidase 2_Mm00439498_m1	NM_008610.2	Fw CCAGCCGGCCACATCTGGCG Rv AAAAAAAAAAAAAAAAAAAAAA
<i>Mmp9</i>	Mouse_Matrix metallopeptidase 9_Mm00442991_m1	NM_013599.3	Fw TGCAAAGGCAGCGTTAGCCA Rv AATGAATATTTACTTATTT
<i>Ctss</i>	Mouse_Cathepsin S_Mm01255859_m1	NM_001267695.2	Fw TTCTCATTGTGGATGCTTC Rv TCTGTCATTTCAAATATCTA
<i>Adams4</i>	Mouse_a disintegrin-like and metallopeptidase with thrombospondin type 1 motif,4_Mm00556068_m1	NM_172845.2	Fw GGGGAGAACCCGGGGAAGAC Rv GAACTAGCATAGAGCCTCTC
<i>Adams5</i>	Mouse_a disintegrin-like and metallopeptidase with thrombospondin type 1 motif,5_Mm00478620_m1	NM_011782.2	Fw GAAATTGCCATTGCAGGATG Rv GCACAGGAATAAAAATCAGT
<i>Timp1</i>	Mouse_Tissue inhibitor of metalloproteinase 1_Mm01341361_m1	NM_001044384.1	Fw AGGCTTTGACTCCAGCGGTG Rv AGCAAAAAAAAAAAAAAAAAAAAA
<i>Timp2</i>	Mouse_Tissue inhibitor of metalloproteinase 2_Mm00441825_m1	NM_011594.3	Fw CCGGCCTGCACTGGCCGCCA Rv AAGAGAAAAAAAAAAAAAAAAAAAA
<i>Timp3</i>	Mouse_Tissue inhibitor of metalloproteinase 3_Mm00441826_m1	NM_011595.2	Fw GCGCCCCCGCCCCGCCCC Rv AGTGGTTTTATTTCTATCAC
<i>Timp4</i>	Mouse_Tissue inhibitor of metalloproteinase 4_Mm01184417_m1	NM_080639.3	Fw GGAGGAGTCTGGAGGGGCT Rv AAGCATTTTCCCTCCAGGTT
<i>Gfap</i>	Mouse_Glial fibrillary acidic protein_Mm01253033_m1	NM_001131020.1	Fw CCAGGAAGTCAGGGCAGAT Rv TGCTCCCTGCTCTTCATTTT
<i>Aqp4</i>	Mouse_Aquaporin 4_Mm00802131_m1	NM_009700.2	Fw AGTGTACTGGAGCCCGGGGG Rv TATATTTGATGGTGTTTAAG
<i>S100a1</i>	Mouse_S100 calcium binding proten A10_Mm00501457_m1	NM_009112.2	Fw GTACCCGCCTCGCGTACAAA Rv TCCTTTTTTTAAGTTCTGAA
<i>Iba1</i>	Mouse_Allograft inflammatory factor 1_Mm00479862_g1	NM_019467.2	Fw AGACGAACCCTCTGATGTGG Rv AATGACGCTCCTAGTGGGTC
<i>Trem2</i>		NM_001272078.1	Fw GCGCCTACCCTAGTCTGAC

	Mouse_triggering receptor expressed on myeloid cells 2_Mm04209424_g1		Rv CAACCCCATTTCTCCACACAC
<i>C1q</i>	Mouse_Complement component 1_Mm07295529_m1	NM_007572.2	Fw ATGAAACTTGGCAGTGTCTCT Rv TCCCCGTCTGTGTCTGTGAC
<i>C3</i>	Mouse_complement component 3_Mm01232779_m1	BC029976.1	Fw CGGACGCGTGGGGGCTGTTA Rv AAAAAAAAAAAAAAAAAAAAAA
<i>Mpo</i>	Mouse_Myeloperoxidase_Mm01298424_m1	NM_010824.2	Fw ATAACCTTCTCAGCTTTAGCT Rv AAAAAAAAAAAAAAAAAAAAAA
<i>Cd68</i>	Mouse_CD68 antigen_Mm03047343_m1	NM_001291058.1	Fw TTTTAGTTAAGGGAAGTGAG Rv AAAACTAAAAAAAAAAAAAAAAA
<i>Cd86</i>	Mouse_CD86 antigen_Mm00444540_m1	NM_019388.3	Fw ATTGCTGAGGAAGAAAGAGG Rv TTTTCTTGAATTTTTTCAAG
<i>Cd13</i>	Mouse_Alanyl (membrane) aminopeptidase_Mm00476227_m1	NM_0048486.2	Fw GGCAGTGGGGCTCCACCCCC Rv TGAAAAAAAAAAAAAAAAAAAAA
<i>Cd47</i>	Mouse_CD47 antigen (Rh-related antigen,integrin-associated signal transducer) Mm00495011_m1	NM_010581.3	Fw CCCGGGCAGCCTGGGCGGCC Rv AAAAAAATCAGAAAAAAAAA
<i>Ccl2</i>	Mouse_Chemokine (C-C motif) ligand 2_Mm00441242_m1	NM_011333.3	Fw GCAGAGAGCCAGACGGGAGG Rv ATATATTATTTTTGTACACC
<i>Tgfb1</i>	Mouse_Transforming growth factor, beta 1_Mm01178820_m1	NM_011577.1	Fw CGCCGCCGCCGCCGCCCTTC Rv GGCCCGCCCGCCCGCCCGCC
<i>Plp1</i>	Mouse_Proteolipid protein (myelin) 1_Mm01297210_m1	NM_001290561.1	Fw AATCAGAAAGCCCTTTTCAT Rv AAATACTTGTCTCAAATTGA
<i>Cspg4</i>	Mouse_Chondroitin sulfate proteoglycan 4_Mm00507257_m1	NM_139001.2	Fw GACTTGC GACTTGC GACTCG Rv TAAATAAATAAATGCTCCCA
<i>Pdgfrb</i>	Mouse_Platelet derived growth factor receptor, beta polypeptide_Mm00435553_m1	NM_001146268.1	Fw GGGGCAGAGAAAGCCACAG Rv TGCTTCTCACTGAATAACCG
<i>Asma</i>	Mouse_actin,apha2, smooth muscle_Mm00725412_s1	NM_007392.3	Fw CAAGGGGCTATATAACCCTT Rv AATAAAATGTGACAACCGGA
<i>Il6</i>	Mouse_Interleukin 6_Mm00446190_m1	NM_031168.1	Fw CCAAGAACGATAGTCAATTC Rv AAATAAATTATATTATATT
<i>Il33</i>	Mouse_Interleukin 33_Mm00505403_m1	NM_001164724.1	Fw AGCTCTCCACCGGGGCTCAC Rv TCAAAACCACGTGTGACCAC
<i>Il1b</i>	Mouse_Interleukin 1 beta_Mm00434228_m1	NM_008361.3	Fw CGAGGCCTAATAGGCTCATC Rv ATTTTCATTAACAAACAAA
<i>Tna</i>	Mouse_Tumor necrosis factor_Mm00443258_m1	NM_001278601.1	Fw AGCAGAAGCTCCCTCAGCGA Rv CGCTTGAAAAGAAATGTGA

Table 3.1 Taqman probes used for real-time PCR analysis.

3.6 SDS-PAGE and Western blot analysis

Brain samples from 12-month-old mice (from the right cortex) were processed using a motorized Teflon-glass homogenizer, performing 12 repetitive strokes. We used a 5 mM Hepes buffer (pH 7.4) containing 0.32 M sucrose and a cocktail of protease inhibitors (Complete; Boehringer Mannheim) at a ratio of 1g (wet weight) brain to 4 ml of buffer. The resulting mixtures were then brought to a 10% (wt/vol) dilution. For a semi-quantitative evaluation of brevicin fragments, samples underwent digestion with chondroitinase ABC (procured from Sigma-Aldrich, St. Louis, USA) under specified conditions, and later prepared in 5x SDS loading buffer. Post boiling at 95°C

for a duration of 10 minutes, samples were loaded onto 5–20% Tris-glycine SDS polyacrylamide gels that contained 2,2,2-trichloroethanol (TCE).

Subsequent to gel electrophoresis, proteins were UV-activated for 5 minutes prior to the Western blot transfer onto PVDF membranes (sourced from Merck Millipore, Burlington, MA, USA). To ensure efficient protein transfer, UV images of the membranes were taken. Membranes, post blocking, were incubated with primary antibodies at 4°C, then followed with secondary antibodies at room temperature. The resultant membranes underwent imaging on an ECL Chemocam Imager (from INTAS Science Imaging Instruments GmbH, Göttingen, Germany).

To ensure uniformity and consistency in the semi-quantitative comparison of immunoblot data, we used a standard sample on every gel to offset potential gel-based discrepancies. We utilized the NHI ImageJ software version 1.52a (offered by US National Institutes of Health, Bethesda, MD, USA) for the quantification of the band intensities. The integrated density of signals was measured by setting identical, rectangular regions of interest around the bands on the same membrane. In the provided figures, the molecular weight of markers is presented in kDa, and antibodies used for Western blot detection are noted.

Buffer	Composition	Composition
10x TG-Running buffer	Tris-HCl (0.25M)	Carl Roth 5429.2
	Glycerol (1.92M)	Carl Roth 3783.2
	SDS (1%)	Carl Roth 2326.3
10x TG-Blot buffer	Tris-HCl (0.25M)	Carl Roth 5429.2
	Glycerol (1.92M)	Carl Roth 3783.2
	SDS (0.2%)	Carl Roth 2326.3
4x SDS-PAGE sample buffer	Tris (250 mM)	Carl Roth 5429.2
	4% SDS	Carl Roth 2326.3
	40% Glycerol	Carl Roth 3783.2
	20% β -Mercaptoethanol	Ferak Berlin 31012
	0.004% Bromphenolblau	Serva 15375
10x TBS	Tris-HCl (0.5M)	Carl Roth 5429.2
	NaCl	Carl Roth 3957.1
TBST	1x TBS	
	Tween 20	Carl Roth 9127.1
5% Milk	Nonfat dried milk powder	PanReac Applichem P100810

Table 3.2 Buffers and solutions for Immunoblotting.

Reagent or Resource	Dilution	Source	Identifier
----------------------------	-----------------	---------------	-------------------

Primary reagents for histochemistry			
Rabbit anti-Smad3 (EP568Y)	1:1000	Abcam, Cambridge, UK, USA	Cat # AB40854
Rabbit anti-Smad3 (phosphor S423+S425) (EP823Y)	1:1000	Abcam, Cambridge, UK, USA	Cat# AB52903
Rabbit anti-TGF beta 1	1:1000	Abcam, Cambridge, UK, USA	Cat#AB215715
Rabbit anti- VCAM1	1:1000	Abcam, Cambridge, UK, USA	Cat# AB134407
Rabbit anti-TIMP-3	1:1000	Abcam, Cambridge, UK, USA	Cat# AB39184
Brevican	1:1000	LIN	
Rabbit anti-ADAMTS-4	1:1000	Abcam, Cambridge, UK, USA	Cat#AB185722
Rabbit anti-PDGFRbeta	1:1000	Abcam, Cambridge, UK, USA	Cat#AB32570
Rabbit anti-Occludin	1:1000	Abcam, Cambridge, UK, USA	Cat# 216327
Secondary reagents for histochemistry			
Donkey anti-rabbit POD	1:10000	JacksonImmunoResearch	Cat#711035152

Table 3.3 Primary and secondary reagents used for Immunoblotting.

3.7 Immunohistochemistry

All sections were washed at room temperature (RT) three times with 120 mM phosphate buffer (PB), pH = 7.2, for 10 min each wash, followed by permeabilization with 0.5% Triton X-100 (Sigma-Aldrich Inc. T9284, St. Louis, MO, USA) in PB for 10 min at RT. The sections were subsequently blocked using a blocking buffer (0.4% Triton X-100 + 10% goat serum (Gibco 16210-064, Amarillo, TX, USA/Thermo Fisher Scientific 16210-064, Waltham, MA, USA) + 0.1% glycine in PB) for 45–60 min at RT. Afterward, sections were either incubated overnight at 37 °C or for 2 days at 4 °C depending on which primary reagents were used (**Table 3.4**). Following three washes with PB, sections were incubated with secondary antibodies (**Table 3.5**) for 2 h at RT. Labeled sections were washed again three times at RT for 10 min in PB and mounted on glass slides using Fluoromount medium (Sigma-Aldrich F4680, St. Louis, MO, USA) (Kaushik, Morkovin et al. 2018).

Buffer	Composition
4% paraformaldehyde (PFA) (w/v)	4 % PFA in PBS, pH 7.4
Phosphate buffer (PB)	0.1 M sodium phosphate dibasic; 0.1 M sodium phosphate monobasic

Pemeabilization solution	0.4 % Triton-X 100 in PB
Blocking Solution	10 % normal goat serum (NGS) in PB, 0.4 % Glycine, 0.4 % Triton-X 100
Floating solution	Ethylene glycol, glycerin, PBS in the ratio 1:1:2

Table 3.4 Buffers and solutions for IHC.

Reagent or Resource	Dilution	Source	Identifier
Primary reagents for histochemistry			
STL-FITC	1:250	Vector Laboratories, Newark, CA, USA	Cat # FL-1161
Rabbit anti-Iba1	1:1000	Wako, Richmond, VA, USA	Cat# 019-19741
Chicken anti-GFAP	1:500	Millipore, Boston, MA, USA	Cat#AB5541
Rabbit anti-C1q	1:1000	Abcam, Cambridge, UK, USA	Cat# ab182451
Rabbit anti-aggrecan (Acan)	1:300	Millipore, Boston, MA, USA	Cat# AB1031
chicken anti-parvalbumin (PV)	1:500	Synaptic Systems, Gottingen, Germany	Cat#195006
Biotinylated-WFA	1:1000	BioLogo (Vector Laboratories), , Burlingame, CA, USA	Cat# B1355
Chicken anti-VGLUT1	1:1000	Synaptic systems, Gottingen, Germany	Cat# 135316
Chicken anti-VGLUT2	1:1000	Synaptic Systems, Gottingen, Germany	Cat# 135416
Guinea pig anti-VGAT	1:500	Synaptic Systems, Gottingen, Germany	Cat# 131004
Guinea pig anti-Homer1	1:500	Synaptic Systems, Gottingen, Germany	Cat# 160004
Rabbit anti-brevican (Bcan)	1:1000	LIN, Magdeburg, Germany	[81] [34]
Rabbit anti-fibrinogen	1:500	Abcam, Cambridge, UK, USA	Cat#ab92572
Secondary reagents for histochemistry			
Goat anti-rabbit Alexa Fluor 546	1:1000	Invitrogen, Waltham, MA, USA	Cat# A-11035
Goat anti-mouse Alexa Fluor 647	1:200	Invitrogen, Waltham, MA, USA	Cat# A-21236
Goat anti-chicken Alexa Fluor 546	1:1000	Invitrogen, Waltham, MA, USA	Cat# A-11039
Goat anti-rabbit Alexa Fluor 405	1:1000	Invitrogen, Waltham, MA, USA	Cat# A-31556
Goat anti-Guinea pig Alexa Fluor 405	1:1000	Invitrogen, Waltham, MA, USA	Cat# A-31553
Streptavidin Alexa Fluor 405	1:1000	Invitrogen, Waltham, MA, USA	Cat# S-32351

Table 3.5 Primary and secondary reagents used for histochemistry.

3.8 Image acquisition and histochemical measurements

To analyze the tissue distribution of mouse immunoglobulin G (IgG) in *Solanum tuberosum* lectin-fluorescein isothiocyanate (STL-FITC)-fluorescent small vessels, the expression of ECM markers, astroglial/microglial cell activation, and synaptic puncta, images were acquired using a Zeiss confocal microscope (LSM 700) and EC Plan-Neofluar 20×/0.50 M27, 40×1.3 oil M27 and 63×/1.40 oil M27 objectives by an experimenter blinded to the experimental groups. Consistent acquisition conditions were upheld across all imaging sessions to ensure accurate fluorescence intensity comparisons among samples. Images were further processed and analyzed using the open software ImageJ (Fiji) (Schindelin, Arganda-Carreras et al. 2012) and MATLAB 2019a (MathWorks, Natick, MA).

3.9 Detection and quantification of IgG leakage as an indicator of BBB breakdown

BBB integrity was assessed by measuring the parenchymal abundance of mouse IgG. Briefly, sections containing the RSC, dorsal striatum (DS), CA1, BG, thalamus, and medial prefrontal cortex (mPFC) from young animals as well as the RSC and CA1 from aged animals were immunostained with anti-mouse IgG antibody and STL-FITC. Accordingly, we calculated the vascular leaks as a percentage of overlap between IgG⁺ area and STL⁺ relative to the total STL⁺ area. To accomplish this, we measured the positive area (in μm^2) represented in each IHC-stained section by using self-developed MATLAB code based on a thresholding technique. Analyses were performed on nine images from each region of each animal.

3.10 Vessel-associated microglia/perivascular macrophages

The association of microglia/perivascular macrophages with blood vessels was quantified in fluorescence microscopy images using Fiji by comparing the vessel area associated with microglia and the total area of blood vessels in FOVs located in the CA1 region. To quantify the associated area, we used color thresholding and binary analysis. Manual thresholds were set according to signal intensities. Then, the selected threshold value was applied to all animals, and the resulting

data represent the percentage of signal colocalization. Ten random images from each group were analyzed.

3.11 Microglia and C1q analyses

The prevailing understanding is that microglia undergo noticeable morphological alterations upon activation, including an expansion of the soma and a decrease in microglial processes (Glenn, Ward et al. 1992, Hovens, Nyakas et al. 2014). Ionized calcium-binding adaptor molecule 1 (Iba1) antibody recognizes the microglial protein Iba1, which is commonly used as a microglia/macrophage-specific marker. For the evaluation of the arborization area, somatic area and number of positive (Iba1⁺) cells, nine images per animal were acquired. Square regions of interest (ROIs) ($374 \times 374 \mu\text{m}^2$) were selected in the RSC and CA1. Thresholding and size exclusion standards were utilized in two distinct ways to determine the overall branching area and the soma area of Iba1⁺ cells. For measuring the entire area encompassed by branching, the first thresholding method employed was autothresholding using the mean dark option. In contrast, for the soma area, the second method utilized autothresholding with the triangle dark option. To compute the total area occupied by Iba1 branching, the soma area was deducted from the entire area. For accurately tallying the number of Iba1⁺ cells, the second thresholding approach was paired with a size-exclusion criterion. In every animal, disparities in the mean arborization area and somatic area for each cell were determined and standardized. The counting of Iba1⁺ cells was done by hand.

For evaluating microglial morphology, we also employed 3DMorph, a script rooted in MATLAB designed for interpreting microglial form in 3D, as elaborated by York, LeDue et al. (2018). In essence, this tool leverages graphical user interfaces to initially set an image threshold, establish noise limits, and stipulate cell dimensions. Users are prompted to input specific threshold values, anticipated cell sizes, and their chosen method for skeletonization. Once these parameters were established, the program proceeded to conduct measurements autonomously. Data produced from this analysis encompassed metrics like cell volume, territorial space, branch length, count of endpoints and branch junctions, and the mean spacing between cells. For the purpose of the 3DMorph analysis, three snapshots for each animal were captured in the CA1 zone utilizing a Zeiss LSM 700 confocal microscope, which was paired with an EC Plan-Neofluar, 63×/1.40 oil M27

lens. The captures were done at 16-bit, encompassing 12 optical layers, with 0.2 μm spacing between layers and resolution at $1,024 \times 1,024$ pixels, each pixel spanning 0.625 μm .

For quantitation of C1q expression in the *stratum radiatum* of the CA1 region and RSC, images were analyzed using Fiji software. Three ROIs (squares) were defined randomly within soma-free ROIs, and the mean pixel intensity per ROI was determined. The mean ROI intensity per animal was obtained by averaging all ROI mean intensities in the sections studied (three sections per region).

3.12 Astroglia analysis

Glial fibrillary acid protein (GFAP) antibody has been extensively used to investigate astrocytic activation (Nolte, Matyash et al. 2001). To count GFAP-positive (GFAP⁺) cells, 3 images per animal were taken in the CA1 region using a Zeiss LSM 700 confocal microscope equipped with an EC Plan-Neofluar, 40 \times 1.3 oil M27 objective (16-bit, 12 optical sections, 1.2 μm intervals between sections, $1,024 \times 1,024$ pixels, pixel size of 0.625 μm). Autothresholding (moments dark option) and size exclusion criteria (size = 20) were applied in Fiji to measure the area and mean intensity of GFAP⁺ cells on the maximum intensity z-projection images. The number of GFAP⁺ cells was counted manually.

3.13 Neural ECM analysis

To count the perineuronal net (PNN)-associated and parvalbumin (PV)-immunopositive (PV⁺) cells, 3 images per animal were taken per RSC and the CA1 region using a Zeiss LSM 700 confocal microscope equipped with an EC Plan-Neofluar, 40 \times 1.3 oil M27 objective (16-bit, 12 optical sections, 1.2 μm intervals between sections, $1,024 \times 1,024$ pixels, pixel size of 0.625 μm). The numbers of PV⁺ Acan-immunopositive (Acan⁺) and PV⁺ Acan-immunonegative (Acan⁻) cells were counted manually. The soma area and intensity were measured on the maximum intensity z-projection images using Fiji as described below.

Biotinylated *Wisteria floribunda* agglutinin (WFA) and anti-Aggrecan antibodies were used to label the ECM of PNNs. WFA labels Gal- and GalNAc-terminated glycoepitopes on core ECM proteins, such as lecticans, whereas Aggrecan antibody labels the Acan core protein (Morawski,

Dityatev et al. 2014, Matuszko, Curreli et al. 2017). High-resolution images for WFA/vesicular GABA transporter (VGAT) analysis were acquired using a Zeiss LSM 700 confocal microscope and the EC Plan Apochromat 63×/1.40 oil M27 objective. For each animal, 3 images of WFA/VGAT cells per animal were acquired in the RSC and CA1 (16-bit, 14 optical sections, 0.170 μm intervals between sections, 1,024 \times 1,024 pixels, pixel size of 0.099 μm).

For soma size and mean intensity quantification, the soma of PV⁺ Acan⁺ cells were manually outlined, and a band of 1.5 μm was then created as the ROI to measure the mean intensity and soma area of PV cells and the mean intensity of Acan signals. In addition, the somatic area of Acan⁺ cells was measured as described. For further analysis, the somatic area and mean intensity of WFA⁺ cells were manually outlined and analyzed by creating a band of 1.5 μm around cells as the ROI.

For the quantification of the expression of VGAT⁺ puncta on WFA⁺ cells, the soma was manually outlined by creating a band of 1.5 μm as the region of interest (ROI). Then, the mean intensities of at least 5 cells were averaged in each region to obtain the mean ROI intensity per animal. At least 5 cells per section were measured and averaged for each mouse (three sections per region).

3.14 Analysis of presynaptic and postsynaptic markers

Past research indicates that the reduction in glutamatergic synapses, along with alterations in the expression of proteins on both the pre- and post-synaptic ends, are associated with cognitive decline in CSVD as well as Alzheimer's disease (AD) (Kirvell, Esiri et al. 2006, Kashani, Lepicard et al. 2008). To count synapses, 3 images per animal were taken per RSC and the CA1 region using a Zeiss LSM 700 confocal microscope equipped with an EC Plan-Neofluar, 40×1.3 oil M27 objective (16-bit, 12 optical sections, 1.2 μm intervals between sections, 1,024 \times 1,024 pixels, pixel size of 0.625 μm). We analyzed the mean ROI intensity and the numbers of presynaptic vesicular glutamate transporter 1 (VGLUT1)- and vesicular glutamate transporter 2 (VGLUT2)-immunopositive puncta in the neuropil area. The expression levels of VGLUT1 and VGLUT2 in the CA1 *stratum radiatum* and RSC were quantified using Fiji software. Three ROIs (squares) were defined randomly within soma-free ROIs, and the mean pixel intensity per ROI was determined. To obtain the mean ROI intensity per animal, three ROI mean intensities in each region were averaged.

Furthermore, we analyzed Homer-1-immunopositive puncta because Homer-1 is a postsynaptic scaffolding protein that regulates glutamatergic synapses and spine morphogenesis. The expression levels of Homer-1 in CA1 *str. radiatum* and RSC were quantified using Fiji. To determine the mean pixel intensity within each ROI, three random ROIs (squares) were defined within soma-free ROIs, and then three ROI mean intensities were averaged in each region to obtain the mean ROI intensity per animal.

3.15 Analysis of VGLUT1⁺ puncta and perisynaptic brevican

In our endeavor to understand synaptic modifications in the mature *Coll8a1*^{-/-} mouse RSC and CA1, and to draw connections to the associated perisynaptic ECM, we introduced a semi-automated open-source Fiji tool dubbed Analysis of PeriSynaptic Matrix (APSM_v1.1) (Strackeljan, Baczynska et al. 2021). This software is tailored for confocal z-stacks, prompting users to pinpoint the most distinct focus plane for evaluation purposes. The tool recognizes high-intensity pixel clusters, indicative of presynaptic boutons amidst a noisy backdrop within brain sections. Additionally, it facilitates the exclusion of puncta that don't typify synaptic boutons based on attributes like intensity, size, and form. Unlike other thresholding techniques available in Fiji, this tool enabled us to seamlessly segment presynaptic boutons, facilitating an assessment of individual synaptic puncta and their associated ECM. These proteins' expression in the CA1 *str. radiatum* was subsequently assessed.

After manual selection of the most vivid VGLUT1 signal, the software proceeds with a maximum intensity projection spanning 3 z-planes (comprising the central chosen plane plus the adjacent top and bottom planes), from where it negates the background and incorporates a Gaussian filter. Subsequently, the Find Maxima algorithm is employed (with a user-specified prominence of 2, excluding maxima on image peripheries) to pinpoint the most luminous VGLUT1⁺ regions of synaptic boutons and record the x-y coordinates of these central pixels.

The software then navigates through all discerned central x-y coordinates, identifying proximate pixels to classify surrounding pixels that are part of the same presynaptic bouton, based on user-set intensity criteria of the central pixel within a defined radius. For our research, proximal pixels within a 1 μm radius from the central pixel, possessing a brightness of at least 75% of the central pixel, were categorized as part of the same bouton. The software then imposes an area constraint

(>0.05 μm^2) to exclude ill-defined structures. It then evaluates the attributes of the retained synaptic puncta and computes the average intensity signals present in perisynaptic layers adjacent to the synaptic puncta (with a width of 0.2 μm in this study) across all channels of the primary image. Post size (ranging from 0.3 to 1 μm^2) and shape (from 0.5 to 1) filtering of puncta, the quantification of puncta count was done. Conclusively, the assortment of binary puncta served as a template to gauge the fluorescence intensity (FI) of the puncta.

3.16 Data analysis and statistics

Data analysis was carried out using Prism GraphPad (v.8.3.0). For comparisons between two sets, we utilized the t-test paired with Welch's correction. For analyzing multiple sets, a regular two-way ANOVA complemented by Sidak's test for multiple comparisons was applied, especially when inspecting the interplay between genotype and age. In addition, a two-way RM ANOVA coupled with Sidak's test for various comparisons was employed to evaluate the interaction between genotype and region. The bar diagrams display the average \pm the standard error of the mean (SEM), and each individual sample's value is represented as points. A p-value of less than 0.05 was deemed statistically significant.

4 RESULT

4.1 Erythrocyte aggregations, microbleeds, and perivascular space in young and aged *Coll8a1*^{-/-} mice

In a rat model with hypertension-induced CSVD, our prior work revealed intravascular accumulations of erythrocytes, known as stases (Braun, Bueche et al. 2012). Thus, we analyzed HE-stained sections from the brains of mice aged 5 and 12 months. As seen in hypertensive rats, there was a notable rise in the number of capillaries with erythrocyte thrombi (Fig. 4.1 a, left) in 5-month-old *Coll8a1*^{-/-} mice relative to their wild-type counterparts (*Coll8a1*^{+/+}) across the investigated brain areas. Namely, the RSC (two-way ANOVA followed by Sidak's post hoc test; $p = 0.0078$), basal ganglia (BG: $p = 0.0099$), the CA1 region of the hippocampus (CA1: $p = 0.0011$), corpus callosum (CC: $p < 0.0001$) and the thalamus ($p = 0.0012$) (**Fig. 4.1 b-f**). For arterioles, there were similar increases in the occurrence of stases at this age in the RSC ($p = 0.0063$), BG ($p = 0.0025$), CA1 ($p = 0.0336$) and thalamus ($p = 0.0154$) but not in the CC ($p = 0.4151$) (**Fig. 4.1 g-k**).

In 12-month-old compared to 5-month-old mice, there was a tendency for an increase in occurrence of stases in *Coll8a1*^{+/+} mice in all studied brain subregions, while in *Coll8a1*^{-/-} mice there was an opposite trends, resulting in similar levels of erythrocyte accumulation in both genotypes in 12-month-old mice and significant interaction between genotype and age (**Fig. 4.1 b-k**). Hence, *Coll8a1*^{-/-} mice show an earlier elevation in stases than wild-type mice and partial recovery/resilience at the age of 12 months.

In *Coll8a1*^{-/-} mice, we found no significant differences in enlarged PVS (**Fig. 4.1 a, right**) across all studied regions and ages in 5- and 12-month-old animals (**Fig. 4.2 a-d**). Both genotypes had no microbleeds in the mentioned brain regions and age groups.

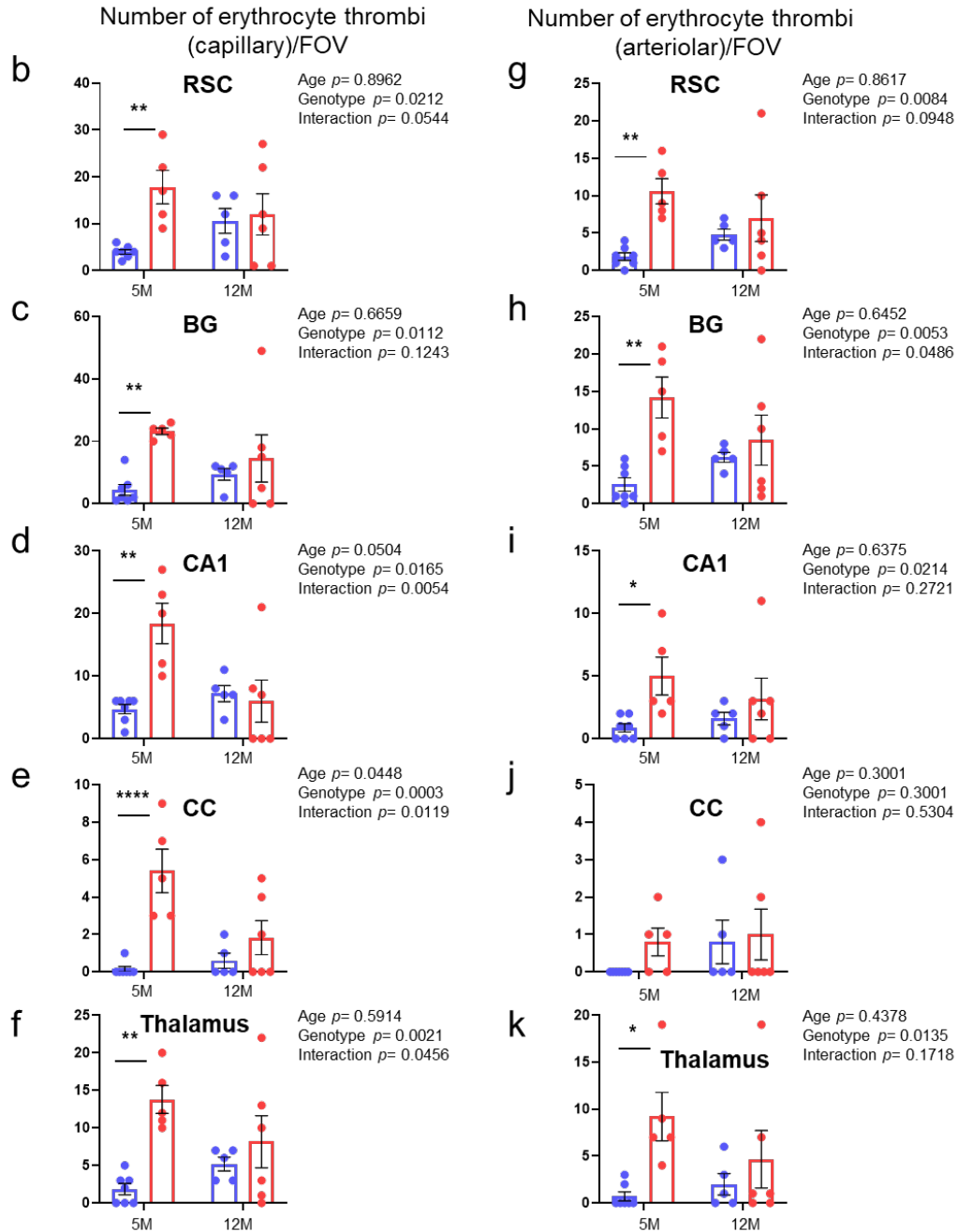
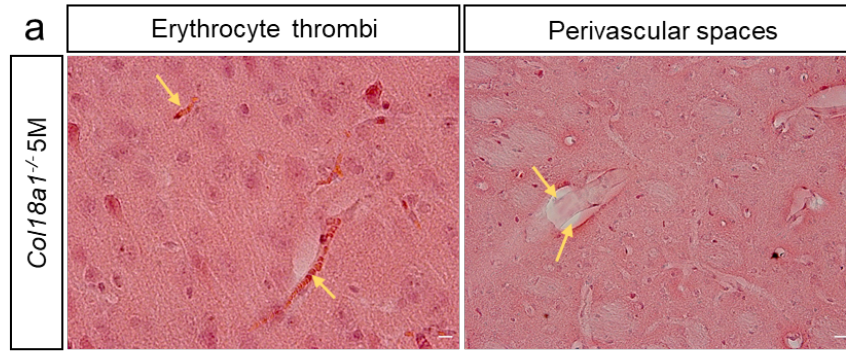


Figure 4.1 Erythrocyte thrombi and enlarged perivascular spaces in the brains of *Col18a1*^{-/-} mice.

(a) Hematoxylin-eosin staining with representative examples of erythrocyte thrombi (arrows) and perivascular spaces (arrows) in 5-month-old *Col18a1*^{-/-} mice. **(b – k)** The mean number (\pm SEM) of capillary and arteriolar thrombi per animal across five brain regions (RSC, BG, CA1, CC and thalamus) in 5- and 12-month-old animals. Each dot represents one animal. * $p < 0.05$, ** $p < 0.01$, *** $p < 0.001$ and **** $p < 0.0001$ represent significant differences between *Col18a1*^{+/+} (5-month-old animals: N=7; 12-month-old animals: N=5) and *Col18a1*^{-/-} mice (5-month-old animals: N=5; 12-month-old animals: N=6) using two-way ANOVA and Sidak's multiple comparisons test. BG, basal ganglia; CA1, CA1 region of the hippocampus; CC, corpus callosum; FOV, field of view; M, months; RSC, retrosplenial cortex. Scale bar = 50 μ m.

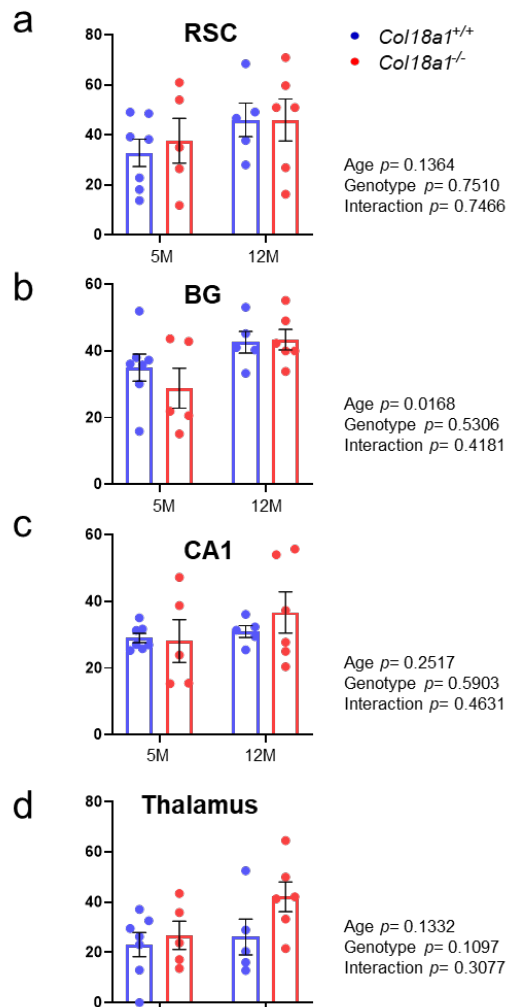


Figure 4.2 (a-d) Percentages of arterioles with enlarged PVS per animal across all brain regions (RSC, BG, CA1 and thalamus) in 5- and 12-month-old animals. Each dot represents one animal. Bar graphs show mean \pm SEM values between *Col18a1*^{+/+} (5-months-old animals: N=7; 12-months-old animals, N=5) and *Col18a1*^{-/-} mice (5-months-old animals: N=5; 12-months-old animals: N=6) using two-way ANOVA, Sidak's multiple comparisons test. BG, basal ganglia; CA1, the CA1 region of the hippocampus; CC, corpus callosum; FOV, field of view; M, months; PVS, perivascular spaces; RSC, retrosplenial cortex. Scale bar = 50 μ m.

4.2 Knockout of *Col18a1* increases BBB leakage in young and aged mice

Next, we examined the effects of collagen XVIII deficiency on BBB breakdown, which was assessed by measuring the leakage of IgG and quantitatively determined as the percentage of STL+ area in which IgG was detected. Data were collected from six brain regions, namely, the RSC, DS, CA1, BG, thalamus and mPFC. In young *Col18a1*^{-/-} animals, we revealed that BBB breakdown was significantly increased by $\approx 20\%$ in the dorsal striatum and by $\approx 25\%$ in the thalamus (Mann-Whitney test: $p = 0.0484$ for both regions), with no significant changes in other brain regions (**Fig. 4.3 a & b**). The Mann-Whitney test was used here for statistical analysis instead of two-way RM ANOVA due to prominent differences in variability between regions and genotypes and for non-Gaussian distribution of values. In 12-month-old mice, the IgG leakage was $\approx 60\%$ higher in the CA1 region and RSC of *Col18a1*^{-/-} mice than in *Col18a1*^{+/+} mice (two-way RM ANOVA, Sidak's multiple comparisons test for CA1 and RSC: $p < 0.0001$) (**Fig. 4.3 c & d**).

As expected for wild-type mice (Acharya, Levin et al. 2013), there was a low IgG signal ($\approx 3\%$ in 12-month-old *Col18a1*^{+/+} mice) in the brain parenchyma of these animals. As we found prominent differences between genotypes, we focused our next analyses on CA1 and RSC, which are highly relevant to CSVD and AD.

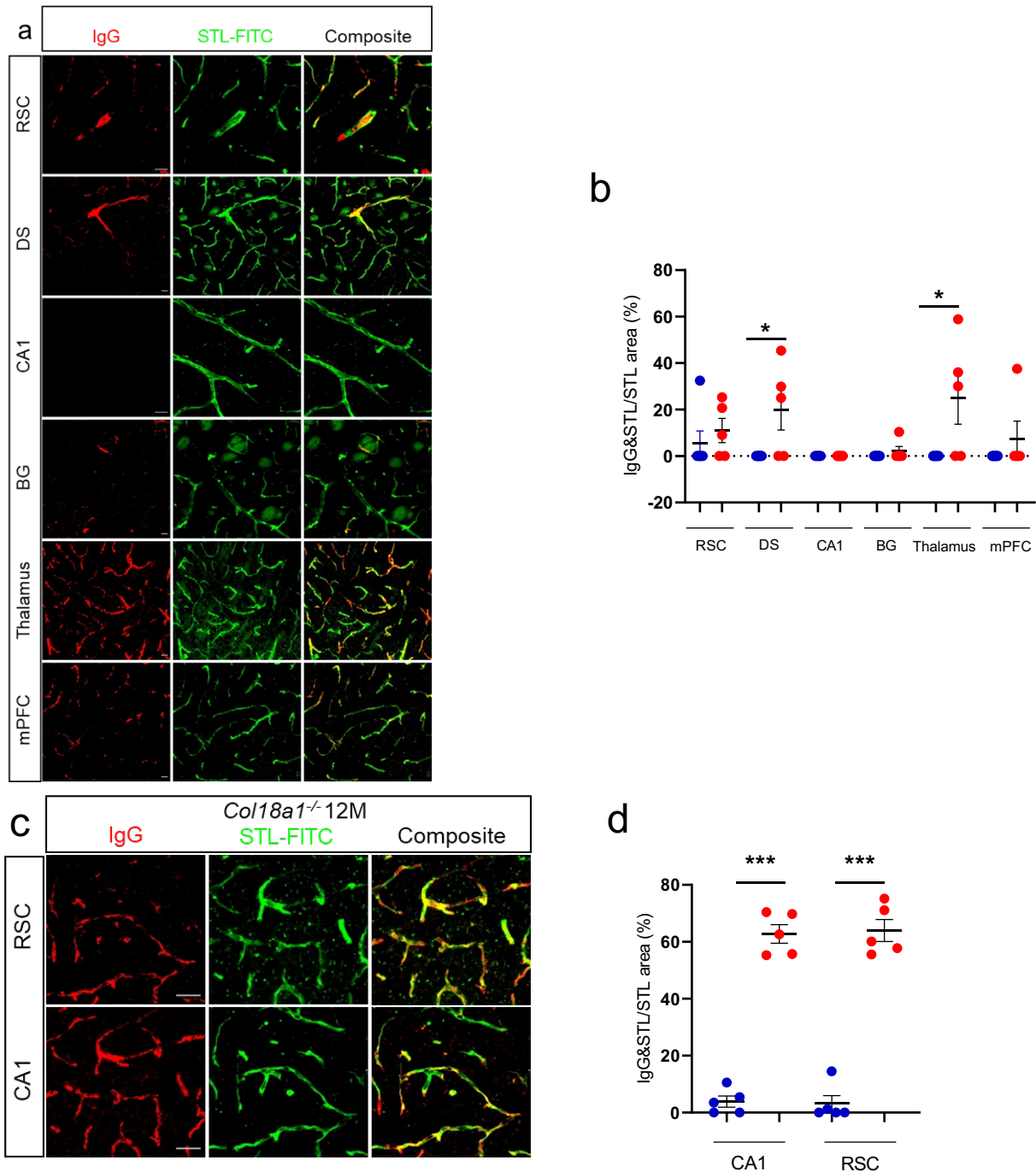


Figure 4.3 Knockout of *Col18a1* induces BBB breakdown and alters the expression of basement membrane proteins.

(a & c) Representative 20x and 40x images of vessels from *Col18a1*^{-/-} and control mice stained with STL-FITC (green) to visualize blood vessels and IgG (red) as a marker of BBB disruption in 5-month-old (5M) and 12-month-old (12M) mice, respectively. The percentage of STL-FITC area that colocalized with IgG (yellow in the composite image in (a & c)) was calculated in 6 brain regions (RSC, DS, CA1, BG, thalamus and mPFC) of 5-month-old animals (a) and 2 brain regions (CA1, RSC) of 12-month-old animals (c). Each dot represents one animal. *p < 0.05, **p < 0.01, ***p < 0.001 and ****p < 0.0001 represent significant differences between

Coll8a1^{+/+} (5-month-old animals: N=6; 12-month-old animals: N=5) and *Coll8a1*^{-/-} mice (5-month-old animals: N=5; 12-month-old animals: N=5) using the Mann-Whitney test for young animals and two-way RM ANOVA and Sidak's multiple comparisons test for old animals. AT, anterior thalamus; BBB, blood-brain barrier; BG, basal ganglia; CA1, CA1 region of the hippocampus; DS, dorsal striatum; GAPDH, glyceraldehyde 3-phosphate dehydrogenase; IgG, immunoglobulin G (BBB breakdown detection); M, months; mPFC, medial prefrontal cortex; RSC, retrosplenial cortex; STL-FITC, *Solanum tuberosum* lectin fluorescein isothiocyanate (endothelial marker). Scale bars=20 μ m.

4.3 Basement membrane remodeling, endothelial cells and pericytes activation in *Coll8a1*^{-/-} mice

We determined the mRNA levels of tight junction proteins (*Cldn5*, *Ocln*, *Zo1*), basement membrane components (*Col3a1*, *Col4a1*, *Col8a1*, *Lama5*, *Nid1*), *Vcam1* and *Loxl2* in hippocampal homogenates (Perosa, Priester et al. 2020). In *Coll8a1*^{-/-} mice, *Col3a1*, *Col4a1*, *Col8a1*, *Nid1*, *Vcam1* and *Loxl2* mRNA expression levels were significantly higher than those in controls (t-test with Welch's correction for *Col3a1*: $p = 0.0180$; *Col4a1*: $p = 0.0112$; *Col8a1*: $p = 0.0119$; *Nid1*: $p = 0.0083$; *Vcam1*: $p = 0.0459$; *Loxl2*: $p = 0.0018$), while the expression of *Ocln* was reduced ($p = 0.0004$), and *Zo1* had a similar tendency ($p = 0.082$), suggesting that endothelial function is altered in *Coll8a1*^{-/-} mice (**Fig. 4.4 a**). However, the protein level of occludin in the cortex region remains unchanged. The protein level of VCAM1, was found to be upregulated in the cortex region in accordance with the mRNA levels of VCAM1 (t-test with Welch's correction $p = 0.0253$).

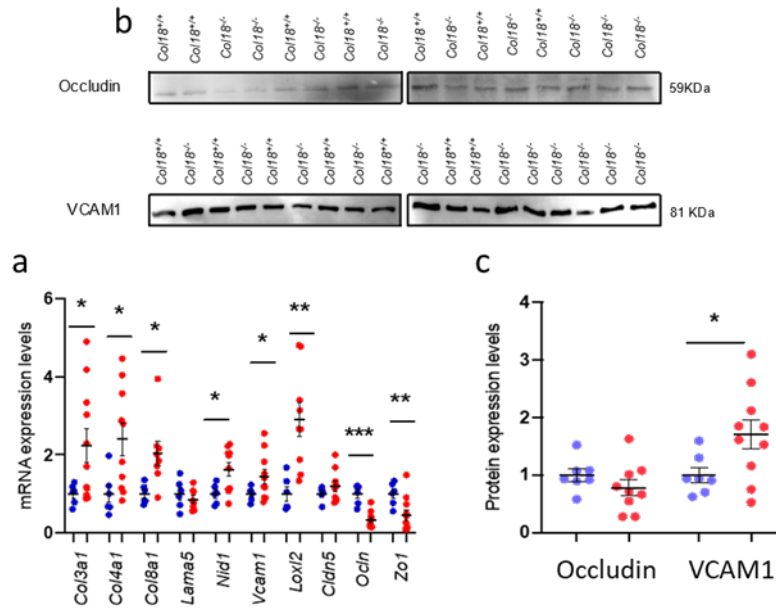


Figure 4.4 (a) The expression of genes involved in the organization of the basement membrane in the hippocampal region of 12-month-old mice was investigated using RT-qPCR and normalized to individual *Gapdh* values. Bar graphs show the mean \pm SEM values; t-test with Welch's correction: * $p < 0.05$, ** $p < 0.01$, *** $p < 0.001$. **(b & c)** Representative western blots for the expression of Occludin and VCAM1 in the cortex region of 12-month-old mice. * $p < 0.05$, ** $p < 0.01$, *** $p < 0.001$ and **** $p < 0.0001$ represent significant differences between *Coll8a1*^{+/+} (N=6) and *Coll8a1*^{-/-} mice (N=11).

4.4 Microglial recruitment to cerebral small blood vessels in *Coll8a1*^{-/-} mice

Using IHC staining with an antibody against the microglial markers Iba1 and STL-FITC labeling, we visualized microglia/perivascular macrophages and blood vessels within the CA1 region, observing some microglia/perivascular macrophages in close association with cerebral vessels (**Fig. 4.5 a**) (Koizumi, Kerkhofs et al. 2019). We quantified the colocalization of vessels and vessel-associated microglia (VAM)/perivascular macrophages using color thresholding and binary analysis (**Fig.4.5 a right**). This colocalization significantly increased by 15% in *Coll8a1*^{-/-} mice compared to *Coll8a1*^{+/+} mice (t-test with Welch's correction $p = 0.0091$; **Fig. 4.5 a & b**), suggesting that microglia/macrophages were recruited to cerebral vessels in *Coll8a1*^{-/-} mice.

To understand the mechanism behind microglial cell migration, we investigated the expression of a chemokine that might be involved in the recruitment of microglia. The mRNA level of chemokine (C-C motif) ligand 2 (*Ccl2*) was elevated in *Coll18a1*^{-/-} mice compared to *Coll18a1*^{+/+} mice (t-test with Welch's correction $p = 0.0077$, **Fig. 4.5 c**).

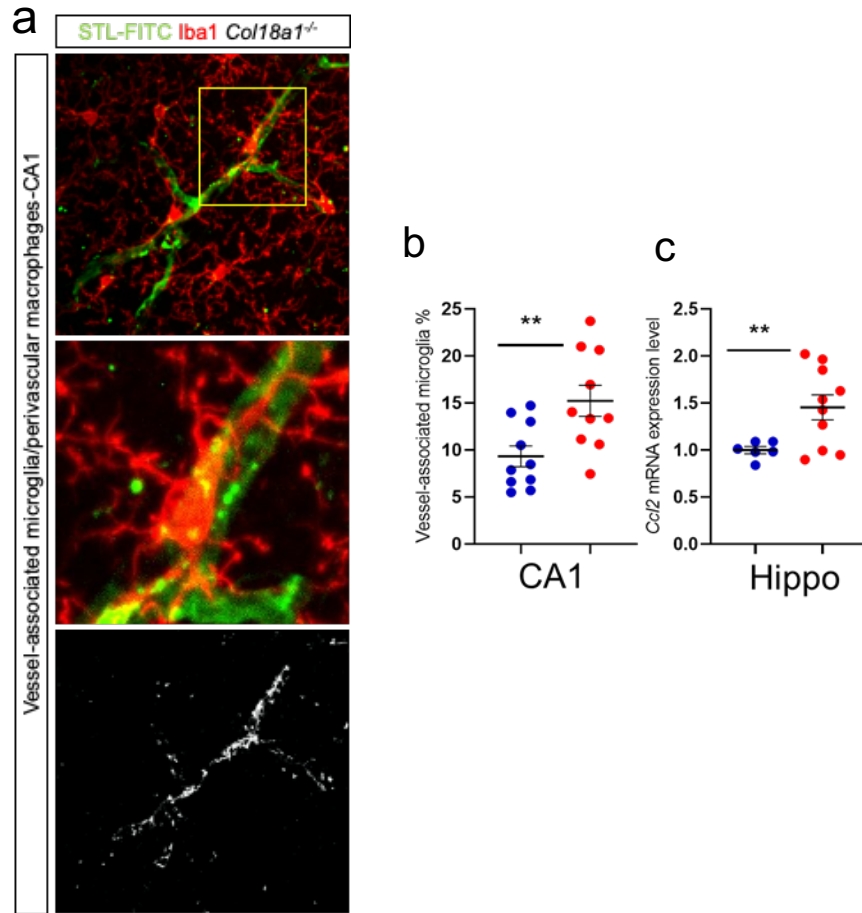


Figure 4.5 Analysis of microglia/perivascular macrophage recruitment to cerebral small blood vessels in *Coll18a1*^{-/-} mice. (a) Representative 40x image of the CA1 area in mice showing microglial/perivascular macrophages (Iba1, red) associated with blood vessels (STL-FITC, green). Middle: magnified part of the image outlined on the left in yellow. Right: colocalization of Iba1 and STL-FITC. (b) Increased colocalization in *Coll18a1*^{-/-} mice. (c) Overexpression of *Ccl2*, a gene involved in microglial recruitment. Data are presented as the mean \pm SEM. Each dot represents one FOV in **b** and one animal in **c**. * $p < 0.05$, ** $p < 0.01$, *** $p < 0.001$ and **** $p < 0.0001$ represent significant differences between *Coll18a1*^{+/+} (N=5) and *Coll18a1*^{-/-} mice (N=5) in 12-month-old animals in (b) and *Coll18a1*^{+/+} (N=6) and *Coll18a1*^{-/-} mice (N=11) in 5-month-old animals in **c** using the t-test with Welch's correction. CA1, CA1 region of the hippocampus; *Ccl2*, (C-C motif) ligand 2; Hippo, hippocampus; Iba1, ionized calcium-binding adapter molecule 1; IgG, immunoglobulin G; STL-FITC, *Solanum tuberosum* lectin fluorescein isothiocyanate (endothelial marker); VAM, vessel-associated microglia/perivascular macrophages.

4.5 Activation of microglia in *Coll8a1*^{-/-} mice

It has been reported that BBB breakdown is associated with increased glial activation and release of neuroinflammatory cytokines (Zlokovic 2008). Therefore, the alterations in the microglial cells and astrocytes in 12-month-old mice were assessed. Analysis of microglial morphology in the RSC and CA1 region revealed that Iba1-labeled microglia appeared to display a more spherical morphology in *Coll8a1*^{-/-} mice compared to the ramified appearance in control mice (**Fig. 4.6 a, c, d & e**). At 12 months, *Coll8a1*^{-/-} mice had a larger microglial somatic area by 20% in CA1 (two-way RM ANOVA, Sidak's multiple comparisons test; $p = 0.0464$) and by 37% in the RSC (two-way RM ANOVA, Sidak's multiple comparisons test; $p = 0.0014$) than in the corresponding regions of *Coll8a1*^{+/+} mice (**Fig. 4.6 c**). The average branch lengths were significantly reduced in CA1 (two-way RM ANOVA, Sidak's multiple comparisons test; $p = 0.0051$; **Fig. 4.6 d**). Additionally, in the CA1 and RSC of *Coll8a1*^{-/-} mice, we revealed an increase in the density of microglial cells (t-test with Welch's correction test; $p = 0.0444$ and $p = 0.0253$, respectively; **Fig. 4.6 e**).

As C1q may promote synaptic phagocytosis by microglia, we examined the association between expression of C1q and collagen XVIII deficiency. Our data revealed that C1q was upregulated by 44% in the neuropil of the CA1 region and by 21% in the RSC (two-way RM ANOVA, Sidak's multiple comparisons test; $p < 0.0001$ and $p = 0.0245$, respectively; **Fig. 4.6 b & f**), although the overall hippocampal mRNA expression of *C1q* remained unchanged (**Fig. 4.6 g**).

Our gene expression evaluation strongly supported these observations, suggesting a contribution of transcriptional regulation (**Fig. 4.6 g**). We detected significant increases in microglial markers: *Iba1* (t-test with Welch's correction here and below $p = 0.027$), *Mpo* ($p = 0.0114$) and *Cd86* ($p = 0.0319$), *Tgfb1* ($p = 0.0487$) and significant decreased in *Trem2* ($p = 0.0275$).

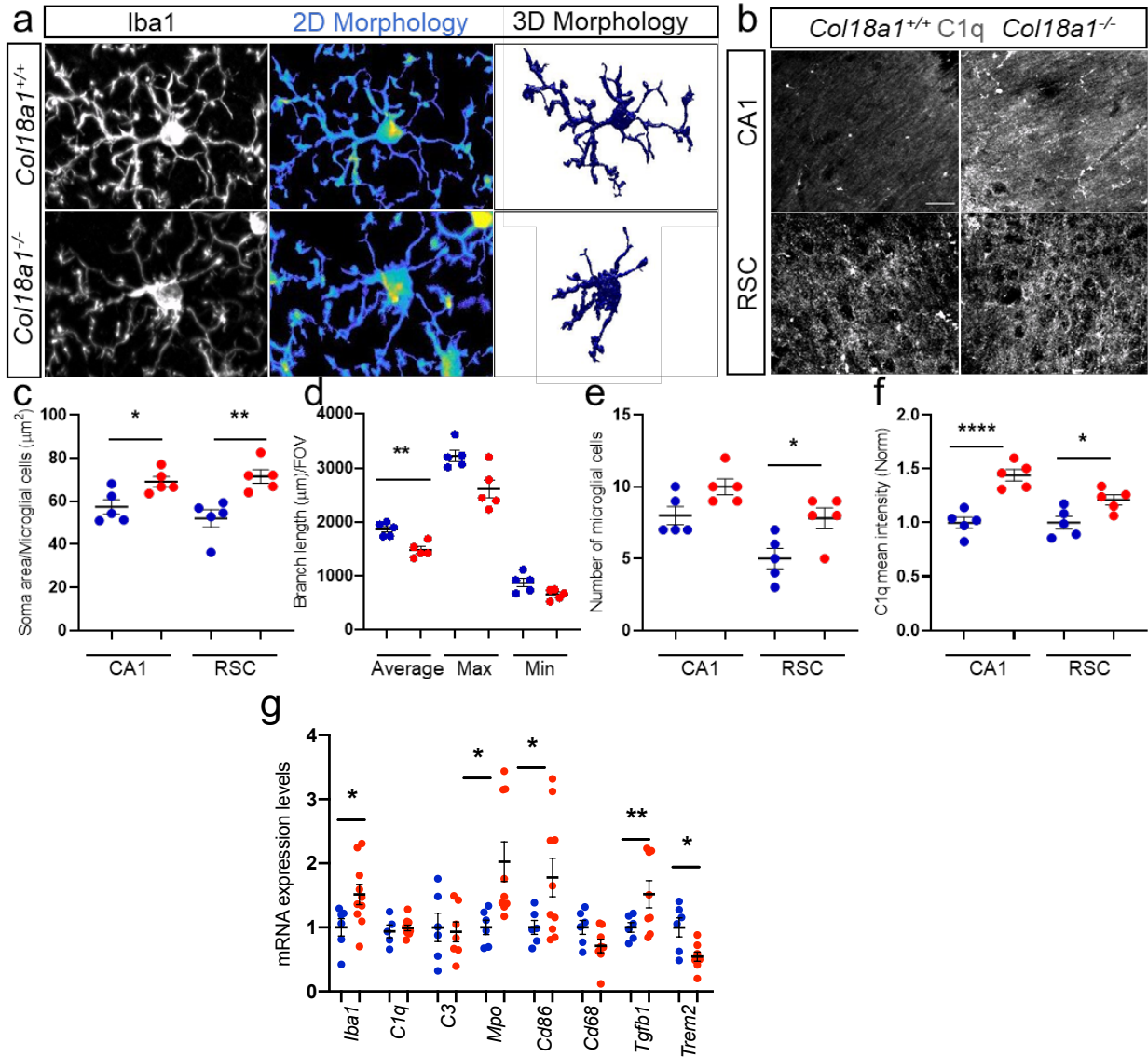


Figure 4.6 (a) Activation of microglia was confirmed by immunostaining in the RSC and hippocampal CA1 area, which revealed an increase in the soma area (c) and a decrease in the branch length (d), which correlated with the increasing number of microglial cells (e) in *Col18a1*^{-/-} mice. (b & f) Representative images showing the upregulation of C1q immunostaining in the CA1 and RSC of *Col18a1*^{-/-} mice. g, Representative expression of genes involved in microglial activation and subtypes differentiation using RT-qPCR and normalized to individual *Gapdh* values. CA1, CA1 region of the hippocampus; RSC, retrosplenial cortex.

4.6 Activation of astroglia in *Coll8a1*^{-/-} mice

Next, we assessed the state of astrocytes by measuring GFAP immunofluorescence within the CA1 region as well as by counting the number of astrocytes. An analysis of GFAP⁺ cell area and mean intensity in *Coll8a1*^{-/-} mice revealed significant increases in both parameters (t-test with Welch's correction $p = 0.0295$ and $p < 0.0001$, respectively), although no changes in the number of GFAP⁺ cells were observed (**Fig. 4.7 a, b, c & d**).

Transcriptional regulation seems to be responsible for these observations, based on our gene expression analysis (**Fig. 4.7 e**). We detected significant increases in astrocytic: *Gfap* (t-test with Welch's correction here and below, $p = 0.0030$) and *Aqp4* ($p = 0.0366$) as astrocytic markers and *S100a10* ($p = 0.0072$) as A2 subtype markers.

As PLP1 is one of the main protein components in myelin of the central nervous system (CNS) and myelination defects are characteristic of the disease and reflected by oligodendrocyte damage, we examined the hippocampal mRNA expression level of *Plp1* and found that it was downregulated (t-test with Welch's correction $p = 0.0218$) (**Fig. 4.7 f**), although *Cspg4* remained unchanged as an OPC marker (**Fig. 4.8 b**).

Furthermore, the hippocampal mRNA expression of the proinflammatory cytokine *Il1b* was significantly increased (t-test with Welch's correction $p = 0.0306$) in *Coll8a1*^{-/-} mice compared to control mice, whereas no changes were seen in the hippocampal levels of a few/certain other proinflammatory cytokines, *Il6*, *Il33* and *Tnfa*, the later is expressed by neurons in an activity-dependent manner to control microglial activity towards the neural ECM (**Fig. 4.7 f**) (Strackeljan, Baczynska et al. 2021).

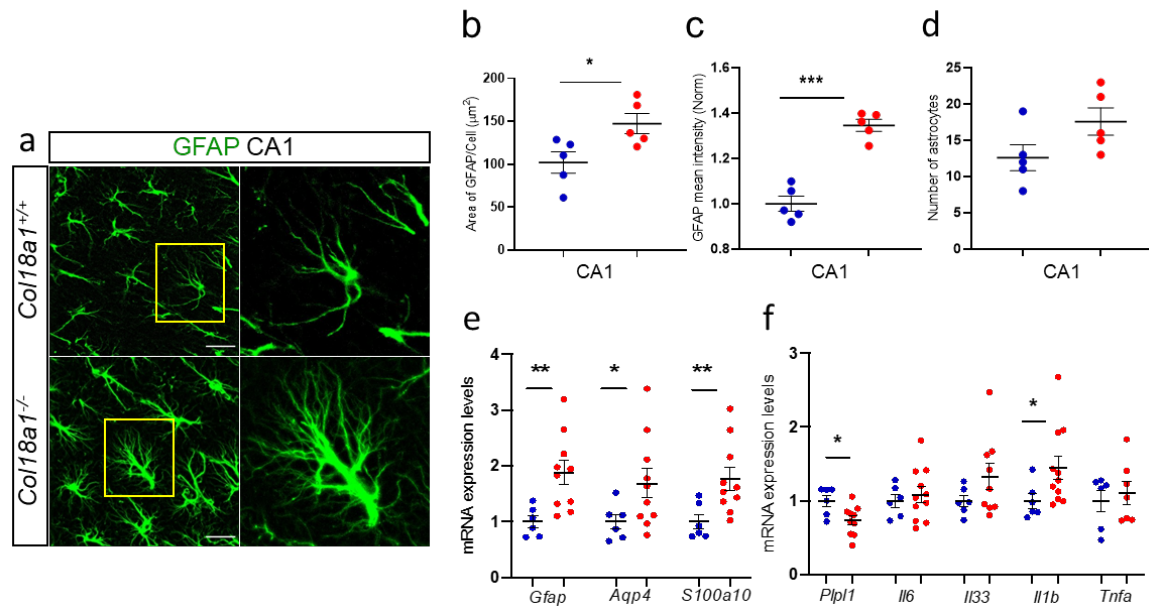


Figure 4.7 (a) Representative fluorescent images showing GFAP-labeled astrocytes (green). (b & c) An increase in GFAP⁺ cell area and mean intensity was observed, while the density of GFAP⁺ cells remained unchanged (d) in the hippocampal CA1 region of *Col18a1*^{-/-} mice. Data are presented as the mean ± SEM, while **p* < 0.05, ***p* < 0.01, ****p* < 0.001 and *****p* < 0.0001 represent significant differences between *Col18a1*^{+/+} (N=5) and *Col18a1*^{-/-} (N=5) mice using two-way RM ANOVA, Sidak's multiple comparisons test for microglial cells and C1q analysis, and t-test with Welch's correction test for GFAP analysis. Scale bars = 20 µm. (e & f) Expression of genes involved in inflammation and related molecules was investigated using RT-qPCR and normalized to individual *Gapdh* values.

4.7 Activation of pericytes in *Col18a1*^{-/-} mice

Pericytes, as a central neurovascular unit component, dynamically and actively respond to injury in various diseases, such as ischemic strokes and AD. Accordingly, Western blot analysis revealed that *Col18a1*^{-/-} mice showed elevated levels of PDGFRβ (t-test with Welch's correction *p* = 0.0288), an indication of pericyte activation (Fig. 4.8 a & b).

Additionally, we examined the hippocampal mRNA level of *Pdgfrb* as a pericyte marker and found that it was overexpressed in *Col18a1*^{-/-} mice compared to control mice (t-test with Welch's correction *p* = 0.0344) (Fig. 4.8 c). However we found a decrease in the mRNA level of alpha smooth muscle actin (*asma*) (t-test with Welch's correction *p* = 0.0399).

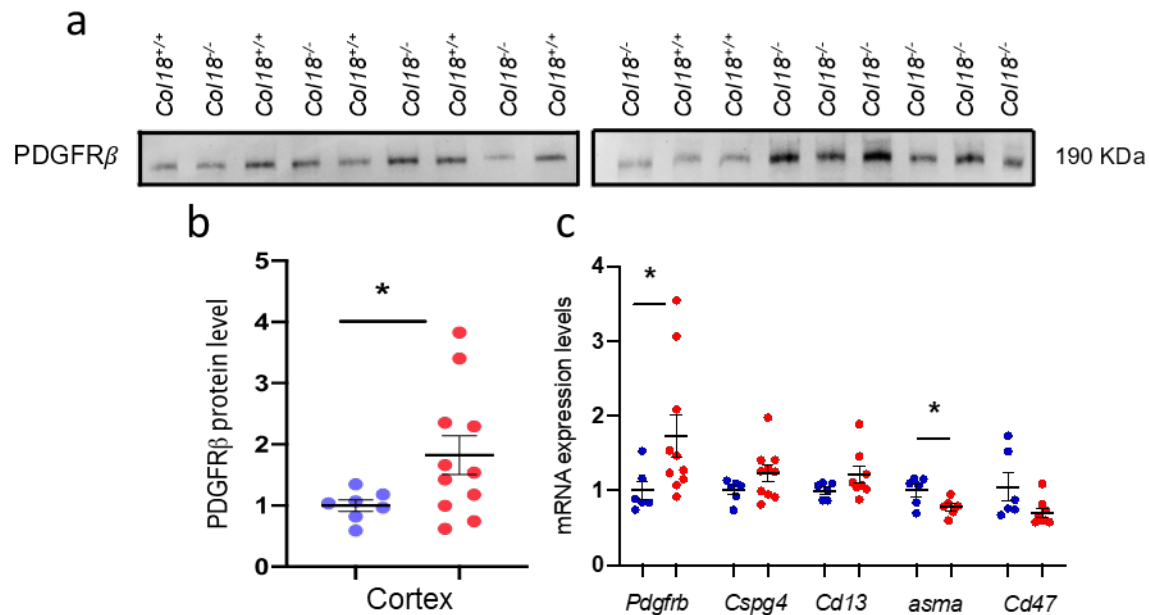


Figure 4.8 (a & b) Represents the upregulation of PDGFR β protein level in the cortex of 12-month-old mice. Bar graphs show the mean \pm SEM values, while * $p < 0.05$, ** $p < 0.01$, *** $p < 0.001$ and **** $p < 0.0001$ represent significant differences between *Coll8a1*^{+/+} (N=6) and *Coll8a1*^{-/-} (N=11) mice using a t-test with Welch's correction test. **(c)** Representative expression of genes involved in pericytes activation and alpha smooth muscle cells differentiation using RT-qPCR and normalized to individual *Gapdh* values.

4.8 Reduced expression of parvalbumin and perineuronal nets in *Coll8a1*^{-/-} mice

Because of microglial activation in *Coll8a1*^{-/-} mice and a strong reported/established interaction between microglia and PV⁺ interneurons (Gervais, Iloun et al. 2021), we studied the effects of collagen XVIII deficiency on the size of PV⁺ cells and the level of their PV expression as measures reflecting their function. Using PV immunolabeling (**Fig. 4.9 a**) and quantitative analysis of 12-month-old mice, we found that the mean intensity of PV⁺ cells in CA1 and RSC decreased by 25% and 44%, respectively (two-way RM ANOVA, Sidak's multiple comparisons test; $p = 0.0128$ and $p < 0.0001$; respectively; **Fig. 4.9 b**) in *Coll8a1*^{-/-} mice when compared to wild-type controls. Furthermore, the area of PV⁺ cells was reduced by 22% in CA1 (two-way RM ANOVA, Sidak's multiple comparisons test $p = 0.0162$; **Fig. 4.9 c**).

Additionally, the mean intensity of the Acan⁺ signal colocalizing with CA1 PV⁺ interneurons (**Fig. 4.9 a**), a measure of the structural integrity of associated PNNs, and the size of Acan⁺ PV⁺ cells

were reduced in *Coll18a1*^{-/-} mice compared to *Coll18a1*^{+/+} mice (two-way RM ANOVA, Sidak's multiple comparisons test; $p = 0.0179$, $p = 0.0182$, respectively; **Fig. 4.9 d & e**); however, these measures were unchanged in the RSC. Moreover, there was a 37% decrease in the fraction of PV⁺Acan⁺ cells per total PV⁺ cell population in the CA1 region of *Coll18a1*^{-/-} mice (**Fig. 4.9 f**). Labeling of PNNs with WFA, which binds to particular glycoepitopes on CSPGs (Fujita, Yamaguchi et al. 2018) (**Fig. 4.9 g**), revealed no changes in the WFA mean intensity per cell, WFA⁺ cell area or cell density in the CA1 and RSC of *Coll18a1*^{-/-} mice (**Fig. 4.9 h, i & j**).

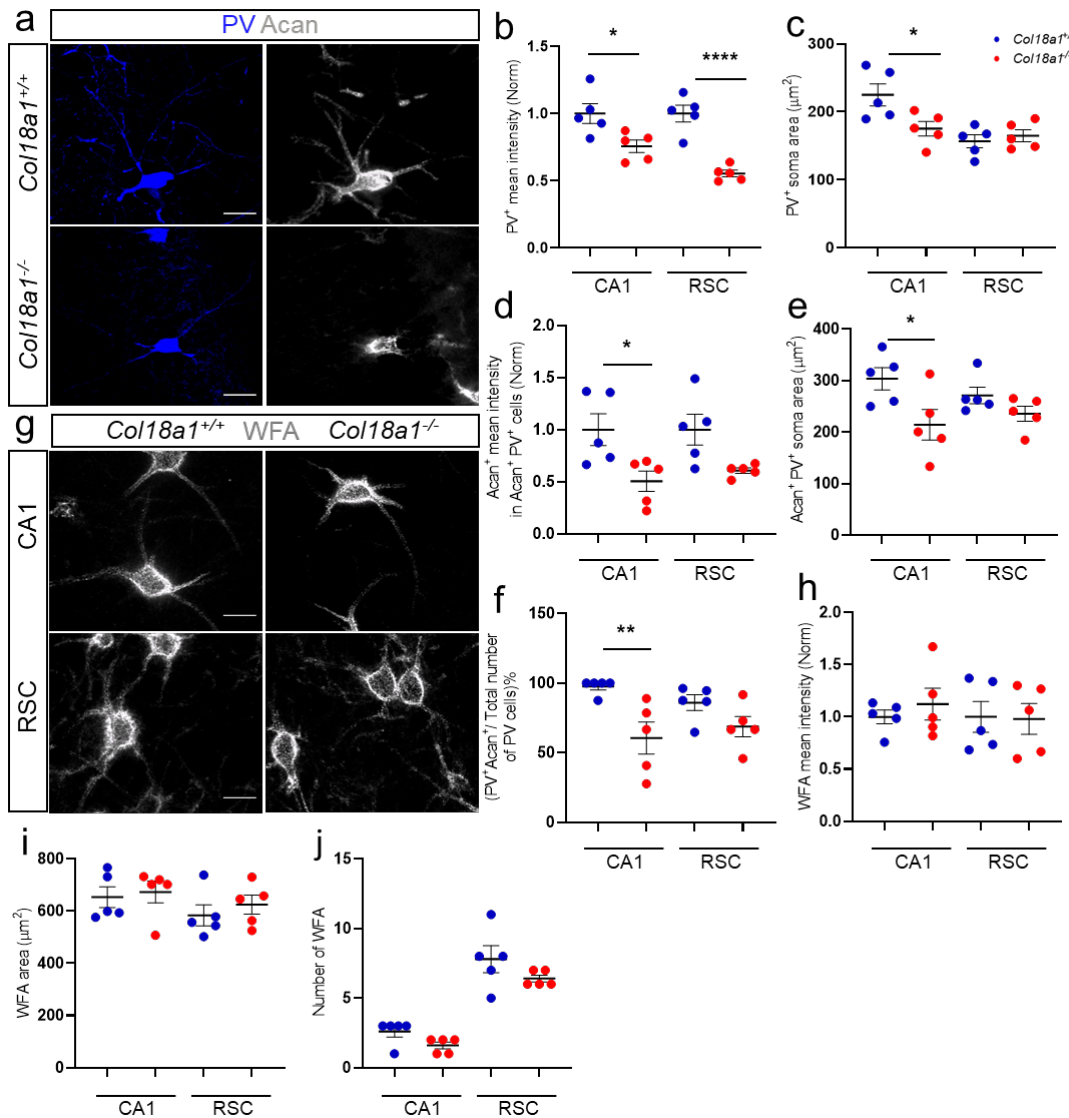


Figure 4.9 Expression of parvalbumin, perineuronal nets, neural ECM genes and ECM proteases in *Coll18a1*^{-/-} mice. (a) Representative 40x images of morphologically dystrophic PV⁺ interneurons associated with Acan in *Coll18a1*^{-/-} mice. (b & c) Quantification of PV⁺ interneurons associated with *Coll18a1*^{-/-} mice revealed significant reductions in the mean PV⁺ intensity and area in the hippocampal CA1 region. (d & e) The mean Acan intensity (d) and area (e) of Acan⁺ PV⁺ cells were significantly reduced in the hippocampal CA1 of *Coll18a1*^{-/-} mice. (f) The percentage of PV⁺ cells surrounded by Acan per total number of PV cells significantly decreased in the hippocampal CA1 of *Coll18a1*^{-/-} mice. (g) Representative images of hippocampal CA1 and RSC regions in *Coll18a1*^{+/+} and *Coll18a1*^{-/-} mice at 12 months stained for WFA. (h–j) No significant difference in the mean intensity, area and density of the WFA⁺ signal in the brain regions or animal groups. Bar graphs show the mean ± SEM values, while * p < 0.05, ** p < 0.01, *** p < 0.001 and **** p < 0.0001 represent significant differences between *Coll18a1*^{+/+} (N=5) and *Coll18a1*^{-/-} (N=5) mice using two-way RM ANOVA and Sidak's multiple comparisons test. Acan, aggrecan; CA1, CA1 region of the hippocampus; ECM, extracellular matrix; PV, parvalbumin; RSC, retrosplenial cortex; WFA, *Wisteria floribunda* agglutinin. Scale bar=20 μm.

4.9 Alterations in glutamatergic synapses in *Coll18a1*^{-/-} mice

Considering the activation of microglia and astrocytes in *Coll18a1*^{-/-} mice, we investigated possible changes in synaptic markers and the associated perisynaptic ECM. The mean fluorescence intensity of the glutamatergic presynaptic marker VGLUT1 was decreased in 12-month-old *Coll18a1*^{-/-} mice in the neuropil of the CA1 region by 45% (two-way RM ANOVA, Sidak's multiple comparisons test; $p = 0.0002$) and in the RSC by 37% (two-way RM ANOVA, Sidak's multiple comparisons test; $p=0.0014$; **Fig. 4.10 a & b**). In contrast, the fluorescence intensity of VGLUT2 (**Fig. 4.10 c & d**), which is predominantly expressed in another subset of glutamatergic presynapses, was not different between genotypes (**Fig. 4.10 d**). Additionally, the expression of the presynaptic GABAergic marker VGAT was not affected by collagen XVIII deficiency (**Fig. 4.10 e & f**).

In line with the observed reduction in presynaptic VGLUT1, the expression of the glutamatergic postsynaptic scaffold protein Homer1 was reduced by 27% in the CA1 region (two-way RM ANOVA, Sidak's multiple comparisons test; $p = 0.0290$; **Fig. 4.10 g & h**). Thus, deficiency in *Coll18a1* results in specific synaptic modifications in VGLUT1⁺ glutamatergic synapses made by intracortical rather than VGLUT2⁺ synapses made by thalamic axons.

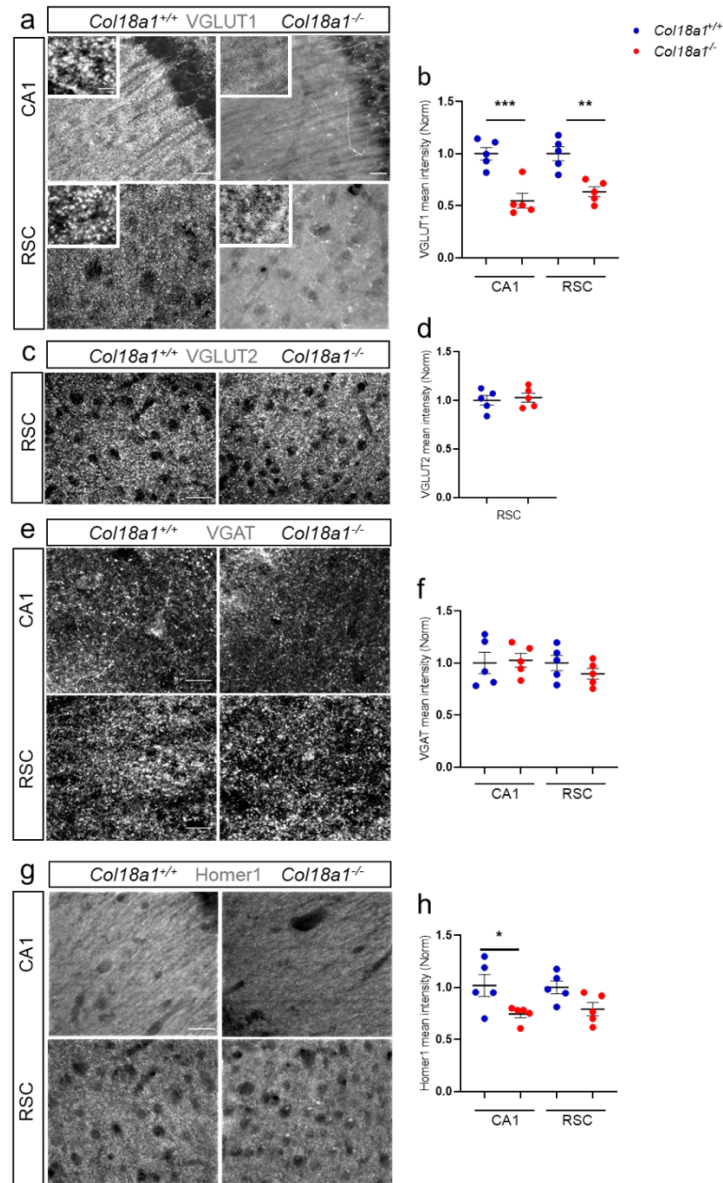


Figure 4.10 Alterations in glutamatergic synapses in *Col18a1*^{-/-} mice. (a, c, e & g) Representative 63x and 40x confocal images of VGLUT1 (63x), VGLUT2 (40x), VGAT (40x) and Homer1 (40x) immunostaining in the CA1 and RSC of 12-month-old *Col18a1*^{-/-} and *Col18a1*^{+/+} mice. There was a significant reduction in the fluorescent intensity of VGLUT1 (b) and Homer1 (h) puncta in *Col18a1*^{-/-} mice in the CA1 and RSC regions, but there was no difference between the genotypes in VGLUT2 expression in the RSC region (d) and VGAT in the CA1 and RSC regions (f). Bar graphs show the mean \pm SEM values, while * $p < 0.05$, ** $p < 0.01$, *** $p < 0.001$ and **** $p < 0.0001$ represent significant differences between *Col18a1*^{+/+} (N=5) and *Col18a1*^{-/-} (N=5) mice using two-way RM ANOVA and Sidak's multiple comparisons test. CA1, CA1 region of the hippocampus; Homer 1, homer protein homolog 1; RSC, retrosplenial cortex; VGAT, vesicular GABA transporter; VGLUT1, vesicular glutamate transporter 1; VGLUT2, vesicular glutamate transporter 2. Scale bars =20 μ m.

4.10 Upregulation of perisynaptic ECM proteoglycan Bcan and downregulation of presynaptic VGLUT1 in *Coll8a1*^{-/-} mice

To count excitatory synapses and measure the expression of perisynaptic ECM associated with them, we performed double VGLUT1/Bcan immunolabeling (**Fig. 4.11 a & b**), confocal imaging and applied a recently developed script for image analysis (Strackeljan, Baczynska et al. 2021). In agreement with ROI measurements (**Fig. 4.11 b**), the analysis of single VGLUT1⁺ puncta intensity revealed a 51% decrease in CA1 (two-way RM ANOVA, Sidak's multiple comparisons test; $p < 0.0001$) and 32% in RSC ($p = 0.001$) (**Fig. 4.11 c**); however, the number of VGLUT1⁺ puncta in the neuropil remained unchanged in *Coll8a1*^{-/-} mice (**Fig. 4.11 d**). In contrast, the total expression of Bcan was upregulated: the mean intensity per ROI was increased by 58% in CA1 (RM two-way ANOVA, Sidak's multiple comparisons test; $p = 0.0118$) and by 75% in the RSC (*one-way* ANOVA; Sidak post hoc test $p = 0.0017$) (**Fig. 4.11 e**). Additionally, the perisynaptic expression of Bcan in bands around presynaptic puncta was elevated by 28% in CA1 (two-way RM ANOVA, Sidak's multiple comparisons test; $p = 0.0357$) and by 33% in the RSC (two-way RM ANOVA, Sidak's multiple comparisons test; $p = 0.0119$) (**Fig. 4.11 f**). Thus, our data revealed reduced expression of pre- and postsynaptic proteins at excitatory synapses and upregulation of perisynaptic ECM around them.

Next, we analyzed the total Bcan expression level in the cortical homogenate. For detection of proteolytically cleaved Bcan, we used the antibody which detects both cleaved fragments with a size of 53 kDa and full-length Bcan with a size 145 kDa (**Fig. 4.11 g**). Our results indicate that the amount of full-length Bcan in *Coll8a1*^{-/-} mice was significantly higher than in *Coll8a1*^{+/+} mice (t-test with Welch's correction $p = 0.0093$), while that the amount of cleaved Bcan remained unchanged (t-test with Welch's correction $p = 0.1073$) although showed a similar tendency as the full-length Bcan.

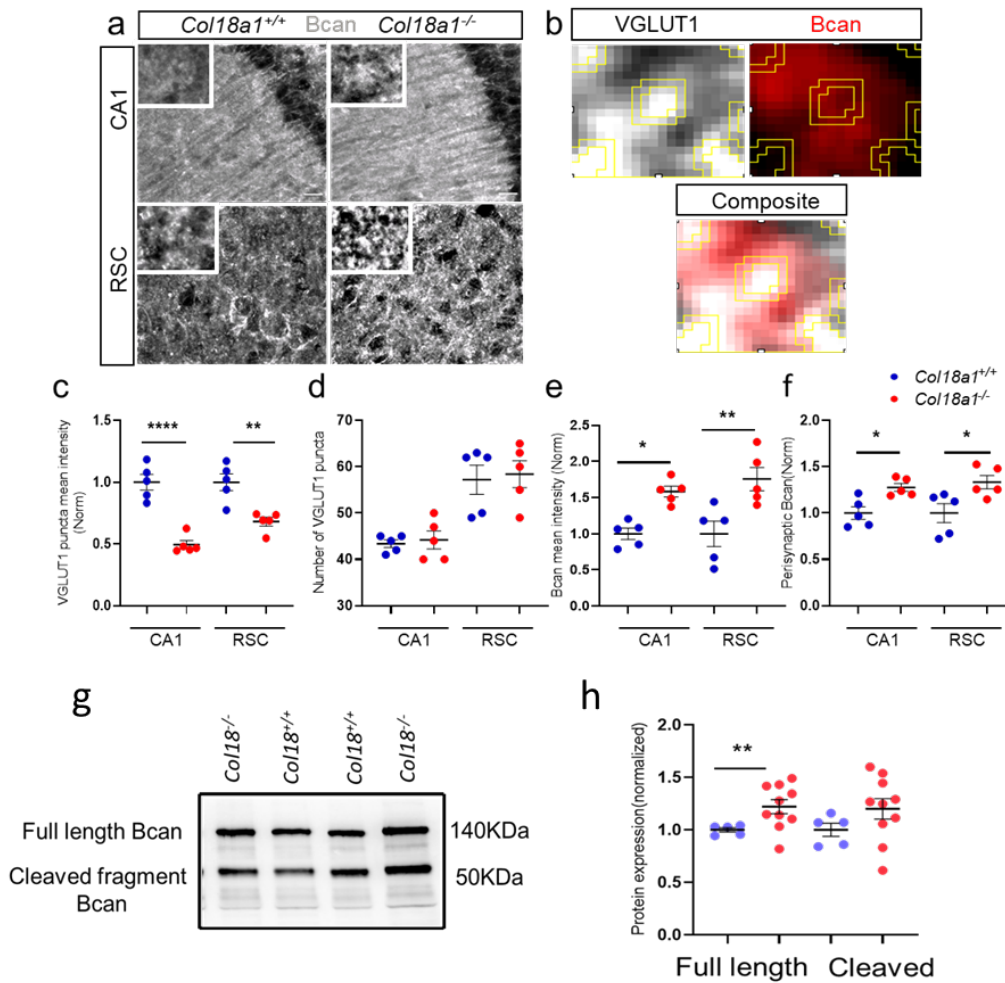


Figure 4.11 Upregulation of perisynaptic ECM proteoglycan Bcan and downregulation presynaptic VGLUT1 in *Col18a1*^{-/-} mice

(a) Representative 63x images of Bcan expression in the CA1 and RSC regions. (b) Magnified image of single presynaptic puncta and surrounding ECM to count excitatory synapses and measure the perisynaptic ECM associated with them. (c & d) Quantification of VGLUT1⁺ puncta within the CA1 and RSC regions of *Col18a1*^{-/-} mice revealed a significant reduction in the intensity of VGLUT1⁺ puncta (c); however, there were no changes in the number of VGLUT1⁺ puncta (d) in the neuropil of *Col18a1*^{-/-} mice. (e) The mean intensity of Bcan was significantly increased in the CA1 and RSC of *Col18a1*^{-/-} mice compared to wild-type animals. (f) The mean intensity of presynaptic Bcan was significantly increased in the CA1 and RSC regions of *Col18a1*^{-/-} mice. Bar graphs show the mean \pm SEM values, while * $p < 0.05$, ** $p < 0.01$, *** $p < 0.001$ and **** $p < 0.0001$ represent significant differences between *Col18a1*^{+/+} mice (N=5) and *Col18a1*^{-/-} (N=5) mice using two-way RM ANOVA and Sidak's multiple comparisons test. (g & h) shows that there is an upregulation in the level of full-length Bcan protein in the cortex of 12-month-old mice, but not the cleaved fragment protein. Bar graphs show the mean \pm SEM values, while * $p < 0.05$, ** $p < 0.01$, *** $p < 0.001$ and **** $p < 0.0001$ represent significant differences between *Col18a1*^{+/+} (N=6) and *Col18a1*^{-/-} (N=11) mice using a t-test with Welch's correction.

4.11 Evaluation of gene expression of CSPGs, enzymes regulating their proteolysis and TGF β 1/SMAD3/TIMP-3 signalling in *Coll8a1*^{-/-} mice

Further, we examined the expression of several key ECM-related genes to gain insight into the mechanisms underlying the dysregulation of neural ECM in *Coll8a1*^{-/-} mice. We observed a significant mRNA overexpression of *Acan* (t-test with Welch's correction here and below, $p = 0.0214$) and downregulation in *Ncan* and *Bcan* ($p = 0.0231$ and $p = 0.0168$, respectively) (**Fig. 4.12 a**). Moreover, the expression of the link protein *Hpln4* and CSPG cross-linking glycoprotein *Tnr* was significantly increased ($p = 0.0081$ and $p = 0.0017$, respectively), while the expression of *Hpln3* was decreased ($p = 0.0297$), and no change in the expression of *Hpln2* was detected ($p = 0.1276$) (**Fig. 4.12 a**). The expression of *Timp3* ($p = 0.0309$), *Adamts4* ($p = 0.0175$), *Mmp2* ($p = 0.0463$) and *Ctss* (t-test $p = 0.0235$) was significantly increased, while the expression of *MMP9* ($p = 0.0086$) was decreased. There were no changes observed in the expression of *Timp1*, *Timp2*, *Timp4* and *Adamts5* (**Fig. 4.12 b**). In summary, these data highlight a complex pattern of changes in the gene expression of proteins controlling the stability and proteolysis of ECM as molecular correlates of detected alterations in perineuronal and perisynaptic ECM.

As TIMP-3 is the regulator of multiple proteinases, including ADAMTS-4 and -5, which cleave CSPGs, we performed Western blot analysis to determine the protein level of TIMP-3 in *Coll8a1*^{-/-} mice, and we found a significant upregulation of this protein level (t-test with Welch's correction, $p = 0.0302$) (**Fig. 4.12 c & d**). In contrast, the protein level of ADAMTS-4 remained unchanged in *Coll8a1*^{-/-} mice (t-test with Welch's correction, $p = 0.2342$) (**Fig. 4.12 c & d**).

To understand the mechanism that underlies the upregulation of TIMP-3, we examined the TGF- β 1 mediated signalling, which elevation has been previously linked to CSVD and diverse vascular diseases in humans, including hereditary hemorrhagic telangiectasia, Loeys-Dietz syndrome, and pulmonary arterial hypertension (Ten Dijke and Arthur 2007, Goumans, Liu et al. 2009). Elevated TGF- β signaling is a strong candidate that may explain matrix accumulation (Yamamoto and Ihara 2017, Kato, Sekine et al. 2020).

Initially, we checked the protein level of TGF- β 1 based on our findings which indicate that there is an overexpression of *Tgfb1* mRNA in the *Coll8a1*^{-/-} mice. Consistently with our qPCR finding, we observed an upregulation of TGF- β 1 protein level in *Coll8a1*^{-/-} mice (t-test with Welch's correction, $p = 0.0220$) (**Fig. 4.12 c & d**).

The TGF- β /SMAD3 pathway has previously been demonstrated to induce ECM production in conjunction with the Ras/MEK/ERK MAP kinase or the p38 MAP kinase pathway. As SMAD3 is the key player in this cascade, we evaluated its expression and found that this protein had become more phosphorylated in the *Col18a1*^{-/-} mice (t-test with Welch's correction for pSMAD3/SMAD3 ratio, $p = 0.0422$). Thus, according to our findings, TGF- β 1-induced upregulation of TIMP-3 expression may be driven via the canonic SMAD3 pathway, resulting in inhibition of proteases and accumulation of perisynaptic ECM molecules.

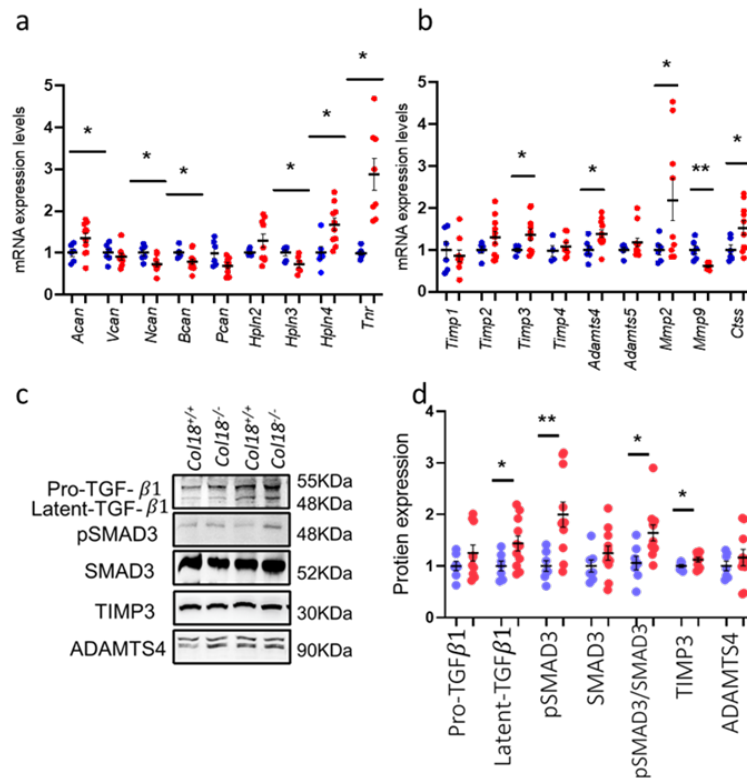


Figure 4.12 Evaluation of gene expression of CSPGs and proteins regulating ECM proteolysis and TGF- β 1/SMAD3/TIMPT-3 cascade in *Col18a1*^{-/-} mice. (a) Hippocampal expression of major genes encoding the PNN CSPGs (*Acan*, *Vcan*, *Ncan*, *Bcan* and *Pcan*), link proteins (*Hpln2*, *Hpln3*, *Hpln4*) and *Tnr*. **(b)** Hippocampal expression of genes encoding the tissue metalloprotease inhibitors *Timp1*, *Timp2*, *Timp3* and *Timp4* and genes encoding major metalloproteases degrading the neural ECM proteins *Adamts4*, *Adamts5*, *Mmp2*, *Mmp9*, and *Ctss*. *Bcan*, brevican; CA1, CA1 region of the hippocampus; CSPG, chondroitin sulfate proteoglycan; ECM, extracellular matrix; PNN, perineuronal net; RSC, retrosplenial cortex; VGLUT1, vesicular glutamate transporter 1. Scale bars = 20 μ m. **(c & d)** Demonstrated cortical western blot analysis of TGF- β 1, pSMAD3/SMAD3, TIMP-3 and ADAMTS-4 in 12-month-old mice. Bar graphs show the mean \pm SEM values, while * $p < 0.05$, ** $p < 0.01$, *** $p < 0.001$ and **** $p < 0.0001$ represent significant differences between *Col18a1*^{+/+} (N=6) and *Col18a1*^{-/-} (N=11) mice using the t-test with Welch's correction.

5 Discussion

Utilizing both histological and immunohistochemical methods, we showcased that a deficiency of collagen XVIII in 5- and 12-month-old *Col18a1* knockout mice leads to microvascular irregularities. These irregularities resemble the preliminary stages of CSVD without any noticeable increase in PVS or significant hemorrhagic or ischemic lesions. Such microvascular irregularities were found alongside glial cell activation, (peri)vascular ECM alterations, and varied shifts in the inhibitory and excitatory neural pathways in the CA1 and RSC. Furthermore, the ECM's perineuronal and perisynaptic structures, which play a crucial role in managing synaptic effectiveness and adaptability within these pathways, were disrupted. Through our qPCR investigations, we pinpointed the altered expression of multiple genes potentially driving these intertwined modifications, which are depicted in **Figure 5.1**. For this research, we selected the hippocampus and RSC as the primary focus due to their involvement in memory and learning processes, and their significance in dementia and cognitive deterioration. Notably, within the RSC, cognitive deficits and memory challenges have been detected after injuries to this region, indicating its pivotal role in maintaining cognitive abilities throughout one's life (Trask and Fournier 2022). Furthermore, a marked reduction in size and neuron count in the hippocampal CA1 area of AD patients stands out as a characteristic symptom of the ailment (Ball 1977). Thus, the *Col18a1*^{-/-} mice offer a representation of the initial or milder phases of CSVD, shedding light on potential ways to understand the defense mechanisms that can halt the disease's advancement. In the sections that follow, we delve into the mechanisms at play and how our discoveries align with clinical observations in CSVD and other well-recognized CSVD experimental models.

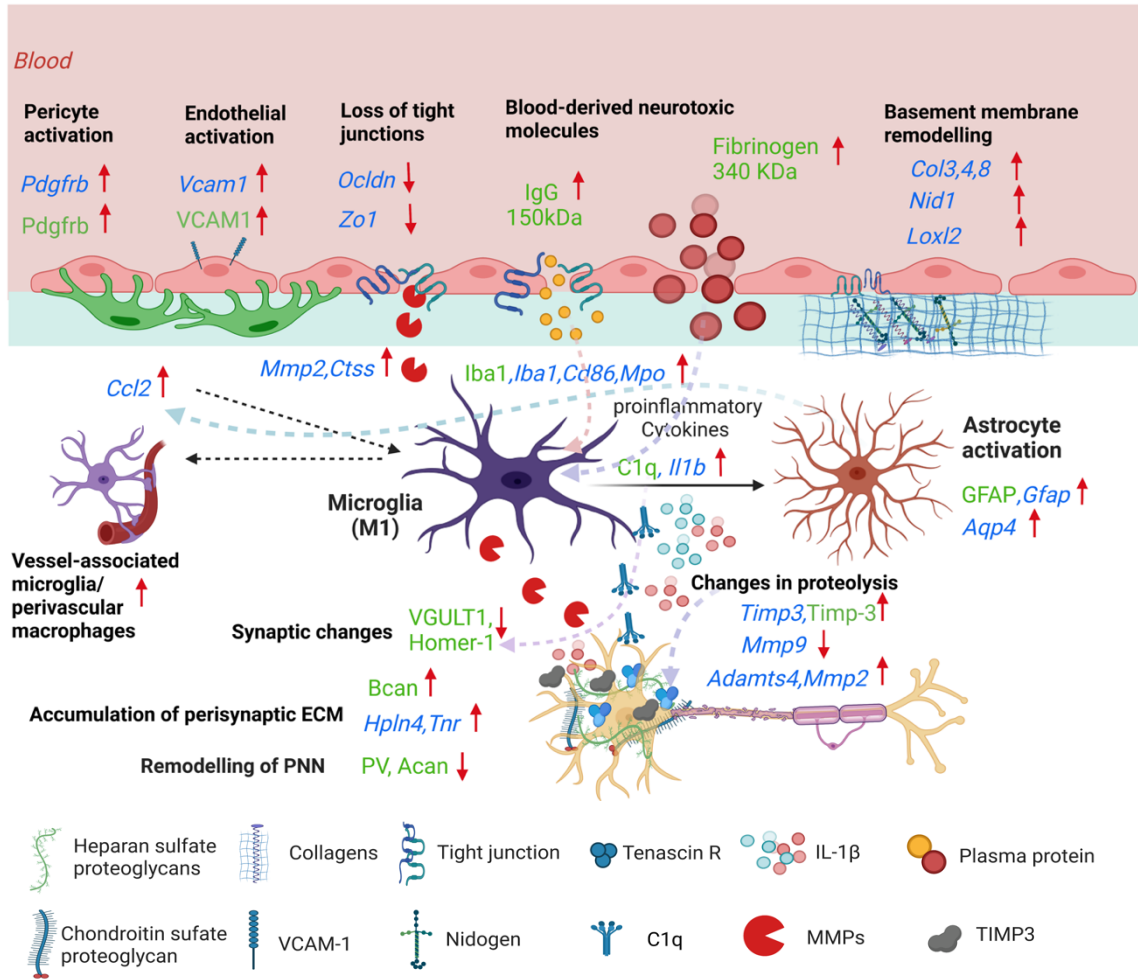


Figure 5.1 Summary of findings in *Col18a1*^{-/-} mice.

In the absence of collagen XVIII, a variety of changes occurs, including the activation of pericytes and endothelial cells, the remodeling of the basement membrane and impaired function of tight junctions that leads to the CNS entry of blood-derived neurotoxic molecules. The BBB damage promotes microglia activation. Activated microglia secrete C1q, IL-1β, MMP2 and CTSS. MMP2 and CTSS may contribute to further degradation of junctional proteins, enlarging the gap between endothelial cells. Following the activation of astrocytes by IL-1β and TGF-β1, reactive astrocytes secrete CCL2, which stimulates migration and recruitment of microglia/perivascular macrophages to damaged vessels. Changes in expression of proteinases and their tissue inhibitors result in remodeling of PNNs, perisynaptic ECM and C1q accumulation, and synaptic modifications. Alterations in protein levels are represented by green and in gene levels by blue. The figure was generated with Biorender.com (Biorender, Toronto, Ontario, Canada). *Aqp4*, aquaporin 4; *Adamts4*, a disintegrin-like and metallopeptidase with thrombospondin type 1 motif 4; *Acan*, Aggrecan; *Bcan*, Brevican; *Col3a1*, collagen 3 alpha 1; *Col4a1*, collagen 4 alpha 1; *Col8a1*, collagen 8 alpha 1; *Cldn5*, claudin 5; *Ccl2*, (C-C motif) ligand 2; *C1q*, complement component 1q; *Gfap*, glial fibrillary acidic protein; *Hpln4*, Hyaluronan and proteoglycan link protein 4; *Iba1*, ionized calcium-binding adapter molecule 1; *Il1b*, interleukin 1 beta; *Loxl-2*, lysyl oxidase homolog 2; *Mmp2,9*, Matrix metallopeptidase 2,9; *Mpo*, myeloperoxidase; *Nid1*, nidogen1; *Ocln*, occludin; *Pdgfrb*, platelet-derived growth factor receptor beta; *PV*, Parvalbumin; *Tnr*, Tenascin-R; *Timp3*, Tissue inhibitor

of metalloproteinase 3; *Vcam-1*, vascular cell adhesion molecule 1; VGLUT1, vesicular glutamate transporter 1; *Zo1*, zonula occludens-1.

5.1 Collagen XVIII deficiency and microvascular pathology

The inception of our research was influenced by an earlier study by Moulton and team, which explored permeability with regard to albumin-bound Evans blue dye in the aorta and tiny vessels in the skin of *Coll8a1^{-/-}* and *Coll8a1^{+/-}* mice. They noted a doubling of permeability under regular conditions and amidst hypercholesterolemia (Moulton, Olsen et al. 2004). The presence of type XVIII collagen at the junction of the fibrillar matrix hints at a possible anchoring role, suggesting that its absence may lead to basement membrane instability.

Our findings highlighted a heightened BBB permeability to mouse IgG in the profound gray matter of 5-month-old *Coll8a1^{-/-}* mice. This was observed along with a widespread accumulation of intravascular erythrocytes in the capillaries and arterioles of the cortex, hippocampus, and deep gray matter, with a subdued presence in the white matter. As the mice aged to 12 months, BBB permeability in the *Coll8a1^{-/-}* mice escalated, predominantly affecting the cortical and hippocampal regions. However, the frequency of intravascular erythrocyte buildup remained consistently high but showed no further increase with age in the *Coll8a1^{-/-}* mice. This contrasted with the continuous rise seen in *Coll8a1^{+/+}* mice. Echoing our findings, erythrocyte stases were pinpointed as the initial histological anomaly of CSVD in hypertensive rats, observable across the brain, especially in the cortex, deep gray matter, and hippocampus, and to a lesser extent in white matter (Braun, Bueche et al. 2012). These stases symbolize endothelial damages, sparking wound healing mechanisms, thrombus formation, and local reductions in cerebral blood flow (Schreiber, Bueche et al. 2013, Jandke, Garz et al. 2018). The dysfunction of endothelial cells (EC) is pivotal in CSVD pathogenesis, even preceding BBB disruption (Rajani, Quick et al. 2018). This dysfunction is perceived to be distinct from but connected to endothelial activation, which is characterized by a rise in the expression of adhesion molecules like *Vcam1* and E-selectin. Such activations usually result from inflammatory triggers, hypertension (Graham, McBride et al. 2007), and as our study suggests, also due to the deficiency of collagen XVIII. VCAM-1 is a critical cell adhesion molecule interacting with integrin receptors, influencing both leukocyte and neuronal activities, and is linked with AD dementia (Huang, Tsai et al. 2015). Erythrocytes also adhere to the endothelium via adhesion molecules like VCAM-1, which is related to a higher chance of

compromised hemodynamics and thrombus formation (Badimon and Vilahur 2014). Given that COL18A1-derived endostatin diminishes *Vcam1* expression, its upregulation aligns with an endostatin deficiency in *Coll18a1*^{-/-} mice, potentially relating to erythrocyte clustering (Kivinen, Felszeghy et al. 2016).

The BBB is crucial for regulating the entry of cells and molecules into the brain tissue. Its functionality hinges on the establishment and sustenance of tight junction protein assemblies among ECs and the structural soundness of the BM. The elevated BBB permeability observed in *Coll18a1*^{-/-} mice could possibly be associated with a weakened synthesis of endothelial tight junction proteins (notably, the downregulation of *Ocln* and *Zo1*), their degradation by enzymes like the elevated *Mmp2*, or inherent structural deficiencies of the BM without COL18A1. It's worth noting that IL-1 β has been found to amplify BBB permeability by suppressing the production of TJ proteins (Laflamme, Lacroix et al. 1999, Blamire, Anthony et al. 2000). Additionally, IL-1 β encourages astrocytes to excrete vascular endothelial growth factor, further elevating BBB permeability (Argaw, Zhang et al. 2006). Consequently, IL-1 β is involved in the deterioration of the BBB through both direct and auxiliary mechanisms (Wang, Jin et al. 2014). Compromised BBB function is a recognized pathological trait in the onset of cognitive deterioration in CSVD as well as in several neurodegenerative conditions, including AD and Parkinson's disease (PD) (Montagne, Barnes et al. 2015, Yamazaki and Kanekiyo 2017, Qin, Li et al. 2019). Diminished production levels of TJ proteins can lead to a weakened barrier, resulting in microbleeds, and might also correlate with heightened endothelial cell growth.

5.2 Collagen XVIII deficiency and activation of glial cells

In the *Coll18a1*^{-/-} mice, glial cells exhibited signs of activation. Specifically, microglia presented a less ramified structure, larger cell bodies, and were observed near blood vessels. Simultaneously, astrocytes had elevated protein levels of the activation marker, GFAP. There's established evidence that microglia take on an activated and phagocytic state in reaction to a compromised BBB (Merlini, Rafalski et al. 2019). These shifts in form and function of the activated glial cells coincide with the release of various chemokines and cytokines, as well as alterations in the expression of surface antigens (Wyss-Coray and Mucke 2002, Vom Berg, Prokop et al. 2012). Through q-PCR analyses, there was an observed increase in the expression of microglial/macrophage markers such

as *Iba1*, *Cd86*, *Mpo*, *Il1b*, *Ccl2*, and the astrocytic marker *Gfap* in *Coll8a1*^{-/-} mice. A more recent investigation highlighted that IL-1 β prompted astrocytes to produce pro-inflammatory chemokines like CCL2, CCL20, and CXCL2. These chemokines further instigate the migration of immune cells, including neutrophils, monocytes, macrophages, dendritic cells, and pathogenic T cells, leading to a disturbed BBB and resultant neuroinflammation (Wang, Jin et al. 2014). Elevated CCL2 levels were detected in the blood of hypertensive patients and were associated with the extent of damage caused by hypertension (Rudemiller and Crowley 2017). Additionally, increased concentrations of CCL2 were identified in brain tissue and CSF of AD patients and were indicative of cognitive decline in early AD stages (Ishizuka, Kimura et al. 1997, Sokolova, Hill et al. 2009, Westin, Buchhave et al. 2012). An earlier investigation demonstrated that CCL2 stimulated and attracted microglia to injury sites (Cherry, Meng et al. 2020). This could explain the observed congregation of microglial cells around compromised blood vessels in *Coll8a1*^{-/-} mice.

The processes of microglial cells are notably dynamic. These cells actively survey the healthy brain, aid in reshaping the ECM, clear malfunctioning synapses, and supply neurons with trophic factors, thereby bolstering the adaptability of neural connections (Nimmerjahn, Kirchhoff et al. 2005). C1q serves as the identifying component of the multi-component classical complement pathway. Earlier research indicated an augmented synthesis of C1q in young AD mouse models, notably before the manifestation of fibrillar amyloid plaques (Benoit, Hernandez et al. 2013). Our current investigation highlights increased C1q protein accumulation, with no evident alterations in *C1q* gene expression in the CA1 and RSC areas of *Coll8a1*^{-/-} mice. This could potentially explain the synaptic modifications detailed in section 5.4.

Microglial activation might stimulate astrocyte activation. When microglia are activated, they release significant quantities of TNF- α and IL1 α/β , driving dormant astrocytes towards the A1 phenotype (Liddelow, Guttenplan et al. 2017). Once activated, A1 astrocytes produce elevated levels of intermediate filaments like glial fibrillary acidic protein (GFAP) and vimentin (Liddelow, Guttenplan et al. 2017). Based on our IHC staining results, we observed a rise in both GFAP coverage and intensity, indicating activation. Additionally, heightened expression of *S100a10* hints at an increase in the A2 astrocyte population (Fujita, Yamaguchi et al. 2018).

5.3 *Col18a1* knockout and remodeling of perineuronal and perisynaptic ECM

The ECM surrounding PV+ interneurons and the perisynaptic ECM on primary cells consists of lecticans, such as Acan, Bcan, Ncan, and Vcan. These lecticans can be cleaved by enzymes like MMP9, ADAMTS-4 and -5, and CTSS. In the CA1 region of *Col18a1*^{-/-} mice, it was observed that 36% of the PV+ interneurons lacked Acan+ PNNs. Moreover, the average intensity of Acan expression in PV+ Acan+ cells was diminished. Given that PNNs regulate excitability and synaptic signals to perisomatic interneurons (Hayani, Song et al. 2018) — essential for synchronizing neural action and managing gamma oscillations — our data indicates that Acan loss could underlie specific cognitive impairments observed in *Col18a1*^{-/-} mice. This Acan reduction corresponded with a surge in the mRNA levels of *Adamts4* and *Ctss*. The heightened expression of these proteases has been documented in several pathologies like AD, ischemic stroke, and others (Sato, Suzuki et al. 2000, Lemarchant, Pomeschik et al. 2016, Lowry and Klegeris 2018). However, their potential role in CSVD warrants further study. Given the potential of *Adamts4* to cleave Vcan found in blood vessels, it was postulated that its increased expression, possibly from activated microglia, could influence BBB opening and PNN abnormalities. Yet, no significant shifts in ADAMTS-4 protein levels were detected in *Col18a1*^{-/-} mice, suggesting an alternate theory wherein microglial activation might instigate vascular and PNN alterations (Nakanishi 2003). Compounding this, hypoxia-induced neuroinflammation can spur microglia/macrophages to produce proteases and free radicals, further exacerbating damage to the ECM and NVU over time. The MMPs, while intended to remodel vascular walls, “unintentionally” compromise the BBB and affect myelinated fibers (Rosenberg 2017).

Conversly, a noticeable accumulation of Bcan was spotted in *Col18a1*^{-/-} mice, both within the general neuropil and specifically at perisynaptic areas. In an AD-like mouse model, escalations in Bcan and other CSPGs corresponded to disruptions in long-term potentiation and memory (Végh, Heldring et al. 2014). Elevated Bcan levels were also documented in models of brain injuries, both at the site of the lesion and surrounding areas (Blamire, Anthony et al. 2000). This accumulation in Bcan aligns with an increased expression of proteins that fortify connections between lecticans and hyaluronic acid (*Hpln4*), link up lecticans (*Tnr*) (Morawski, Dityatev et al. 2014), and stave off the proteolytic division of lecticans by ADAMTS-4/5 (*Timp3*). Significantly, in the CADASIL

variant of CSVD, an upswing in TIMP-3 was observed, and eliminating TIMP-3 was shown to mitigate CADASIL's pathological effects (Capone, Cognat et al. 2016).

In conclusion, *Coll8a1*^{-/-} mice exhibited contrasting changes in the perineuronal and perisynaptic ECM. This demands a more nuanced assessment of the spatial shifts in the expression of lecticans and associated stabilizing proteins.

5.4 *Coll8a1* knockout and defects in glutamatergic synapses

Prior studies have indicated that alterations and reductions in glutamatergic synapses are closely associated with cognitive deficits seen in both vascular dementia and AD (Kirvell, Esiri et al. 2006; Kashani, Lepicard et al. 2008; Kirvell, Elliott et al. 2010). A consistent feature of the pathological transformations linked to dementia, synaptic deterioration has been shown to be the most precise indicator of the progression of AD (DeKosky and Scheff 1990). There is also a crucial role for synaptic plasticity in the development of VaD. Synapse damage occurs in the early stages of VaD, and the degree of damage is related to the degree of cognitive impairment. It has been demonstrated that cognitive dysfunction is closely linked to synaptic plasticity dysfunction in animal models of VaD (Lisman, Schulman et al. 2002, Xiao, Wang et al. 2018). N-methyl-D-aspartic acid receptor (NMDAR; comprising subunits NR2A and NR2B) and calmodulin-dependent protein kinase II (CaMKII) play pivotal roles in modulating synaptic plasticity. They are intimately linked with processes related to learning and memory (Lisman, Schulman et al. 2002; Hussain, Ringsevjen et al. 2016). Studies have found that a decrease in CaMKII protein levels is correlated with damage to LTP induction in the hippocampus of VaD rats (Yang, Yao et al. 2017). Our study indicated a notable decrease in VGLUT1 mean intensity in the CA1 area, while VGLUT2 concentrations stayed consistent. In a similar trend to VGLUT1, we observed diminished expression of the glutamatergic postsynaptic scaffold protein, Homer1. Yet, the count of VGLUT1 puncta appeared unaltered, pointing to synaptic alterations in *Coll8a1*^{-/-} mice rather than a complete loss of excitatory synapses. Past research has highlighted fluctuations in VGLUT1 and VGLUT2 following instances of transient global cerebral ischemia (Llorente, Pérez-Rodríguez et al. 2013). Furthermore, a decline in VGLUT1 has been associated with cognitive function in individuals with vascular dementia (Kirvell, Elliott et al. 2010). In a separate study involving an AD mouse model, it was found that fibrinogen, present at vascular injury sites, fosters spine loss and cognitive

deterioration through a harmful microglial reaction (Merlini, Rafalski et al. 2019). Future investigations should determine whether these synaptic variations are connected to the increased presence of perisynaptic ECM or other inflammatory factors, such as elevated deposits of C1q/fibrinogen, playing a vital role in modulating microglia and synapse interactions.

5.5 TGF- β 1/SMAD3/TIMP-3 signalling play a role in *Col18a1*^{-/-} mice ECM alterations

The TGF- β /SMAD signaling route, one of the most intricate and predominant pathways in vascular development, holds diverse roles in brain vessel development and stability. Abnormalities in this pathway have been linked to numerous cerebrovascular issues (Park, Wankhede et al. 2009, Nguyen, Lee et al. 2011, Maddaluno, Rudini et al. 2013). TGF- β signaling is known to be involved in the formation and permeability of the BBB, influencing tight and adherens junctions. TGF- β 1, originating from pericytes, increases the levels of claudin-5 and aids in the maturation of the BBB, primarily through the reduction of endothelial CD146 expression (Chen, Luo et al. 2017). It has been observed that pericytes stimulate and enhance BBB functionalities via consistent TGF- β synthesis (Dohgu, Takata et al. 2005). ALK5 in pericytes increases tissue TIMP-3, which regulates endothelial morphogenesis in the germinal matrix. A deficiency of *Alk5* in embryonic mouse pericytes results in a pronounced germinal matrix hemorrhage-intraventricular hemorrhage (GMH-IVH), a consequence of the increased matrix metalloproteinases (MMPs) breaking down the basement membrane (Dave, Mirabella et al. 2018). A recent study posits that impaired BBBs in aging populations, both human and rodent, are connected to overstimulation of TGF- β signaling in astrocytes. The use of conditional genetic knockdown techniques on astrocytic TGF- β receptor-coding genes or the pharmacological obstruction of TGF- β signaling remedies these manifestations in older mice (Senatorov Jr, Friedman et al. 2019).

Current research underscores that abnormalities in TGF- β signaling correlate with human cerebrovascular ailments (Zhang and Yang 2020). Several genome-wide association studies (GWAS) or whole exome trio sequencing have identified multiple pathogenic gene variants in the TGF- β trajectory, correlating with conditions like small vessel ischemic strokes, intracerebral hemorrhages, and sporadic brain conditions (Yılmaz, Toktaş et al. 2016, Liu, Li et al. 2022). After an ischemic stroke event, a heightened expression of TGF- β 1 has been documented in brain tissue,

as well as in hereditary cerebral hemorrhage cases with the amyloidosis-Dutch type (Krupinski, Kumar et al. 1996). Due to the limited number of studies focusing on the mechanisms connecting cerebrovascular diseases with TGF- β dysfunction, our exploration sought to discern TGF- β 1's potential role in vascular irregularities in *Coll18a1*^{-/-} mice. Our findings emphasize the augmented signaling via the TGF- β 1/SMAD3/TIMP-3 sequence (**Figure 5.2**).

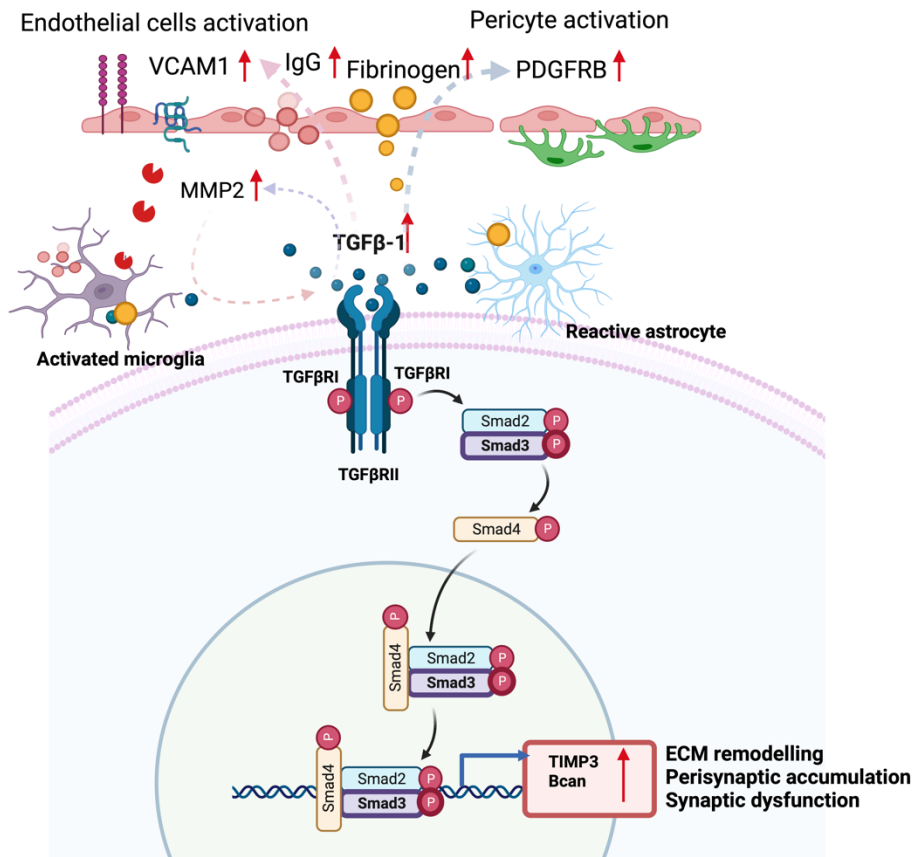


Figure 5.2 Illustration of TGF- β 1/SMAD3 signalling. In the absence of Collagen XVIII, the BBB breaks down, fibrinogen and albumin are extravasated, and microglia and astrocytes become activated. Activated microglia and reactive astrocytes secrete TGF- β 1 and MMP2. In turn, TGF- β 1 might stimulate endothelial cells and modulate pericytes' inflammatory response. Meanwhile, TGF- β 1 ligand binds to TGF- β receptor to form a complex. Receptor-induced phosphorylation of receptor activated Smads (R-Smads) leads to binding to cytoplasmic Smad2/3. Phosphorylated Smads form complexes with Smad4, which are then translocated to the nucleus where they bind to transcription factors that are crucial for gene expression of TIMP-3 and Bcan.

6 Conclusions

1. Our histological, immunohistochemical, q-PCR and western blot analyses revealed several hallmarks of CSVD in *Coll8a1*^{-/-} mice (**Figure 5.1 and 5.2**) such as:
 - erythrocyte aggregation in capillaries and arterioles,
 - opening of the BBB,
 - activation of pericytes and endothelial cells,
 - basement membrane remodeling,
 - activation of microglia and astroglia,
 - dysregulation of extracellular proteolysis resulting in removal of PNNs and accumulation of perisynaptic ECM,
 - reduced expression of key pre- and postsynaptic molecules.
2. Activation of TGF- β 1/SMAD3/TIMP-3 cascade, culminating in upregulation of TIMP-3 expression, appeared as a potential molecular mechanism linking together most of these changes.
3. Despite the *Coll8a1*^{-/-} mice not exhibiting characteristic markers of advanced CSVD stages, such as expanded perivascular space, significant hemorrhages, or infarcts, and given the reduced incidence of erythrocyte thrombi in capillaries and arterioles as these mice aged, this CSVD model might prove pivotal in examining the factors contributing to resistance or resilience against the progression of CSVD.

7 Future directions

A well-functioning brain relies on the balanced expression of extracellular proteases, their associated tissue inhibitors, and the extracellular matrix (ECM) molecules to sustain ECM turnover, which is crucial for adaptive synaptic and vascular plasticity. Yet, in numerous CNS diseases, the tension between tissue remodeling and maintaining homeostasis often results in an ECM pathology, which is potentially a key factor in advancing these conditions, especially in the cognitive domain. As highlighted, a number of experimental findings and biomarker research point to an altered MMP/TIMP balance in cases of stroke, CNS trauma, and CSVD. This is alongside evidence of an increase in ECM molecules in the prolonged phases of these conditions and even depression, and PNN reduction in epilepsy. This imbalance in ECM and extracellular proteolytic activity results in tangible symptoms via the engagement of TLRs and RPTPs, altering integrins, and variances in ion channel expressions and cellular adhesion molecules. Our proposed theory suggests a two-phase pathophysiological ECM regulation observed in both clinical and animal studies of varying CNS ailments, emphasizing the significance of the diffusion of ECM components, extracellular proteases, and their inhibitors between perivascular and perineuronal regions. Moreover, the activation of astrocytes prompted by BBB leakage is pivotal. These components might offer insight into why vascular impairment and BBB breaches are crucial pathological traits of neurodegenerative diseases, possibly culminating in a combination of hampered energy provision and the inhibition of synaptic plasticity due to ECM upregulation. Despite this, our understanding of the molecular dynamics governing ECM adjustments in human conditions remains in its infancy. Given the higher astrocyte-to-neuron ratio in human brains versus rodent brains, and the significance of astrocyte activation in the overproduction of neural ECM, it is conceivable that ECM-driven mechanisms might have a heightened role in humans. With the recent progress in neural ECM research, there is hope that ECM-centered therapies might emerge as potential treatments for neurological and psychiatric disorders. However, clinical trials centered around MMP inhibitors have largely been underwhelming. For example, using MMP inhibitors a week post-stroke led to amplified ischemic brain damage and hampered recovery two weeks later (Zhao, Wang et al. 2006). Another investigation revealed that nullifying MMP2/9 temporarily decreased the infarct size 24 hours post focal ischemia but didn't offer lasting protection. This seeming ineffectiveness might be attributed to various constraints, some technical, like MMP inhibitor specificity, and some rooted in biology. As previously outlined in our review

(Ulbrich, Khoshneviszadeh et al. 2021), MMPs' roles might pivot from being harmful to helpful over the disease's progression, making treatment timing crucial. Additionally, considering the spatial dynamics is essential, especially in CSVD, given the overlay of processes instigated by multiple BBB failures at different intervals. Consequently, a more nuanced approach, like utilizing prodrugs activated under specific inflammatory conditions or targeting specific cell types, might be beneficial. Delving into cell-specific proteomes through systems biology analysis and employing single-cell genomic evaluations could potentially aid in formulating such strategies.

8 References

Abbott, N. J., et al. (2010). "Structure and function of the blood–brain barrier." Neurobiology of Disease **37**(1): 13-25.

Abbott, N. J., et al. (2006). "Astrocyte–endothelial interactions at the blood–brain barrier." Nature Reviews Neuroscience **7**(1): 41-53.

Acharya, N. K., et al. (2013). "Diabetes and hypercholesterolemia increase blood-brain barrier permeability and brain amyloid deposition: beneficial effects of the LpPLA2 inhibitor darapladib." Journal of Alzheimer's Disease **35**(1): 179-198.

Al'Qteishat, A., et al. (2006). "Changes in hyaluronan production and metabolism following ischaemic stroke in man." Brain **129**(8): 2158-2176.

Alistair, D. G. (2002). "Hypertensive cerebral small vessel disease and stroke." Brain Pathology **12**(3): 358-370.

Argaw, A. T., et al. (2006). "IL-1 β regulates blood-brain barrier permeability via reactivation of the hypoxia-angiogenesis program." The Journal of Immunology **177**(8): 5574-5584.

Armulik, A., et al. (2005). "Endothelial/pericyte interactions." Circulation research **97**(6): 512-523.

Armulik, A., et al. (2010). "Pericytes regulate the blood–brain barrier." Nature **468**(7323): 557-561.

Arpino, V., et al. (2015). "The role of TIMPs in regulation of extracellular matrix proteolysis." Matrix Biology **44**: 247-254.

Asahi, M., et al. (2001). "Effects of matrix metalloproteinase-9 gene knock-out on the proteolysis of blood–brain barrier and white matter components after cerebral ischemia." Journal of Neuroscience **21**(19): 7724-7732.

Badimon, L. and G. Vilahur (2014). "Thrombosis formation on atherosclerotic lesions and plaque rupture." Journal of internal medicine **276**(6): 618-632.

Bager, C. and M. Karsdal (2016). Type XVIII Collagen. Biochemistry of Collagens, Laminins and Elastin, Elsevier: 113-121.

Bailey, E., et al. (2011). "Cerebral small vessel endothelial structural changes predate hypertension in stroke-prone spontaneously hypertensive rats: a blinded, controlled immunohistochemical study of 5-to 21-week-old rats." Neuropathology applied neurobiology **37**(7): 711-726.

- Balabanov, R. and P. Dore-Duffy (1998). "Role of the CNS microvascular pericyte in the blood-brain barrier." Journal of neuroscience research **53**(6): 637-644.
- Ball, M. (1977). "Neuronal loss, neurofibrillary tangles and granulovacuolar degeneration in the hippocampus with ageing and dementia." Acta neuropathologica **37**(2): 111-118.
- Banerjee, G., et al. (2017). "The increasing impact of cerebral amyloid angiopathy: essential new insights for clinical practice." Journal of Neurology **88**(11): 982-994.
- Bell, R. D. and B. V. Zlokovic (2009). "Neurovascular mechanisms and blood-brain barrier disorder in Alzheimer's disease." Acta neuropathologica **118**(1): 103-113.
- Benagiano, V., et al. (1996). "VIP-like immunoreactivity within neurons and perivascular neuronal processes of the human cerebral cortex." European Journal of Histochemistry **40**(1): 53-56.
- Benoit, M. E., et al. (2013). "C1q-induced LRP1B and GPR6 proteins expressed early in Alzheimer disease mouse models, are essential for the C1q-mediated protection against amyloid- β neurotoxicity." Journal of Biological Chemistry **288**(1): 654-665.
- Blamire, A., et al. (2000). "Interleukin-1 β -induced changes in blood-brain barrier permeability, apparent diffusion coefficient, and cerebral blood volume in the rat brain: a magnetic resonance study." Neurosci **20**(21): 8153-8159.
- Bobńska, K., et al. (2016). "The role of MMP genes in recurrent depressive disorders and cognitive functions." Acta neuropsychiatrica **28**(4): 221-231.
- Bonnans, C., et al. (2014). "Remodelling the extracellular matrix in development and disease." Nature reviews Molecular cell biology **15**(12): 786-801.
- Brauer, K., et al. (1993). "Distribution of parvalbumin-containing neurons and lectin-binding perineuronal nets in the rat basal forebrain." Brain research **631**(1): 167-170.
- Braun, H., et al. (2012). "Stases are associated with blood-brain barrier damage and a restricted activation of coagulation in SHRSP." Neurol Sci **322**(1-2): 71-76.
- Breteler, M. M. (2000). "Vascular risk factors for Alzheimer's disease:: An epidemiologic perspective." Neurobiology of aging **21**(2): 153-160.
- Brodsky, B. and N. K. Shah (1995). "The triple-lielix motif in proteins." The FASEB journal **9**(15): 1537-1546.

Capone, C., et al. (2016). "Reducing Timp3 or vitronectin ameliorates disease manifestations in CADASIL mice." Annals of neurology **79**(3): 387-403.

Capone, C., et al. (2016). "Mechanistic insights into a TIMP3-sensitive pathway constitutively engaged in the regulation of cerebral hemodynamics." Elife **5**: e17536.

Carare, R., et al. (2008). "Solutes, but not cells, drain from the brain parenchyma along basement membranes of capillaries and arteries: significance for cerebral amyloid angiopathy and neuroimmunology." Neuropathology applied neurobiology **34**(2): 131-144.

Cargill, R., et al. (2012). "Astrocytes in aged nonhuman primate brain gray matter synthesize excess hyaluronan." Neurobiology of aging **33**(4): 830. e813-830. e824.

Chabriat, H., et al. (2009). "Cadasil." The Lancet Neurology **8**(7): 643-653.

Charidimou, A., et al. (2017). "Emerging concepts in sporadic cerebral amyloid angiopathy." Brain **140**(7): 1829-1850.

Charlton, R. A., et al. (2006). "The cognitive profiles of CADASIL and sporadic small vessel disease." Neurology **66**(10): 1523-1526.

Chen, J., et al. (2017). "CD146 coordinates brain endothelial cell–pericyte communication for blood–brain barrier development." Proceedings of the National Academy of Sciences **114**(36): E7622-E7631.

Cherry, J. D., et al. (2020). "CCL2 is associated with microglia and macrophage recruitment in chronic traumatic encephalopathy." Journal of neuroinflammation **17**(1): 1-12.

Cines, D. B., et al. (1998). "Endothelial cells in physiology and in the pathophysiology of vascular disorders." The Journal of the American Society of Hematology **91**(10): 3527-3561.

Cordonnier, C. and W. M. van der Flier (2011). "Brain microbleeds and Alzheimer's disease: innocent observation or key player?" Brain **134**(2): 335-344.

Craggs, L. J., et al. (2013). "Quantitative vascular pathology and phenotyping familial and sporadic cerebral small vessel diseases." Brain Pathology **23**(5): 547-557.

Cuadrado-Godia, E., et al. (2018). "Cerebral small vessel disease: a review focusing on pathophysiology, biomarkers, and machine learning strategies." Journal of stroke **20**(3): 302.

Dave, J. M., et al. (2018). "Pericyte ALK5/TIMP3 axis contributes to endothelial morphogenesis in the developing brain." Developmental cell **44**(6): 665-678. e666.

Dehouck, M.-P., et al. (1997). "Endothelin-1 as a mediator of endothelial cell-pericyte interactions in bovine brain capillaries." Journal of Cerebral Blood Flow

17(4): 464-469.

DeKosky, S. T. and S. W. Scheff (1990). "Synapse loss in frontal cortex biopsies in Alzheimer's disease: correlation with cognitive severity." Annals of neurology **27**(5): 457-464.

Deli, M. A. (2009). "Potential use of tight junction modulators to reversibly open membranous barriers and improve drug delivery." Biochimica et Biophysica Acta -Biomembranes **1788**(4): 892-910.

Dityatev, A. (2010). "Remodeling of extracellular matrix and epileptogenesis." Epilepsia **51**: 61-65.

Dityatev, A., et al. (2007). "Activity-dependent formation and functions of chondroitin sulfate-rich extracellular matrix of perineuronal nets." Developmental neurobiology **67**(5): 570-588.

Dityatev, A. and M. Schachner (2003). "Extracellular matrix molecules and synaptic plasticity." Nature Reviews Neuroscience **4**(6): 456-468.

Djrbal, L., et al. (2017). "Chondroitin sulfates and their binding molecules in the central nervous system." Glycoconjugate journal **34**(3): 363-376.

Dohgu, S., et al. (2005). "Brain pericytes contribute to the induction and up-regulation of blood-brain barrier functions through transforming growth factor- β production." Brain research **1038**(2): 208-215.

Dong, S., et al. (2003). "Expression of collagen XVIII and localization of its glycosaminoglycan attachment sites." Journal of Biological Chemistry **278**(3): 1700-1707.

Doubal, F. N., et al. (2010). "Enlarged perivascular spaces on MRI are a feature of cerebral small vessel disease." Stroke **41**(3): 450-454.

Duering, M., et al. (2012). "Incident subcortical infarcts induce focal thinning in connected cortical regions." Neurology **79**(20): 2025-2028.

Dziewulska, D., et al. (2017). "Changes in the vascular extracellular matrix as a potential cause of myocyte loss via anoikis in cerebral autosomal dominant arteriopathy with subcortical infarcts and leukoencephalopathy." J Clin Exp Pathol **7**(332): 2161-0681.1000332.

Dzwonek, J., et al. (2004). "Matrix metalloproteinases and their endogenous inhibitors in neuronal physiology of the adult brain." FEBS letters **567**(1): 129-135.

Elfont, R. M., et al. (1989). "Adrenergic receptors on cerebral microvessels: pericyte contribution." American Journal of Physiology **256**(1): R224-R230.

Engelhardt, B. and S. Liebner (2014). "Novel insights into the development and maintenance of the blood–brain barrier." Cell adhesion & migration **355**(3): 687-699.

Erdő, F., et al. (2017). "Age-associated physiological and pathological changes at the blood–brain barrier: a review." Journal of Cerebral Blood Flow **37**(1): 4-24.

Fassbender, K., et al. (1999). "Adhesion molecules in cerebrovascular diseases: evidence for an inflammatory endothelial activation in cerebral large- and small-vessel disease." Stroke **30**(8): 1647-1650.

Fu, Y. and Y. J. F. i. I. Yan (2018). "Emerging role of immunity in cerebral small vessel disease." Frontiers in Immunology **9**: 67.

Fujita, A., et al. (2018). "Connexin 30 deficiency attenuates A2 astrocyte responses and induces severe neurodegeneration in a 1-methyl-4-phenyl-1, 2, 3, 6-tetrahydropyridine hydrochloride Parkinson's disease animal model." Journal of neuroinflammation **15**(1): 1-20.

Fukai, N., et al. (2002). "Lack of collagen XVIII/endostatin results in eye abnormalities." The EMBO journal **21**(7): 1535-1544.

Gao, Y., et al. (2022). "Cerebral small vessel disease: Pathological mechanisms and potential therapeutic targets." Frontiers in aging neuroscience: 938.

Gautam, J., et al. (2016). "The role of pericytic laminin in blood brain barrier integrity maintenance." Scientific reports **6**(1): 1-13.

Gervais, É., et al. (2021). "Structural analysis of the microglia-interneuron interactions in the CA1 hippocampal area of the APP/PS1 mouse model of Alzheimer's disease." Journal of Comparative Neurology.

Ghosh, M., et al. (2015). "Pericytes are involved in the pathogenesis of cerebral autosomal dominant arteriopathy with subcortical infarcts and leukoencephalopathy." Annals of neurology **78**(6): 887-900.

Girouard, H. and C. Iadecola (2006). "Neurovascular coupling in the normal brain and in hypertension, stroke, and Alzheimer disease." Journal of applied physiology **100**(1): 328-335.

Glenn, J., et al. (1992). "Characterisation of ramified microglial cells: detailed morphology, morphological plasticity and proliferative capability." Journal of anatomy **180**(Pt 1): 109.

Göhring, W., et al. (1998). "Mapping of the binding of platelet-derived growth factor to distinct domains of the basement membrane proteins BM-40 and perlecan and distinction from the BM-40 collagen-binding epitope." European journal of biochemistry **255**(1): 60-66.

Gottschall, P. E. and M. D. Howell (2015). "ADAMTS expression and function in central nervous system injury and disorders." Matrix Biology **44**: 70-76.

Goumans, M.-J., et al. (2009). "TGF- β signaling in vascular biology and dysfunction." Cell research **19**(1): 116-127.

Graham, D., et al. (2007). "Candidate genes that determine response to salt in the stroke-prone spontaneously hypertensive rat: congenic analysis." Hypertension **50**(6): 1134-1141.

Greenberg, S. M., et al. (2009). "Cerebral microbleeds: a guide to detection and interpretation." The Lancet Neurology **8**(2): 165-174.

Grossetete, M., et al. (2009). "Elevation of matrix metalloproteinases 3 and 9 in cerebrospinal fluid and blood in patients with severe traumatic brain injury." Neurosurgery **65**(4): 702-708.

Gu, Z., et al. (2005). "A highly specific inhibitor of matrix metalloproteinase-9 rescues laminin from proteolysis and neurons from apoptosis in transient focal cerebral ischemia." Journal of Neuroscience **25**(27): 6401-6408.

Guerrini, U., et al. (2002). "New insights into brain damage in stroke-prone rats: a nuclear magnetic imaging study." Stroke **33**(3): 825-830.

Günzel, D. and A. S. Yu (2013). "Claudins and the modulation of tight junction permeability." Physiological reviews **93**(2): 525-569.

Gurney, K. J., et al. (2006). "Blood-brain barrier disruption by stromelysin-1 facilitates neutrophil infiltration in neuroinflammation." Neurobiology of Disease **23**(1): 87-96.

Haarmann, A., et al. (2010). "Evaluation of soluble junctional adhesion molecule-A as a biomarker of human brain endothelial barrier breakdown." PloS one **5**(10): e13568.

Hainsworth, A. H. and H. S. Markus (2008). "Do in vivo experimental models reflect human cerebral small vessel disease? A systematic review." Journal of Cerebral Blood Flow **28**(12): 1877-1891.

Hainsworth, A. H., et al. (2015). "Endothelial cells and human cerebral small vessel disease." Brain Pathology **25**(1): 44-50.

Hajdu, M. A., et al. (1990). "Effects of aging on mechanics and composition of cerebral arterioles in rats." Circulation research **66**(6): 1747-1754.

Haorah, J., et al. (2007). "Oxidative stress activates protein tyrosine kinase and matrix metalloproteinases leading to blood-brain barrier dysfunction." Journal of neurochemistry **101**(2): 566-576.

Hayani, H., et al. (2018). "Increased excitability and reduced excitatory synaptic input into fast-spiking CA2 interneurons after enzymatic attenuation of extracellular matrix." Frontiers in cellular neuroscience **12**: 149.

Healy, D. P. and S. Wilk (1993). "Localization of immunoreactive glutamyl aminopeptidase in rat brain. II. Distribution and correlation with angiotensin II." Brain research **606**(2): 295-303.

Held, F., et al. (2017). "Vascular basement membrane alterations and β -amyloid accumulations in an animal model of cerebral small vessel disease." Clinical science **131**(10): 1001-1013.

Herve, D. and H. J. J. o. g. p. Chabriat (2010). "Cadasil." Journal of geriatric psychiatry **23**(4): 269-276.

Hopperton, K., et al. (2018). "Markers of microglia in post-mortem brain samples from patients with Alzheimer's disease: a systematic review." Molecular psychiatry **23**(2): 177-198.

Hovens, I. B., et al. (2014). "A novel method for evaluating microglial activation using ionized calcium-binding adaptor protein-1 staining: cell body to cell size ratio." Neuroimmunology Neuroinflammation **1**: 82-88.

Hu, X., et al. (2015). "Microglial and macrophage polarization—new prospects for brain repair." Nature Reviews Neurology **11**(1): 56-64.

Huang, C.-W., et al. (2015). "Clinical significance of circulating vascular cell adhesion molecule-1 to white matter disintegration in Alzheimer's dementia." Thrombosis haemostasis **114**(12): 1230-1240.

Huisa, B. N., et al. (2015). "Long-term blood–brain barrier permeability changes in Binswanger disease." Stroke **46**(9): 2413-2418.

Hussain, S., et al. (2016). "SNARE protein syntaxin-1 colocalizes closely with NMDA receptor subunit NR2B in postsynaptic spines in the hippocampus." Frontiers in molecular neuroscience **9**: 10.

Hußler, W., et al. (2022). "Brevican and Neurocan Cleavage Products in the Cerebrospinal Fluid-Differential Occurrence in ALS, Epilepsy and Small Vessel Disease." Frontiers in cellular neuroscience **16**.

Iemolo, F., et al. (2016). "The prognostic value of biomarkers in stroke." Immunity & Ageing **13**(1): 19.

Ihara, M. and Y. Yamamoto (2016). "Emerging evidence for pathogenesis of sporadic cerebral small vessel disease." Stroke **47**(2): 554-560.

Inzitari, D., et al. (2009). "Changes in white matter as determinant of global functional decline in older independent outpatients: three year follow-up of LADIS (leukoaraiosis and disability) study cohort." BMJ open **339**.

Ishizuka, K., et al. (1997). "Identification of monocyte chemoattractant protein-1 in senile plaques and reactive microglia of Alzheimer's disease." Psychiatry clinical neurosciences **51**(3): 135-138.

Jalal, F. Y., et al. (2015). "Hypoxia-induced neuroinflammatory white-matter injury reduced by minocycline in SHR/SP." Journal of Cerebral Blood Flow & Metabolism **35**(7): 1145-1153.

Jandke, S., et al. (2018). "The association between hypertensive arteriopathy and cerebral amyloid angiopathy in spontaneously hypertensive stroke-prone rats." Brain Pathology **28**(6): 844-859.

Jiménez, A. J., et al. (2014). "Structure and function of the ependymal barrier and diseases associated with ependyma disruption." Tissue barriers **2**(1): e28426.

Jonesco, D. S., et al. (2020). "The CNS-specific proteoglycan, brevican, and its ADAMTS4-cleaved fragment show differential serological levels in Alzheimer's disease, other types of dementia and non-demented controls: A cross-sectional study." PloS one **15**(6): e0234632.

Joutel, A., et al. (2000). "The ectodomain of the Notch3 receptor accumulates within the cerebrovasculature of CADASIL patients." The Journal of clinical investigation **105**(5): 597-605.

Joutel, A., et al. (1996). "Notch3 mutations in CADASIL, a hereditary adult-onset condition causing stroke and dementia." Nature **383**(6602): 707-710.

Joutel, A., et al. (2016). "Perturbations of the cerebrovascular matrisome: A convergent mechanism in small vessel disease of the brain?" Journal of Cerebral Blood Flow & Metabolism **36**(1): 143-157.

Kalaria, R. N. and C. Ballard (1999). "Overlap between pathology of Alzheimer disease and vascular dementia." Alzheimer disease associated disorders.

Kashani, A., et al. (2008). "Loss of VGLUT1 and VGLUT2 in the prefrontal cortex is correlated with cognitive decline in Alzheimer disease." Neurobiology of aging **29**(11): 1619-1630.

Kato, T., et al. (2020). "Excessive production of transforming growth factor β 1 causes mural cell depletion from cerebral small vessels." Frontiers in aging neuroscience **12**: 151.

Kaushik, R., et al. (2018). "Traditional Japanese herbal medicine Yokukansan targets distinct but overlapping mechanisms in aged mice and in the 5xFAD mouse model of Alzheimer's disease." Frontiers in aging neuroscience **10**: 411.

Kirvell, S., et al. (2010). "Vesicular glutamate transporter and cognition in stroke: a case-control autopsy study." Neurology **75**(20): 1803-1809.

Kirvell, S. L., et al. (2006). "Down-regulation of vesicular glutamate transporters precedes cell loss and pathology in Alzheimer's disease." Journal of neurochemistry **98**(3): 939-950.

Kivinen, N., et al. (2016). "Absence of collagen XVIII in mice causes age-related insufficiency in retinal pigment epithelium proteostasis." Biogerontology **17**(4): 749-761.

Knobloch, W. H. and J. M. Layer (1972). "Clefting syndromes associated with retinal detachment." American Journal of Ophthalmology **73**(4): 517-530.

Koizumi, T., et al. (2019). "Vessel-associated immune cells in cerebrovascular diseases: From perivascular macrophages to vessel-associated microglia." Frontiers in neuroscience: 1291.

Koskinen, M.-K., et al. (2020). "From stress to depression: development of extracellular matrix-dependent cognitive impairment following social stress." Scientific reports **10**(1): 1-12.

Krupinski, J., et al. (1996). "Increased expression of TGF- β 1 in brain tissue after ischemic stroke in humans." Stroke **27**(5): 852-857.

Laflamme, N., et al. (1999). "An essential role of interleukin-1 β in mediating NF- κ B activity and COX-2 transcription in cells of the blood-brain barrier in response to a systemic and localized inflammation but not during endotoxemia." Journal of Neuroscience **19**(24): 10923-10930.

Lasek, A. W. (2016). "Effects of ethanol on brain extracellular matrix: implications for alcohol use disorder." Alcoholism: Clinical and Experimental Research **40**(10): 2030-2042.

Lau, L. W., et al. (2013). "Pathophysiology of the brain extracellular matrix: a new target for remyelination." Nature Reviews Neuroscience **14**(10): 722-729.

Launer, L. (2002). "Demonstrating the case that AD is a vascular disease: epidemiologic evidence." Ageing research reviews **1**(1): 61-77.

Lee, J.-M., et al. (2007). "Vascular permeability precedes spontaneous intracerebral hemorrhage in stroke-prone spontaneously hypertensive rats." Stroke **38**(12): 3289-3291.

Lemarchant, S., et al. (2016). "ADAMTS-4 promotes neurodegeneration in a mouse model of amyotrophic lateral sclerosis." Molecular neurodegeneration **11**(1): 1-24.

Li, Q., et al. (2018). "Cerebral small vessel disease." Cell transplantation **27**(12): 1711-1722.

Li, Y.-J., et al. (2013). "Disruption of the blood-brain barrier after generalized tonic-clonic seizures correlates with cerebrospinal fluid MMP-9 levels." Journal of neuroinflammation **10**(1): 848.

Liddelw, S. A., et al. (2017). "Neurotoxic reactive astrocytes are induced by activated microglia." Nature **541**(7638): 481-487.

Liebner, S., et al. (2018). "Functional morphology of the blood–brain barrier in health and disease." Acta neuropathologica **135**(3): 311-336.

Liebner, S., et al. (2000). "Claudin-1 and claudin-5 expression and tight junction morphology are altered in blood vessels of human glioblastoma multiforme." Acta neuropathologica **100**(3): 323-331.

Lin, J.-X., et al. (2001). "White matter lesions and alteration of vascular cell composition in the brain of spontaneously hypertensive rats." Neuroreport **12**(9): 1835-1839.

Lischper, M., et al. (2010). "Metalloproteinase mediated occludin cleavage in the cerebral microcapillary endothelium under pathological conditions." Brain research **1326**: 114-127.

Lisman, J., et al. (2002). "The molecular basis of CaMKII function in synaptic and behavioural memory." Nature Reviews Neuroscience **3**(3): 175-190.

Liu, J., et al. (2022). "Associated genetic variants and potential pathogenic mechanisms of brain arteriovenous malformation." Journal of NeuroInterventional Surgery.

Llorente, I. L., et al. (2013). "Age and meloxicam modify the response of the glutamate vesicular transporters (VGLUTs) after transient global cerebral ischemia in the rat brain." Brain research bulletin **94**: 90-97.

Lowry, J. R. and A. Klegeris (2018). "Emerging roles of microglial cathepsins in neurodegenerative disease." Brain research bulletin **139**: 144-156.

Maddaluno, L., et al. (2013). "EndMT contributes to the onset and progression of cerebral cavernous malformations." Nature **498**(7455): 492-496.

Marneros, A. G., et al. (2004). "Collagen XVIII/endostatin is essential for vision and retinal pigment epithelial function." The EMBO journal **23**(1): 89-99.

Marneros, A. G. and B. R. Olsen (2001). "The role of collagen-derived proteolytic fragments in angiogenesis." Matrix Biology **20**(5-6): 337-345.

Matuszko, G., et al. (2017). "Extracellular matrix alterations in the ketamine model of schizophrenia." Neuroscience Biobehavioral Reviews **350**: 13-22.

McColl, B. W., et al. (2008). "Systemic inflammation alters the kinetics of cerebrovascular tight junction disruption after experimental stroke in mice." Journal of Neuroscience **28**(38): 9451-9462.

McKee, K. K., et al. (2007). "Role of laminin terminal globular domains in basement membrane assembly." Journal of Biological Chemistry **282**(29): 21437-21447.

Meldgaard, M., et al. (2006). "Validation of two reference genes for mRNA level studies of murine disease models in neurobiology." Journal of neuroscience methods **156**(1-2): 101-110.

Merlini, M., et al. (2019). "Fibrinogen induces microglia-mediated spine elimination and cognitive impairment in an Alzheimer's disease model." Neuron **101**(6): 1099-1108. e1096.

Minta, K., et al. (2019). "Dynamics of extracellular matrix proteins in cerebrospinal fluid and serum and their relation to clinical outcome in human traumatic brain injury." Clinical Chemistry and Laboratory Medicine **57**(10): 1565-1573.

Miosge, N., et al. (2003). "The collagen type XVIII endostatin domain is co-localized with perlecan in basement membranes in vivo." Journal of Histochemistry Cytochemistry **51**(3): 285-296.

Mizoguchi, H. and K. Yamada (2013). "Roles of matrix metalloproteinases and their targets in epileptogenesis and seizures." Clinical Psychopharmacology and Neuroscience **11**(2): 45.

Montagne, A., et al. (2015). "Blood-brain barrier breakdown in the aging human hippocampus." Neuron **85**(2): 296-302.

Montaner, J., et al. (2001). "Matrix metalloproteinase expression is related to hemorrhagic transformation after cardioembolic stroke." Stroke **32**(12): 2762-2767.

Morawski, M., et al. (2014). "Tenascin-R promotes assembly of the extracellular matrix of perineuronal nets via clustering of aggrecan." Philosophical Transactions of the Royal Society B: Biological Sciences **369**(1654): 20140046.

Morgan, R. G., et al. (2014). "Role of arterial telomere dysfunction in hypertension: relative contributions of telomere shortening and telomere uncapping." Journal of hypertension **32**(6): 1293.

Morita, K., et al. (1999). "Endothelial claudin: claudin-5/TMVCF constitutes tight junction strands in endothelial cells." The Journal of cell biology **147**(1): 185-194.

Moulton, K. S., et al. (2004). "Loss of collagen XVIII enhances neovascularization and vascular permeability in atherosclerosis." Circulation **110**(10): 1330-1336.

Muoio, V., et al. (2014). "The neurovascular unit—concept review." Acta physiologica **210**(4): 790-798.

Muragaki, Y., et al. (1995). "Mouse Col18a1 is expressed in a tissue-specific manner as three alternative variants and is localized in basement membrane zones." Proceedings of the National Academy of Sciences **92**(19): 8763-8767.

Nakanishi, H. (2003). "Microglial functions and proteases." Molecular neurobiology **27**(2): 163-176.

Nguyen, H.-L., et al. (2011). "TGF- β signaling in endothelial cells, but not neuroepithelial cells, is essential for cerebral vascular development." Laboratory investigation **91**(11): 1554-1563.

Nimmerjahn, A., et al. (2005). "Resting microglial cells are highly dynamic surveillants of brain parenchyma in vivo." Science **308**(5726): 1314-1318.

Nimmerjahn, A., et al. (2005). "Resting microglial cells are highly dynamic surveillants of brain parenchyma in vivo." Science translational medicine **308**(5726): 1314-1318.

Nolte, C., et al. (2001). "GFAP promoter-controlled EGFP-expressing transgenic mice: a tool to visualize astrocytes and astrogliosis in living brain tissue." Glia **33**(1): 72-86.

O'Reilly, M. S., et al. (1997). "Endostatin: an endogenous inhibitor of angiogenesis and tumor growth." cell **88**(2): 277-285.

O'Sullivan, M., et al. (2001). "MRI hyperintensities of the temporal lobe and external capsule in patients with CADASIL." Neurology **56**(5): 628-634.

Oh, S. P., et al. (1994). "Cloning of cDNA and genomic DNA encoding human type XVIII collagen and localization of the $\alpha 1$ (XVIII) collagen gene to mouse chromosome 10 and human chromosome 21." Genomics **19**(3): 494-499.

Omar, M. H., et al. (2017). "CNS neurons deposit laminin $\alpha 5$ to stabilize synapses." Cell reports **21**(5): 1281-1292.

Osada, T., et al. (2011). "Interendothelial claudin-5 expression depends on cerebral endothelial cell-matrix adhesion by $\beta 1$ -integrins." Journal of Cerebral Blood Flow & Metabolism **31**(10): 1972-1985.

Pantoni, L. (2010). "Cerebral small vessel disease: from pathogenesis and clinical characteristics to therapeutic challenges." The Lancet Neurology **9**(7): 689-701.

Park, S. O., et al. (2009). "Real-time imaging of de novo arteriovenous malformation in a mouse model of hereditary hemorrhagic telangiectasia." The Journal of clinical investigation **119**(11): 3487-3496.

Perosa, V., et al. (2020). "Hippocampal vascular reserve associated with cognitive performance and hippocampal volume." Brain **143**(2): 622-634.

Piccardi, B., et al. (2018). "Reperfusion Injury after ischemic Stroke Study (RISKS): single-centre (Florence, Italy), prospective observational protocol study." BMJ open **8**(5): e021183.

Poggesi, A., et al. (2016). "Circulating biologic markers of endothelial dysfunction in cerebral small vessel disease: a review." Journal of Cerebral Blood Flow and Metabolism **36**(1): 72-94.

Qin, W., et al. (2019). "Melatonin protects blood-brain barrier integrity and permeability by inhibiting matrix metalloproteinase-9 via the NOTCH3/NF- κ B pathway." Aging **11**(23): 11391.

Rajani, R. M., et al. (2018). "Reversal of endothelial dysfunction reduces white matter vulnerability in cerebral small vessel disease in rats." Science translational medicine **10**(448): eaam9507.

Rajani, R. M. and A. Williams (2017). "Endothelial cell–oligodendrocyte interactions in small vessel disease and aging." Clinical science **131**(5): 369-379.

Rajashekhar, G., et al. (2006). "Continuous endothelial cell activation increases angiogenesis: evidence for the direct role of endothelium linking angiogenesis and inflammation." Journal of vascular research **43**(2): 193-204.

Rehn, M., et al. (1994). "Primary structure of the alpha 1 chain of mouse type XVIII collagen, partial structure of the corresponding gene, and comparison of the alpha 1 (XVIII) chain with its homologue, the alpha 1 (XV) collagen chain." Journal of Biological Chemistry **269**(19): 13929-13935.

Rehn, M. and T. Pihlajaniemi (1994). "Alpha 1 (XVIII), a collagen chain with frequent interruptions in the collagenous sequence, a distinct tissue distribution, and homology with type XV collagen." Proceedings of the National Academy of Sciences **91**(10): 4234-4238.

Rehn, M. and T. Pihlajaniemi (1995). "Identification of Three N-terminal Ends of Type XVIII Collagen Chains and Tissue-specific Differences in the Expression of the Corresponding Transcripts: THE LONGEST FORM CONTAINS A NOVEL MOTIF HOMOLOGOUS TO RAT AND DROSOPHILA FRIZZLED PROTEINS (*)." Journal of Biological Chemistry **270**(9): 4705-4711.

Reijerkerk, A., et al. (2006). "Diapedesis of monocytes is associated with MMP-mediated occludin disappearance in brain endothelial cells." The FASEB journal **20**(14): 2550-2552.

Reijmer, Y. D., et al. (2016). "Ischemic brain injury in cerebral amyloid angiopathy." Journal of Cerebral Blood Flow & Metabolism **36**(1): 40-54.

Réus, G. Z., et al. (2015). "The role of inflammation and microglial activation in the pathophysiology of psychiatric disorders." Neuroscience **300**: 141-154.

Revesz, T., et al. (2009). "Genetics and molecular pathogenesis of sporadic and hereditary cerebral amyloid angiopathies." Acta neuropathologica **118**(1): 115-130.

Ricard-Blum, S. (2011). "The collagen family." Cold Spring Harbor perspectives in biology **3**(1): a004978.

Riga, D., et al. (2017). "Hippocampal extracellular matrix alterations contribute to cognitive impairment associated with a chronic depressive-like state in rats." Science translational medicine **9**(421): eaai8753.

Rooney, P. and S. Kumar (1993). "Inverse relationship between hyaluronan and collagens in development and angiogenesis." Differentiation **54**(3): 1-9.

Rosenberg, G. A. (2016). "Matrix metalloproteinase-mediated Neuroinflammation in vascular cognitive impairment of the Binswanger type." Cellular and Molecular Neurobiology **36**(2): 195-202.

Rosenberg, G. A. (2017). "Extracellular matrix inflammation in vascular cognitive impairment and dementia." Clinical science **131**(6): 425-437.

Rosenberg, G. A., et al. (2001). "Immunohistochemistry of matrix metalloproteinases in reperfusion injury to rat brain: activation of MMP-9 linked to stromelysin-1 and microglia in cell cultures." Brain research **893**(1-2): 104-112.

Rosenberg, G. A. J. G. (2002). "Matrix metalloproteinases in neuroinflammation." **39**(3): 279-291.

Rouhl, R. P., et al. (2012). "Vascular inflammation in cerebral small vessel disease." Neurobiology of aging **33**(8): 1800-1806.

Rudemiller, N. P. and S. D. Crowley (2017). "The role of chemokines in hypertension and consequent target organ damage." Pharmacological research **119**: 404-411.

Sá-Pereira, I., et al. (2012). "Neurovascular unit: a focus on pericytes." Molecular neurobiology **45**(2): 327-347.

Sadoshima, S. and D. Heistad (1982). "Sympathetic nerves protect the blood-brain barrier in stroke-prone spontaneously hypertensive rats." Hypertension **4**(6): 904-907.

Santisteban, M. M. and C. Iadecola (2018). "Hypertension, dietary salt and cognitive impairment." Journal of Cerebral Blood Flow & Metabolism **38**(12): 2112-2128.

Sasaki, T., et al. (1998). "Structure, function and tissue forms of the C-terminal globular domain of collagen XVIII containing the angiogenesis inhibitor endostatin." The EMBO journal **17**(15): 4249-4256.

Sato, Y., et al. (2019). "Ventricular–subventricular zone fractones are speckled basement membranes that function as a neural stem cell niche." Molecular biology of the cell **30**(1): 56-68.

Satoh, K., et al. (2000). "ADAMTS-4 (a disintegrin and metalloproteinase with thrombospondin motifs) is transcriptionally induced in beta-amyloid treated rat astrocytes." Neuroscience letters **289**(3): 177-180.

Schindelin, J., et al. (2012). "Fiji: an open-source platform for biological-image analysis." Nature methods **9**(7): 676-682.

Schreiber, S., et al. (2013). "Blood brain barrier breakdown as the starting point of cerebral small vessel disease?-New insights from a rat model." Experimental & translational stroke medicine **5**(1): 1-8.

Senatorov Jr, V. V., et al. (2019). "Blood-brain barrier dysfunction in aging induces hyperactivation of TGF β signaling and chronic yet reversible neural dysfunction." Science translational medicine **11**(521): eaaw8283.

Senkov, O., et al. (2014). Neural ECM molecules in synaptic plasticity, learning, and memory. Progress in brain research, Elsevier. **214**: 53-80.

Seppinen, L. and T. Pihlajaniemi (2011). "The multiple functions of collagen XVIII in development and disease." Matrix Biology **30**(2): 83-92.

Sertié, A. L., et al. (2000). "Collagen XVIII, containing an endogenous inhibitor of angiogenesis and tumor growth, plays a critical role in the maintenance of retinal structure and in neural tube closure (Knobloch syndrome)." Human molecular genetics **9**(13): 2051-2058.

Shen, Y., et al. (2009). "PTP σ is a receptor for chondroitin sulfate proteoglycan, an inhibitor of neural regeneration." Science **326**(5952): 592-596.

Simpson, J., et al. (2007). "Microglial activation in white matter lesions and nonlesional white matter of ageing brains." Neuropathology applied neurobiology **33**(6): 670-683.

Sironi, L., et al. (2004). "Analysis of pathological events at the onset of brain damage in stroke-prone rats: a proteomics and magnetic resonance imaging approach." Journal of neuroscience research **78**(1): 115-122.

Sladojevic, N., et al. (2014). "Inhibition of junctional adhesion molecule-A/LFA interaction attenuates leukocyte trafficking and inflammation in brain ischemia/reperfusion injury." Neurobiology of Disease **67**: 57-70.

Sokolova, A., et al. (2009). "Monocyte chemoattractant protein-1 plays a dominant role in the chronic inflammation observed in Alzheimer's disease." Brain Pathology **19**(3): 392-398.

Song, I. and A. Dityatev (2018). "Crosstalk between glia, extracellular matrix and neurons." Brain research bulletin **136**: 101-108.

Stevenson, T. (2018). Role of Tissue Plasminogen Activator in Central Nervous System Physiology and Pathology.

Strackeljan, L., et al. (2021). "Microglia Depletion-Induced Remodeling of Extracellular Matrix and Excitatory Synapses in the Hippocampus of Adult Mice." Cells **10**(8): 1862.

Su, J., et al. (2012). "Target-derived matricryptins organize cerebellar synapse formation through $\alpha 3\beta 1$ integrins." Cell reports **2**(2): 223-230.

Sweeney, M. D., et al. (2016). "Pericytes of the neurovascular unit: key functions and signaling pathways." Nature neuroscience **19**(6): 771-783.

T Ronaldson, P. and T. P Davis (2012). "Blood-brain barrier integrity and glial support: mechanisms that can be targeted for novel therapeutic approaches in stroke." Current pharmaceutical design **18**(25): 3624-3644.

Ten Dijke, P. and H. M. Arthur (2007). "Extracellular control of TGF β signalling in vascular development and disease." Nature reviews Molecular cell biology **8**(11): 857-869.

Thomsen, M. S., et al. (2017). "The vascular basement membrane in the healthy and pathological brain." Journal of Cerebral Blood Flow & Metabolism **37**(10): 3300-3317.

Tornavaca, O., et al. (2015). "ZO-1 controls endothelial adherens junctions, cell–cell tension, angiogenesis, and barrier formation." Journal of Cell Biology **208**(6): 821-838.

Trask, S. and D. I. Fournier (2022). "Examining a role for the retrosplenial cortex in age-related memory impairment." Neurobiology of Learning and Memory **189**: 107601.

Ulbrich, P., et al. (2021). "Interplay between perivascular and perineuronal extracellular matrix remodelling in neurological and psychiatric diseases." European journal of Neuroscience **53**(12): 3811-3830.

Urabe, N., et al. (2002). "Basement membrane type IV collagen molecules in the choroid plexus, pia mater and capillaries in the mouse brain." Archives of histology and cytology **65**(2): 133-143.

Van Zwieten, E., et al. (1988). "Immunocytochemically stained vasopressin binding sites on blood vessels in the rat brain." Brain research **474**(2): 369-373.

Végh, M. J., et al. (2014). "Reducing hippocampal extracellular matrix reverses early memory deficits in a mouse model of Alzheimer's disease." Acta neuropathologica communications **2**(1): 1-11.

Ventura Ferreira, M. S., et al. (2018). "Comprehensive characterization of chorionic villi-derived mesenchymal stromal cells from human placenta." Stem Cell Research & Therapy **9**(1): 1-17.

Vernooij, M., et al. (2008). "Prevalence and risk factors of cerebral microbleeds: the Rotterdam Scan Study." Neurology **70**(14): 1208-1214.

Vinters, H. V. (1987). "Cerebral amyloid angiopathy. A critical review." Stroke **18**(2): 311-324.

Viswanathan, A. and S. M. Greenberg (2011). "Cerebral amyloid angiopathy in the elderly." Annals of neurology **70**(6): 871-880.

Vom Berg, J., et al. (2012). "Inhibition of IL-12/IL-23 signaling reduces Alzheimer's disease-like pathology and cognitive decline." Nature Med **18**(12): 1812-1819.

Wagner, S., et al. (2011). "The MMP inhibitor (R)-2-(N-benzyl-4-(2-[18F] fluoroethoxy) phenylsulphonamido)-N-hydroxy-3-methylbutanamide: Improved precursor synthesis and fully automated radiosynthesis." Applied Radiation and Isotopes **69**(6): 862-868.

Wang, Y., et al. (2014). "Interleukin-1 β induces blood-brain barrier disruption by downregulating sonic hedgehog in astrocytes." PloS one **9**(10): e110024.

Wardlaw, J. M., et al. (2020). "Perivascular spaces in the brain: anatomy, physiology and pathology." Nature Reviews Neurology: 1-17.

Wardlaw, J. M., et al. (2017). "Blood-brain barrier failure as a core mechanism in cerebral small vessel disease and dementia: evidence from a cohort study." Alzheimer's Dementia **13**(6): 634-643.

Wardlaw, J. M., et al. (2013). "Neuroimaging standards for research into small vessel disease and its contribution to ageing and neurodegeneration." The Lancet Neurology **12**(8): 822-838.

Westin, K., et al. (2012). "CCL2 is associated with a faster rate of cognitive decline during early stages of Alzheimer's disease." PloS one **7**(1): e30525.

Whitelock, J. M., et al. (2008). "Diverse cell signaling events modulated by perlecan." Biochemistry **47**(43): 11174-11183.

Wilkinson, R. D., et al. (2015). "Cathepsin S: therapeutic, diagnostic, and prognostic potential." Biological chemistry **396**(8): 867-882.

Woo, D., et al. (2002). "Genetic and environmental risk factors for intracerebral hemorrhage: preliminary results of a population-based study." Stroke **33**(5): 1190-1196.

Worthmann, H., et al. (2010). "The temporal profile of inflammatory markers and mediators in blood after acute ischemic stroke differs depending on stroke outcome." Cerebrovascular Diseases **30**(1): 85-92.

Wyss-Coray, T. and L. Mucke (2002). "Inflammation in neurodegenerative disease—a double-edged sword." Neuron **35**(3): 419-432.

Xiao, L.-Y., et al. (2018). "Acupuncture prevents the impairment of hippocampal LTP through β 1-AR in vascular dementia rats." Molecular neurobiology **55**(10): 7677-7690.

Yamamoto, Y. and M. Ihara (2017). "Disruption of transforming growth factor- β superfamily signaling: A shared mechanism underlying hereditary cerebral small vessel disease." Neurochemistry International **107**: 211-218.

Yamazaki, Y. and T. Kanekiyo (2017). "Blood-brain barrier dysfunction and the pathogenesis of Alzheimer's disease." Int J Mol Sci **18**(9): 1965.

Yang, J., et al. (2017). "Gastrin-releasing peptide facilitates glutamatergic transmission in the hippocampus and effectively prevents vascular dementia induced cognitive and synaptic plasticity deficits." Experimental Neurology **287**: 75-83.

Yang, Q., et al. (2022). "Cerebral small vessel disease alters neurovascular unit regulation of microcirculation integrity involved in vascular cognitive impairment." Neurobiology of Disease: 105750.

Yang, Y., et al. (2007). "Matrix metalloproteinase-mediated disruption of tight junction proteins in cerebral vessels is reversed by synthetic matrix metalloproteinase inhibitor in focal ischemia in rat." Journal of Cerebral Blood Flow **27**(4): 697-709.

Yilmaz, B., et al. (2016). "Familial occurrence of brain arteriovenous malformation: a novel ACVRL1 mutation detected by whole exome sequencing." Journal of neurosurgery **126**(6): 1879-1883.

Ylikärppä, R., et al. (2003). "Double knockout mice reveal a lack of major functional compensation between collagens XV and XVIII." Matrix Biology **22**(5): 443-448.

Yong, V. W., et al. (2001). "Metalloproteinases in biology and pathology of the nervous system." Nature **2**(7): 502-511.

York, E. M., et al. (2018). "3DMorph automatic analysis of microglial morphology in three dimensions from ex vivo and in vivo imaging." eNeuro **5**(6).

Yousif, L. F., et al. (2013). "Laminin isoforms in endothelial and perivascular basement membranes." Cell adhesion & migration **7**(1): 101-110.

Yurchenco, P. D. (2015). Integrating activities of laminins that drive basement membrane assembly and function. Current topics in membranes, Elsevier. **76**: 1-30.

Yurchenco, P. D., et al. (2004). "Basement membrane assembly, stability and activities observed through a developmental lens." Matrix Biology **22**(7): 521-538.

Zhang, C. E., et al. (2017). "Blood–brain barrier leakage is more widespread in patients with cerebral small vessel disease." Neurology **88**(5): 426-432.

Zhang, Y. and X. Yang (2020). "The roles of TGF- β signaling in cerebrovascular diseases." Frontiers in Cell and Developmental Biology **8**: 567682.

Zhao, B.-Q., et al. (2006). "Role of matrix metalloproteinases in delayed cortical responses after stroke." Nature medicine **12**(4): 441-445.

Zhong, C., et al. (2017). "Serum matrix metalloproteinase-9 levels and prognosis of acute ischemic stroke." Neurology **89**(8): 805-812.

Zlokovic, B. V. (2008). "The blood-brain barrier in health and chronic neurodegenerative disorders." Neuron **57**(2): 178-201.

9 Appendix

A. Declaration of Honour

“I hereby declare that I prepared this thesis without the impermissible help of third parties and that none other than the aids indicated have been used; all sources of information are clearly marked, including my own publications.

In particular I have not consciously:

- fabricated data or rejected undesirable results,
- misused statistical methods with the aim of drawing other conclusions than those warranted by the available data,
- plagiarized external data or publications,
- presented the results of other researchers in a distorted way.

I am aware that violations of copyright may lead to injunction and damage claims by the author and also to prosecution by law enforcement authorities.

I hereby agree that the thesis may be electronically reviewed with the aim of identifying plagiarism.

This work has not been submitted as a doctoral thesis in the same or a similar form in Germany, nor in any other country. It has not yet been published as a whole.”

Magdeburg 29.01.2023

Mahsima Khoshneviszadeh

